

AD-A032 010

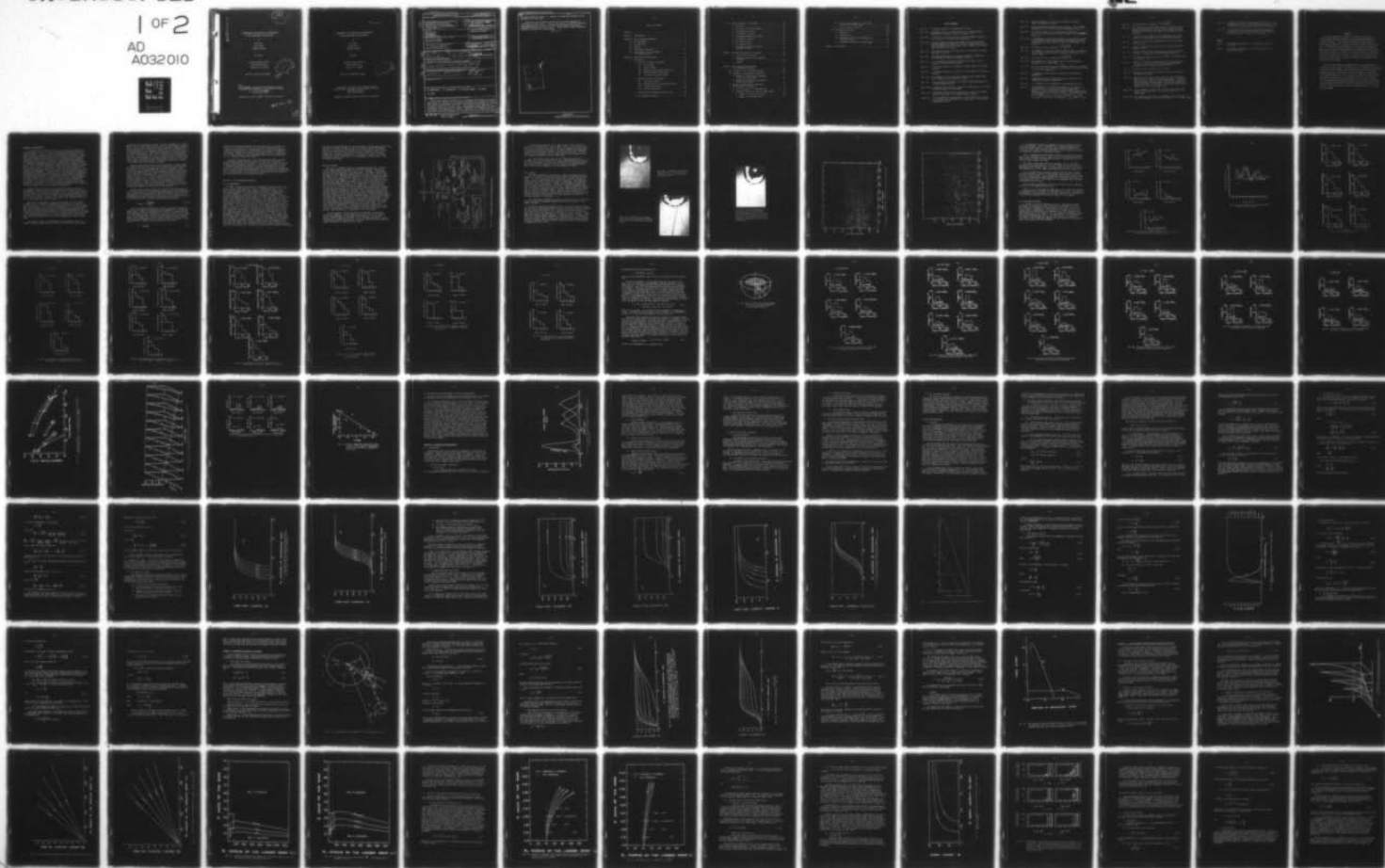
TEL-AVIV UNIV (ISRAEL) DEPT OF GEOPHYSICS AND PLANET--ETC F/G 4/1  
EXPERIMENTAL AND THEORETICAL INVESTIGATION OF THE COALESCENCE 0--ETC(U)  
MAY 76 Z LEVIN, B MACHNES, N ARBEL

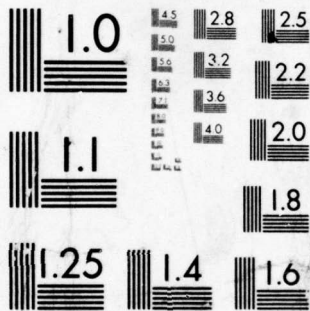
DA-ERO-124-74-G-0058

NL

UNCLASSIFIED

1 OF 2  
AD  
A032010





MICROCOPY RESOLUTION TEST CHART  
NATIONAL BUREAU OF STANDARDS-1963-A

ADA032010

AD 12

EXPERIMENTAL AND THEORETICAL INVESTIGATION  
OF THE COALESCENCE OF WATER DROPS

by

Zev Levin

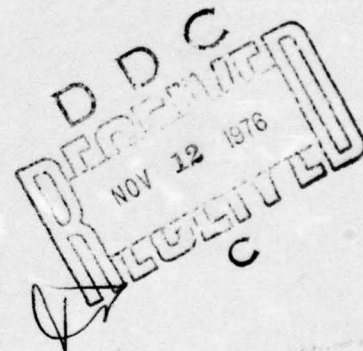
Nitza Arbel

Benjamin Machnes

May 1976

European Research Office  
United States Army  
London N.W.1, England

Grant No. DA-ERO-124-74-G0058



③ Department of Geophysics and Planetary Sciences,  
(previous name: Department of Environmental Sciences)  
① Tel Aviv University  
Ramat Aviv, Israel.

Approved for public release: distribution unlimited

409 921 Now

VB

AD \_\_\_\_\_

EXPERIMENTAL AND THEORETICAL INVESTIGATION  
OF THE COALESCENCE OF WATER DROPS

by

Zev Levin  
Nitza Arbel  
Benjamin Machnes

May 1976

European Research Office  
United States Army  
London N.W.1, England

Grant No. DA-ERO-124-74-G0058



Department of Geophysics and Planetary Sciences  
(previous name: Department of Environmental Sciences)  
Tel Aviv University  
Ramat Aviv, Israel.

Approved for public release: distribution unlimited

UNCLASSIFIED

SECURITY CLASSIFICATION OF THIS PAGE (When Data Entered)

REPORT DOCUMENTATION PAGE		READ INSTRUCTIONS BEFORE COMPLETING FORM
1. REPORT NUMBER	2. GOVT ACCESSION NO.	3. RECIPIENT'S CATALOG NUMBER
4. TITLE (and Subtitle) EXPERIMENTAL AND THEORETICAL INVESTIGATION OF THE COALESCENCE OF WATER DROPS.		5. TYPE OF REPORT & PERIOD COVERED FINAL TECHNICAL REPORT, OCT 75-JUN 76
7. AUTHOR(s) DR. ZEV LEVIN NITZA ARBEL BENJAMIN MACHNES		6. PERFORMING ORG. REPORT NUMBER
9. PERFORMING ORGANIZATION NAME AND ADDRESS TEL AVIV UNIVERSITY RAMAT AVIV, ISRAEL		8. CONTRACT OR GRANT NUMBER(s) DAERO-124-74-G0058 new
11. CONTROLLING OFFICE NAME AND ADDRESS U.S. ARMY R&S GROUP (EUR) BOX 65, FPO NEW YORK 09510		10. PROGRAM ELEMENT, PROJECT, TASK AREA & WORK UNIT NUMBERS 6 1102A-2M061103B53B-00-350
14. MONITORING AGENCY NAME & ADDRESS (if different from Controlling Office) Zev/Levin Benjamin/Machnes Nitza/Arbel		12. REPORT DATE MAY 1976 12/1/76
		13. NUMBER OF PAGES 107
		15. SECURITY CLASS. (of this report) UNCLASSIFIED
16. DISTRIBUTION STATEMENT (of this Report) APPROVED FOR PUBLIC RELEASE DISTRIBUTION UNLIMITED DA-ERO-124-74-G-0058		15a. DECLASSIFICATION/DOWNGRADING SCHEDULE
17. DISTRIBUTION STATEMENT (of the abstract entered in Block 20, if different from Report) 2M061103B53B 17 00		
18. SUPPLEMENTARY NOTES		
19. KEY WORDS (Continue on reverse side if necessary and identify by block number) (U) ATMOSPHERIC: (U) COALESCENCE: (U) ELECTRIC CHARGE: (U) DROPS: (U) WATER		
20. ABSTRACT (Continue on reverse side if necessary and identify by block number) This report summarises results of the coalescence efficiency of colliding drops which were obtained from laboratory experiments and a theoretical model. Both theory and experiment suggest that the coalescence efficiency is a function of both drop radii and drop size ratio. Even though no clear dependence of coalescence efficiency on impact speed was observed experimentally, the theory does predict some dependence on velocity. Generally it is observed that the coalescence efficiency decreases with increase in the size of the large drop,		

DD FORM 1 JAN 73 1473

EDITION OF 1 NOV 65 IS OBSOLETE

409 921

UNCLASSIFIED

SECURITY CLASSIFICATION OF THIS PAGE (When Data Entered)

R(L)

$R_L$ , and the drop size ratio,  $p$ . However, for small  $R_L$  a decrease in the efficiency was also shown.

R(L)

Both theory and experiment demonstrate the strong dependence of coalescence on impact angle. From the experiments two empirical equations were obtained which relate the coalescence efficiencies and partial coalescence efficiencies with  $p$  and  $R_L$ . These could be used in numerical models of cloud and rain development.

R(L)

ACCESSION FOR	
RTIS	W/IN SCHED <input checked="" type="checkbox"/>
RTIS	OUT SCHED <input type="checkbox"/>
UNANNOUNCED JUSTIFICATION	
BY	
DISTRIBUTION/AVAILABILITY CODE	
Dist.	Avail. and/or Sp. Dist.
A	

UNCLASSIFIED

## Table of Contents

Abstract. . . . .	1
Chapter 1: Introduction. . . . .	2
Chapter 2: The Coalescence Experiment. . . . .	4
2-1. The experiment. . . . .	4
2-2. The apparatus . . . . .	5
2-3. Results . . . . .	7
2-4. Coalescence efficiency. . . . .	12
2-5. The effects on the development of the raindrop spectra . . . . .	34
Chapter 3: Theoretical Considerations. . . . .	34
3-1. Introduction . . . . .	34
a. Effects that hinder coalescence . . . . .	34
(i) The air gap. . . . .	34
(ii) Surface energy . . . . .	36
(iii) Aging of the gas liquid interface. . . . .	36
(iv) Drop oscillation after impact. . . . .	36
(v) The electrical double layer. . . . .	37
b. Effects that assist coalescence . . . . .	37
(i) Electrical effects . . . . .	37
(ii) Oscillations on the deformed surfaces. . . . .	37
(iii) Internal circulation . . . . .	38
(iv) Van der Waals force. . . . .	38
c. The shape of the deformation and its size . . . . .	38
d. The coalescence distance. . . . .	39

3-2. Head on approach of two drops. . . . .	39
a. The model. . . . .	39
b. The forces and the deformation . . . . .	40
c. The equation of motion . . . . .	43
d. The numerical solution . . . . .	45
e. A comparison between the forces. . . . .	48
f. The analytic solution. . . . .	54
g. The viscous force. . . . .	57
h. The approach time. . . . .	57
i. The range in which the analytic solution is valid. . . . .	58
Chapter 4. Non-Head-On approach of two drops. . . . .	60
a. The equations of motion. . . . .	60
b. Numerical solution of the equation of motion. . . . .	63
c. Summary. . . . .	67
Chapter 5. The coalescence problem and the coalescence efficiency . . . . .	69
5-1. An answer to the coalescence problem . . . . .	69
5-2. Regions of bouncing and coalescence . . . . .	69
i. Regions of bouncing and coalescence in the $(R_g,  V_i )$ plane. . . . .	69
ii. Regions of bouncing and coalescence in the $(p, R_L)$ plane. . . . .	70
5-3. Regions of bouncing and coalescence in non-head-on collisions. . . . .	76
i. Critical angle for coalescence, CAC. . . . .	76
ii. Available data on the critical impact angle. . . . .	79
a. Impact on a stationary target. . . . .	79
b. Impact of two moving drops . . . . .	79

iii. Critical impact angle for coalescence, CAC, from the present model. . . . .	80
iv. Critical impact velocity . . . . .	80
5-4. Coalescence efficiency. . . . .	83
i. Definitions. . . . .	83
ii. Available data . . . . .	84
iii. Coalescence efficiency for impacts on a stationary target. . . . .	85
iv. Coalescence efficiency of moving drops . . . . .	94
Chapter 6: Conclusions . . . . .	94

List of Figures

- Fig. 2-1. A schematic diagram of the experimental set-up.
- Fig. 2-2a. Coalescence event of two drops 2200 and 110 microns diameter impacting at a velocity of 1m/sec. and angle of 38°.
- Fig. 2-2b. A bouncing of two drops 2180 and 130 microns diameter impacting at a velocity of 1.0 m/sec. and an angle of 8°.
- Fig. 2-2c. A partial coalescence event when drops of 2160 and 120 microns diameter impact at a velocity of 0.5 m/sec. and an angle of 29°. After separation the smaller droplet has a diameter of 80 microns and a velocity of 0.34 m/sec.
- Fig. 2-3a. Experimental observation of coalescence as a function of velocity and angle of contact.
- Fig. 2-3b. Experimental observation of bouncing and partial coalescence as a function of velocity and angle of contact.
- Fig. 2-4. % of coalescence frequency for different velocities of small droplets for various contact angles.
- Fig. 2-5. Coalescence frequency as a function of impact speed for different p ratios.
- Fig. 2-6. Coalescence frequency as a function of impact angle for different p ratios.
- Fig. 2-7a-f. The dependence of the coalescence frequency on the impact angle for a variety of drop sizes and p ratios.
- Fig. 2-8. The projected cross sectional area seen by impacting droplets of a certain angle interval.
- Fig. 2-9a-f. Coalescence efficiencies as a function of impact angle for different p ratios and sizes of large drops.
- Fig. 2-10. Coalescence efficiencies as a function of p ratios for different sizes of large drops. a's represent drops' diameter.
- Fig. 2-11. A three dimensional representation of the coalescence efficiency as a function of p ratio and size of large drops. Dots represent experimental results.

- Fig. 2-12. Partial coalescence efficiencies as a function of impact angle for different  $p$  ratios.
- Fig. 2-13. Partial coalescence efficiency versus  $p$  ratios. Dots represent experimental results and the curve is represented by Eq. 2-2.
- Fig. 2-14. The drop size spectra after 600 seconds for different  $E$  (a)  $E = 1$ , (b)  $E$  as described by Eq. 1-2 and (c)  $E$  as described by Eq. 2-1.
- Fig. 3-1a. The dependence of the approach velocity of the deformed surfaces on the distance between the surfaces for different  $R_s$  when the deformation  $R_D = 0.5R_s$ . Here  $R_L = 250\mu$ ,  $v_0 = -600 \text{ cm-sec}^{-1}$  and large  $D_0$ .
- Fig. 3-1b. The same as in part a except  $R_D = \frac{0.5 \times 10^{-5} R_s}{D}$ .
- Fig. 3-2a. The dependence of approach velocity on the distance of separation for different initial velocities. Here  $R_D = 0.5R_s$ ,  $R_s = 50\mu$  and  $R_L = 250\mu$ .
- Fig. 3-2b. The same as in part a except  $R_D = \frac{0.5 \times 10^{-5} R_s}{D}$ .
- Fig. 3-3a. The dependence of the approach velocity on the deformation constant  $\alpha$ .  $R_D = \alpha R_s$ ,  $R_s = 50\mu$ .
- Fig. 3-3b. The same as in part a except  $R_D = \frac{\beta R_s}{D}$  where curves 1-5 represent,  $\beta = 0.3 \times 10^{-5}$ ,  $\beta = 0.4 \times 10^{-5}$ ,  $\beta = 0.5 \times 10^{-5}$ ,  $\beta = 0.6 \times 10^{-5}$  and  $\beta = 0.7 \times 10^{-5}$  respectively.
- Fig. 3-4. A comparison of the forces as a function of the distance of separation.
- Fig. 3-5. Normalized velocity and viscous force as a function of the normalized distance of separation.
- Fig. 4-1. An illustration of the geometry of a non-head-on collision.
- Fig. 4-2. The dependence of the normalized velocity on the distance of separation for  $R_D = 0.5R_s$  in a non-head-on coalescence. Here  $R_s = 50\mu$ ,  $R_L = 250\mu$  and the relative terminal velocity was chosen as the initial velocity at large  $r_0$ . The curves represent the following: 1.  $x_i = 0$ ,  $\theta_i = 0$ , 2.  $x_i = 67\mu$ ,  $\theta_i = 1/14\pi$ , 3.  $x_i = 130\mu$ ,  $\theta_i = 1/7\pi$ , 4.  $x_i = 187\mu$ ,  $\theta_i = 3/14\pi$ , 5.  $x_i = 234\mu$ ,  $\theta_i = 2/7\pi$ , 6.  $x_i = 270\mu$ ,  $\theta_i = 5/14\pi$  and 7.  $x_i = 292\mu$ ,  $\theta_i = 3/7\pi$ .

- Fig. 4-3. The same as Fig. 4-2 except  $R_D = \frac{0.5 \times 10^{-5} R_S}{D}$ .
- Fig. 4-4. The viscous and the centrifugal forces as a function of the distance of separation. Here  $R_S = 50\mu$ ,  $R_L = 250\mu$ ,  $R_D = 0.5R_S$  and the initial velocity was taken as the relative terminal velocity.
- Fig. 5-1. A schematic graph representing the dependence of  $D_s$  on the radius of the small drop,  $R_S$ , and on the initial velocity.
- Fig. 5-2. Regions of bouncing and coalescence in the  $(|V_i|, R_S)$  plane. Here  $R_D = \alpha R_S$ .
- Fig. 5-3. Regions of bouncing and coalescence in the  $(|V_i|, R_S)$  plane. Here  $R_D = \beta R_S/D$ .
- Fig. 5-4. Regions of bouncing and coalescence in the  $(p, R_L)$  plane for  $R_D = \alpha R_S$ . The enclosed area is enlarged in Fig. 5-6.
- Fig. 5-5. The same as in Fig. 5-4 but for  $R_D = \beta R_S/D$ . The enclosed area is enlarged in Fig. 5-7.
- Fig. 5-6. Regions of coalescence and bouncing in the  $(p, R_L)$  plane for  $R_D = \alpha R_S$ . x and  $\dashv$  represent bouncing and coalescence, respectively in the data of Levin et al (1973).
- Fig. 5-7. The same as Fig. 5-6 except for  $R_D = \beta R_S/D$ .
- Fig. 5-8. Regions of bouncing and coalescence in the  $(\theta_i, V_i)$  plane for two different p ratios.
- Fig. 5-9. Comparison of the present results with the data of Whelpdale and List (1971). Dotted areas represent regions of bouncing. Dashed areas are regions of partial coalescence. Regions in white are regions of coalescence. Based on the present work bouncing will occur to the right of the dotted line and coalescence to the left of the dashed line.
- Fig. 5-10. The coalescence efficiency as a function of the ratio of the radii, p, for  $R_D = 0.5R_S$ . (a) for small drops and (b) for larger drops.
- Fig. 5-11. The coalescence efficiency as a function of the p ratio for  $R_D = 0.5 \times 10^{-5} R_S/D$ . (a) for small drops and (b) for larger drops.

Fig. 5-12. A comparison between the coalescence efficiencies according to Whelpdale and List (1971) and the present results. Curve 1 is for  $R_D = 0.5R_S$  and curve 2 for  $R_D = 0.5 \times 10^{-5}R_S/D$ .

Fig. 5-13. A three dimensional representation of the coalescence efficiency as a function of the radius of the large drop,  $R_L$ , and the p ratio. Here  $R_D = 0.5 \times 10^{-5}R_S/D$ .

#### Tables

Table 1. Coalescence efficiencies as a function of  $R_L$  and p for  $R_D = 0.5R_S$ .

Table 2. Coalescence efficiencies as a function of  $R_L$  and p for  $R_D = 0.5 \times 10^{-5}R_S/D$ .

Abstract

This report summarises results of coalescence efficiency of colliding drops which were obtained from laboratory experiments and a theoretical model. Both theory and experiment suggest that the coalescence efficiency is a function of both drop radii and drop size ratio. Even though no clear dependence of coalescence efficiency on impact speed was observed experimentally, the theory does predict some dependence on velocity. Generally it is observed that the coalescence efficiency decreases with increase in the size of the large drop,  $R_L$ , and the drop size ratio,  $p$ . However, for small  $R_L$  a decrease in the efficiency was also shown.

Both theory and experiment demonstrate the strong dependence of coalescence on impact angle. The theory is able to predict the efficiency of coalescence for different impact speeds and not only the relative terminal velocities of the drops. It is also capable of calculating the coalescence efficiency of all impacts on stationary targets and the coalescence efficiencies for moving drops when the  $p$  ratio is small. From the experiments two empirical equations were obtained which relate the coalescence efficiencies and partial coalescence efficiencies with  $p$  and  $R_L$ . These could easily be used in numerical models of cloud and rain development.

## CHAPTER 1: INTRODUCTION

The growth of warm clouds is understood to take place by three distinct processes: a) the nucleation process, whereby droplet embryos are formed on aerosol particles (called cloud condensation nuclei), b) the growth process by condensation which is the process of diffusion of vapor from the environment to the drops, and c) the growth by the collision-coalescence process in which drops grow by capturing smaller droplets during their fall or rise in the cloud. It was believed that the growth by condensation dominates the growth of droplets up to a radius of about  $20\mu$ , while the collision-coalescence process dominates the growth of larger drops. Fog, on the other hand, grows initially by the nucleation process and continues to grow by condensation. Since very little convection exists, the fog droplets tend to remain small and their growth by collision-coalescence is negligible. However, some of the artificial fog dispersal attempts have used different techniques such as the creation of convection, introduction of steam, spread of hygroscopic particles and the spraying of highly charged droplets. The dispersal of the fog is then accomplished by either evaporation of the droplets by mixing them in a subsaturated environment or by forcing the droplets to grow to such sizes that they precipitate to the ground. The latter growth is achieved either by condensation of excess water vapor onto the existing droplets or by coalescence of the fog droplets with the artificially produced ones.

A great deal of theoretical work has been done on the collision efficiencies of water drops in the atmosphere (e.g. Hocking, 1959, Shafrir and Neiburger, 1963, and Hocking and Jonas, 1970). All the results indicate that the larger the drop gets, the higher is its collision efficiency for the same  $p = r/R$  ratio. As  $p$  increases (for the same large drop size) from 0 to 0.5 the efficiency increases. For larger  $p$  the efficiency drops off only to rise again at  $p$  closer to unity.

The number of experiments testing these theories have been limited in number and, as a result of experimental difficulties, also limited to very low  $p$  ratios ( $< 0.3$ ) and to the very high ones ( $\sim 1.0$ ) (e.g. Picknett, 1960, Woods and Mason, 1964, Beard and Pruppacher, 1971). In these experiments the collision efficiency could not be measured independently and could only be deduced from measurements of collection efficiency by assuming a unity coalescence efficiency. Since their results agreed fairly well with the theoretical predictions of the collision efficiencies, they concluded that, in the range they have tested, the coalescence efficiency is indeed unity.

Most numerical models for the growth of cloud droplets or the dispersal of fog by introducing larger drops have, for lack of better values,

assumed that the coalescence is unity. Recently Neiburger et al. (1972) and Levin et al. (1973) have reported results of some laboratory experiments in which drops of various sizes were suspended in moving clouds of smaller droplets. The liquid water content, the size distribution of the smaller droplets, the temperature and saturation ratio were carefully controlled and monitored. Their results indicated that drops smaller than  $40\mu$  in radius did not grow at all by the collision-coalescence process after being suspended in a cloud of droplets of mean radius of  $12\mu$ . Larger drops ( $>55\mu$ ) grew by collecting smaller droplets ( $p \sim 0.2$ ) but at a much slower rate than predicted. When electric charges were applied to the drops, their rate of growth increased.

Their conclusions were that: a) the coalescence efficiency cannot be considered unity for all  $p$  ratios; b) that as the  $p$  ratio increases (at least to  $p = 0.35$ ) the coalescence efficiency decreases. These results have grave consequences on the theory of growth of warm clouds or the effectiveness of the collision-coalescence mechanism in the artificial dispersion of warm fogs, since if the coalescence efficiency is lower than unity, it is difficult to understand how these clouds, for example, can grow at all. In fact some doubt has already been cast on the effectiveness of the collection mechanism process to account for the rapid growth of warm clouds even with coalescence efficiency of unity (see Bartlett, 1970). Since the results of Levin et al. (1973) indicate even lower coalescence efficiencies, it is even more difficult to explain the growth of these clouds by this mechanism.

However, their conclusions were also based on the observations of the collection and not on an independent investigation of the coalescence. They assumed that the theoretically computed collision efficiencies that had been previously proposed were correct, and from the ratio of their experimentally obtained collection efficiencies and the theoretical collision efficiencies, they computed the coalescence efficiencies

$$E_{\text{coales}} = \frac{E_{\text{collect}}}{E_{\text{collis}}} \quad (1-1)$$

Only a few reported experimental results are available in which the coalescence efficiency was independently investigated (e.g. Charles and Mason, 1960). Recently Whelpdale and List (1971) have reported results of an experiment in which coalescence on drops with  $p$  ratios of the order of 0.1 were investigated. Although the sizes they used and the  $p$  ratios apply to rain drops, their results indicate somewhat the same trends in the coalescence efficiencies as was found by Levin et al. (1973). They found that their results could be described by the equation

$$E = \frac{1}{(1 + p)^2} \quad (1-2)$$

However, since their measurements were carried out in a narrow range of  $p$  ratios and only with a few drop sizes the above equation could be considered as an extrapolation. Braizer-Smith et al (1972) investigated the separation conditions for interacting drops and the number of fragments so produced. However, their results were limited only to  $p$  ratios between 0.4 - 1 and as a result of their experimental set up, did not eliminate the flow around both interacting drops.

Our aims in this work were: (1) To experimentally extend the range of measurements carried out by Whelpdale and List (1971) to include a variety of drop sizes and drop ratios. (2) To obtain an empirical equation to describe the coalescence and partial coalescence efficiencies for use in numerical models of cloud growth, electrical development and fog dispersal. (3) To theoretically investigate some of the main forces hindering the coalescence process and mathematically describe the motion of approaching drops. The main point in this theoretical investigation is the effect of the drop deformation on the coalescence process.

## CHAPTER 2: THE COALESCENCE EXPERIMENT

### 2-1. THE EXPERIMENT

In order to separate the problem of coalescence from that of the collision we used a similar approach to that of Whelpdale and List (1971). In this experiment large drops were suspended from a small capillary tube. A small droplet generated by a drop generator, impacted the larger drop on its lower hemisphere. Viewing the interactions from two perpendicular directions permitted the identification of the angle of impact. The interactions were simultaneously photographed by a 35mm camera and by a television camera. This method of viewing was thought to be an improvement over the method used by Whelpdale and List who observed the interaction from a single direction and, hence, could have had difficulties in determining the exact impact angle. As will be shown later the impact angle is an important parameter for the coalescence and uncertainty in its determination could lead to great inaccuracies. In order to separate the collision from the coalescence problem one has to eliminate the flow around the interacting drops. This is an impossible task. However, the method used by Whelpdale and List and also used here seems to be a close approximation to it. When a small drop approaches a larger falling drop it enters the region of the boundary layer of the larger drop. Within this region the flow decreases as one approaches the drop surface. For large drops the flow does not diminish at the surface due to internal circulation in them. However, as the drops approach each other the flow between them is probably controlled by the drainage of the intervening air layer. This drainage depends on the speed of the approaching drops and their deformation. Therefore it seems that the experiment of Whelpdale

and List and the one proposed here are applicable to interaction of drops in the atmosphere, at least for small  $p$  ratios. At larger  $p$  ratios and larger drops it is possible that the leading surface of the smaller droplet enters the boundary layer while the other side is still affected by the air flow further out. In such a situation the flow will tend to move the droplet sideways and reduce the probability of coalescence. Hence for such cases the results that we obtain here can be considered as an upper limit to the coalescence efficiency.

## 2-2. THE APPARATUS

Fig. 2-1 is a schematic diagram of the experimental set up. The size of the larger collector drop was controlled by a micrometer syringe and could be varied from 200 microns to over 2.5mm in diameter. Its position in space could be changed by a micromanipulator. The smaller droplet was generated by a drop generator similar but more powerful than that of Abbott and Cannon (1972). The generator consists of an acoustic suspension speaker with a metal rod connected to the center of its cone. The other side of the rod is bent and immersed in a water bath. An electrical pulse of known amplitude and shape pushes the speaker's cone up and forces the rod out of the water and produces a droplet. The droplet size is controlled by the size of the rod, the pulse shape and its amplitude. It was constructed in such a way as to be able to eject vertically upward single small droplets. The generator was directed with a slight angle to the vertical and therefore ejected droplets in a parabolic trajectory. This trajectory prevented the droplets from falling back into the water reservoir and disturbing the next generated droplet. By positioning the large drop at different heights along the upward trajectory of the droplet different impact velocities were obtained. By horizontally varying the position of the collector drop the impact angles could be varied. Each interaction was simultaneously photographed on a 35mm film and recorded on a video tape by a television camera which was mounted at a right angle to the viewing direction of the still camera. The interaction zone was illuminated by a continuous flood light (1000w) with a water filter in front, and by a stroboscope flashing at exactly 1000 cycles per sec. The position of the flood light and the stroboscope were at  $160^\circ$  and  $180^\circ$  from the direction of observation of the 35mm camera.

Once the position of the trajectory was determined the electronic circuit was triggered. The drop generator was the first to be triggered and was followed after pre-set delays by the opening of the camera's shutter and ten flashes of the strobe. Then the camera shutter was closed automatically and the film advanced. During this whole period the television camera continuously recorded the entire event.

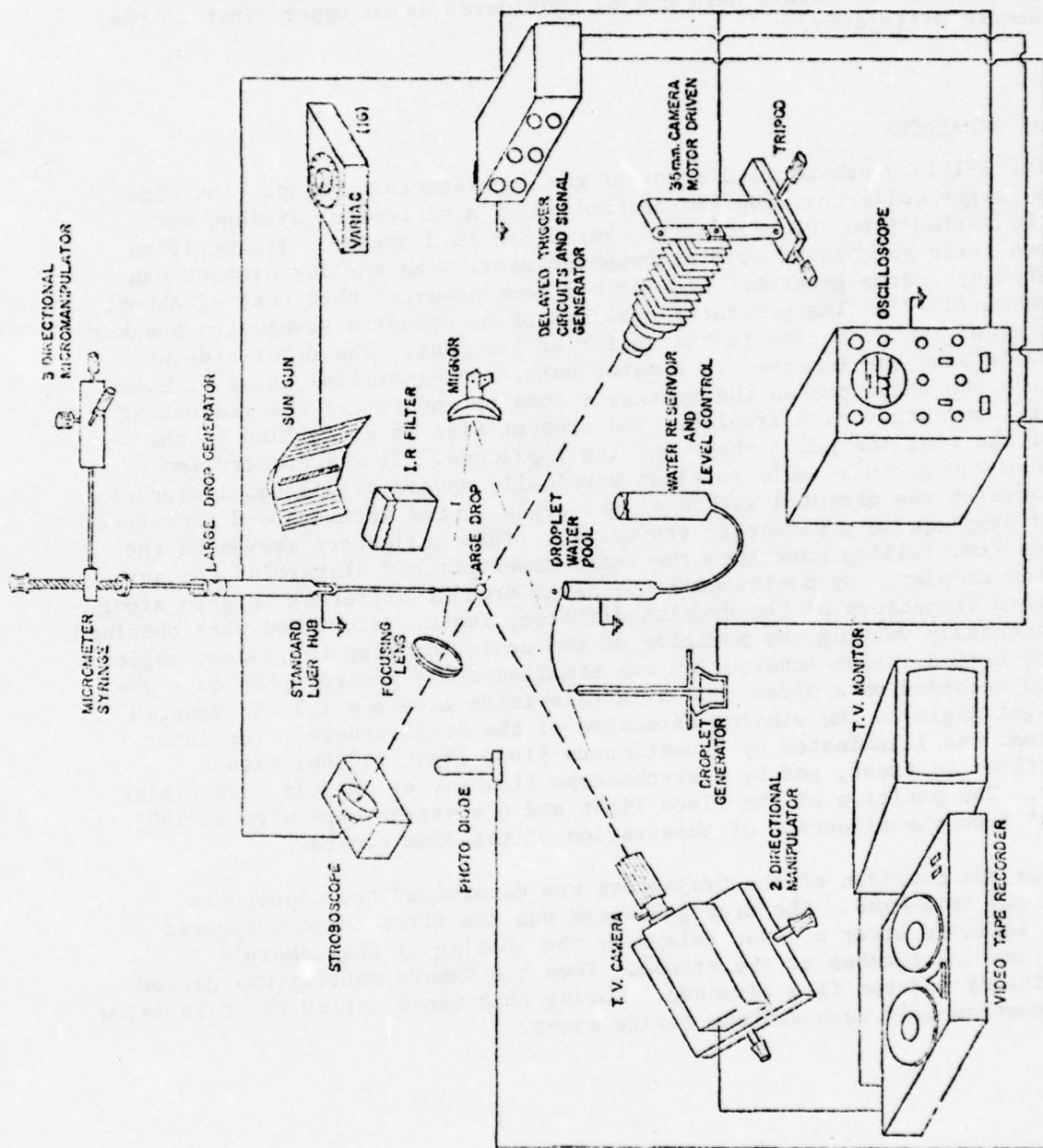


Fig. 2-1. A schematic diagram of the experimental set-up.

By adjusting the position of the impact place so that collisions would occur at precisely the vertical great circle of the collector drop and in the focal plane of the camera, the exact angle and drop size could be determined from the photographs. The impact velocity was determined from the distance between successive light spots on the film. The exact trajectory was determined from the streak produced by the droplet due to the continuous illumination by the flood light.

Both the collector drop holder and the droplet generator were grounded. This eliminated electrical charges from the collector drop but not from the droplets. However, it was estimated that the maximum charge they carried did not exceed  $10^{-5}$  esu and, hence, was believed to have little effect on the coalescence (eg. Neiburger et al, 1974).

## 2-3. RESULTS

About 8000 photographs were taken out of which over 3000 were found adequate for analysis. Collisions studied could be classified into three types: (1) those resulting in full coalescence, (2) those resulting in bouncing and (3) those resulting in partial coalescence. The difference between the first and the last two types of interactions could easily be identified from the photographs. However, the differences between the last two types was more difficult to resolve. Partial coalescence events were identified as such when the size of the outgoing droplet was smaller than its original size before impact. However, since differences of only about 20 microns in diameter could be resolved, many interaction which actually resulted in partial coalescence may have been classified as bounce. This may mean that the efficiency of partial coalescence we obtained actually represents a lower bound.

Fig. 2-2a,b and c represent interactions which resulted in coalescence, bounce, and partial coalescence respectively (details are given in the figure captions).

In order to resolve the possible effect of the impact angle and impact velocity on the coalescence and bouncing events all the results were gathered into two graphs Fig. 2-3a and 2-3b. In here no reference is made to the drop size or drop size ratio. It is observed that up to a velocity of 2.4 m/sec there is no clear dependence on the impact velocity, however, a dependence on the impact angle is observed. Coalescence occurs at angles close to head-on collision and decreases as the angle increases. The reverse is true for bouncing. However, an important conclusion can already be drawn: bouncing is observed at very low impact angles in contrast to observations by Whelpdale and List (1971).

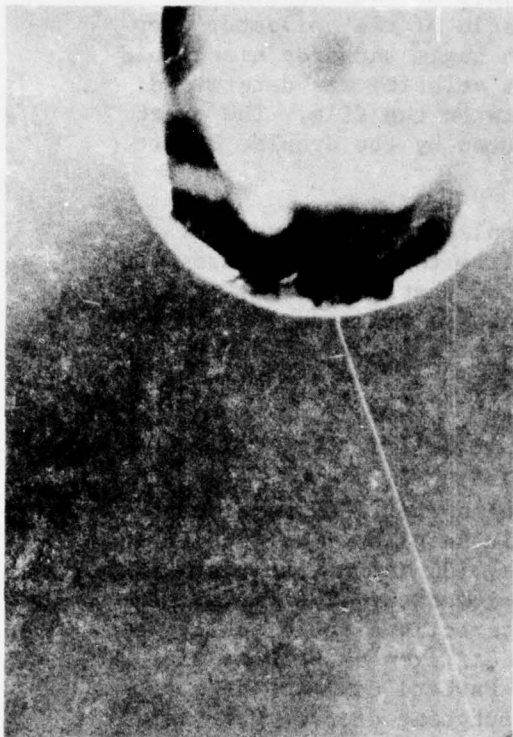


Fig. 2-2a. Coalescence event of two drops 2200 and 110 microns diameter impacting at a velocity of 1m/sec and angle of  $38^\circ$ .

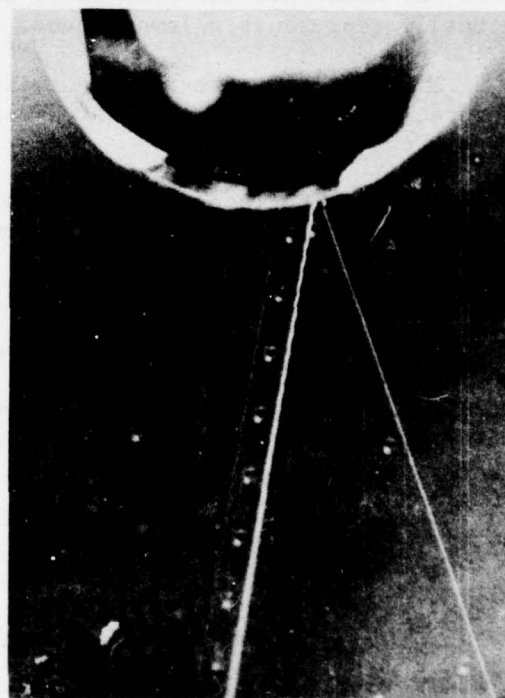


Fig. 2-2b. A bouncing of two drops 2180 and 130 microns diameter impacting at a velocity of 1.0m/sec and an angle of  $8^\circ$ .



Fig. 2-2c. A partial coalescence event when drops of 2160 and 120 microns diameter impact at a velocity of 0.5m/sec and an angle of  $29^\circ$ . After separation the smaller droplet has a diameter of 80 microns and a velocity of 0.34m/sec.

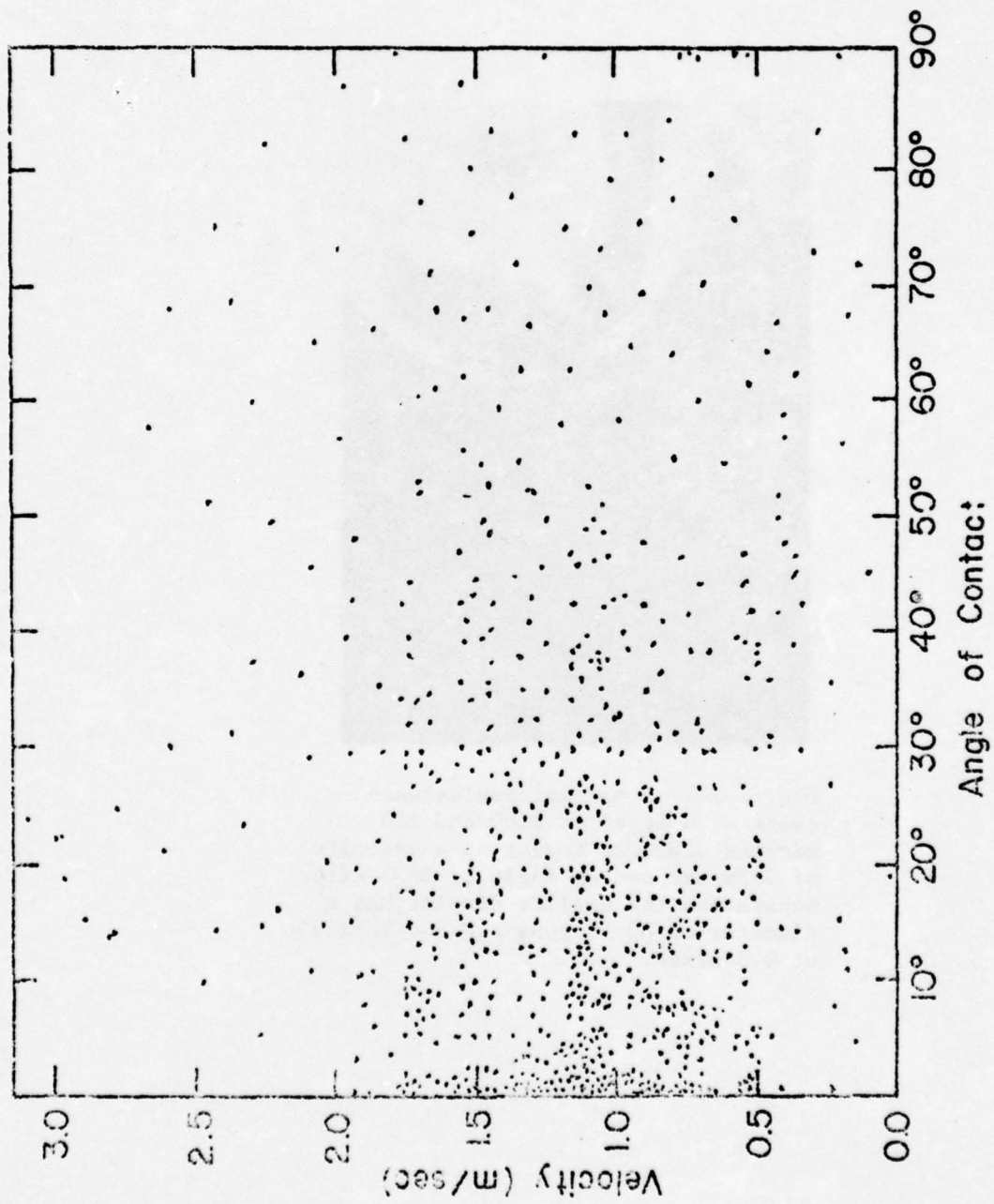


Fig. 2-3a. Experimental observation of coalescence as a function of Velocity and angle of contact.

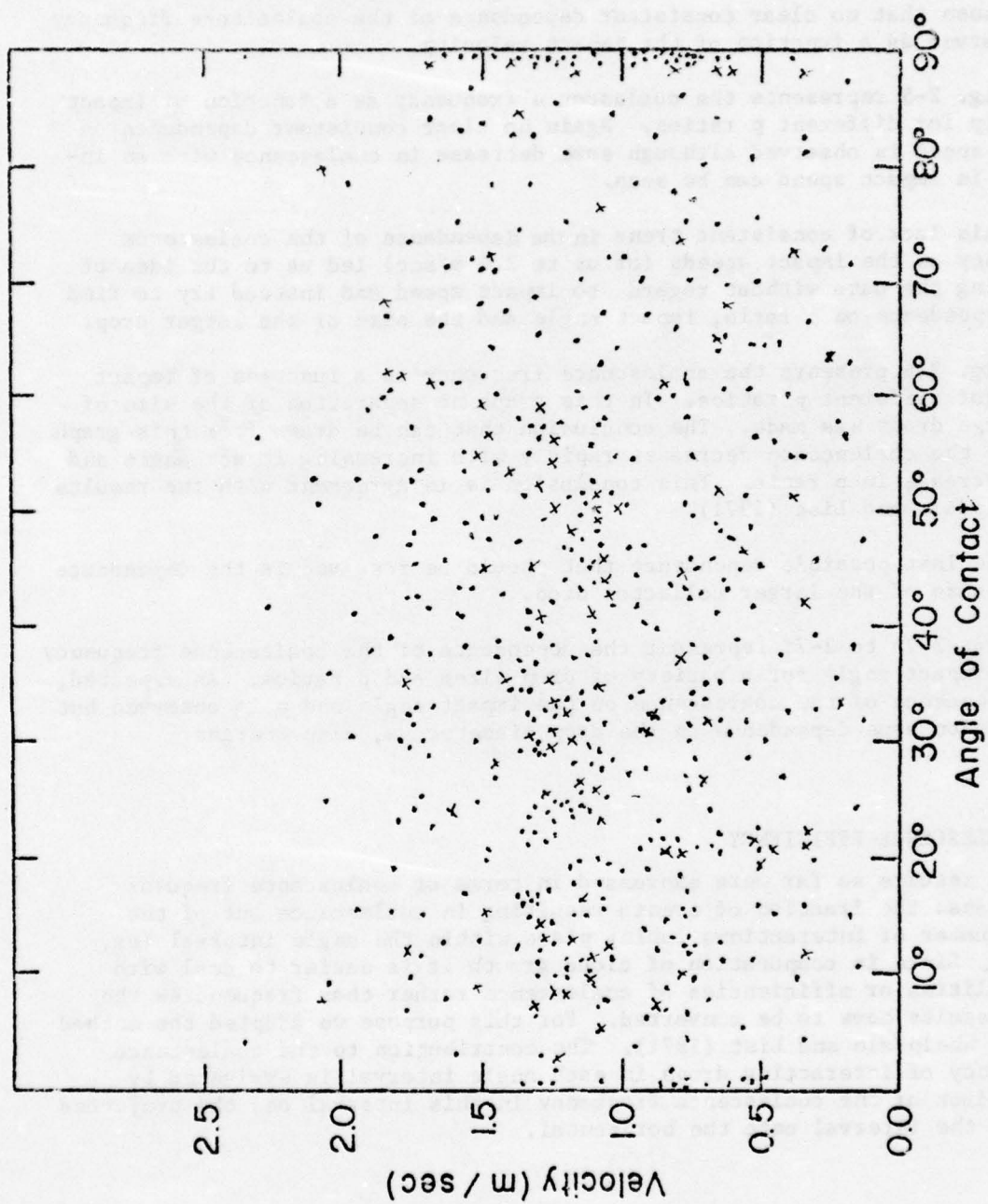


Fig.2-3b. Experimental observation of bouncing (•) and partial coalescence (x) as a function of velocity and angle of contact.

It is important to check the dependence of the coalescence frequency on the impact angle. Fig. 2-4 represents the coalescence frequency as a function of impact angle for four equal angle intervals between  $0^{\circ}$ - $90^{\circ}$ . It is seen that no clear consistent dependence of the coalescence frequency is observed as a function of the impact velocity.

Fig. 2-5 represents the coalescence frequency as a function of impact velocity for different p ratios. Again no clear consistent dependence on impact speed is observed although some decrease in coalescence with an increase in impact speed can be seen.

This lack of consistent trend in the dependence of the coalescence frequency on the impact speeds (of up to 2.4 m/sec) led us to the idea of gathering the data without regard to impact speed and instead try to find some dependence on p ratio, impact angle and the size of the larger drop.

Fig. 2-6 presents the coalescence frequency as a function of impact angle for different p ratios. In this graph no separation of the size of the large drops was made. The conclusion that can be drawn from this graph is that the coalescence decreases rapidly with increasing impact angle and with increase in p ratio. This conclusion is in agreement with the results of Whelpdale and List (1971).

The last possible dependence that should be resolved is the dependence on the size of the larger collector drop.

Figs. 2-7a to 2-7f represent the dependence of the coalescence frequency on the impact angle for a variety of drop sizes and p ratios. As expected, the dependence of the coalescence on the impact angle and p is observed but in addition some dependence on the drop diameter,  $a$ , also emerges.

#### 2-4. COALESCENCE EFFICIENCY

The results so far were expressed in terms of coalescence frequency. This means: the fraction of events resulting in coalescence out of the total number of interactions taking place within the angle interval (eg.  $0$ - $22.5$ ). Since in computation of cloud growth it is easier to deal with probabilities or efficiencies of coalescence rather than frequencies the above results have to be converted. For this purpose we adapted the method used by Whelpdale and List (1971). The contribution to the coalescence efficiency of interacting drops in each angle interval is evaluated by the product of the coalescence frequency in this interval and the projected area of the interval onto the horizontal.

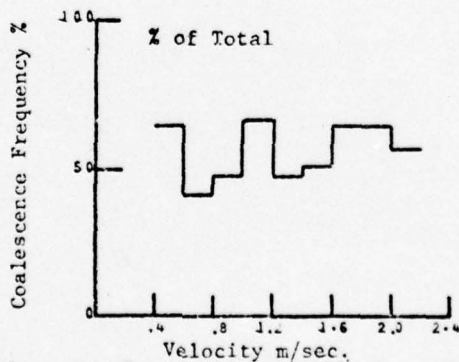
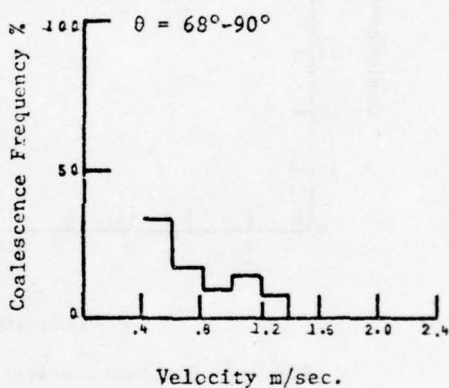
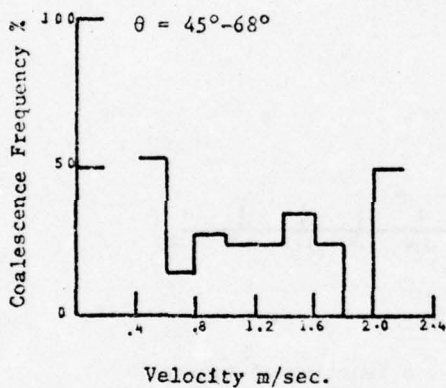
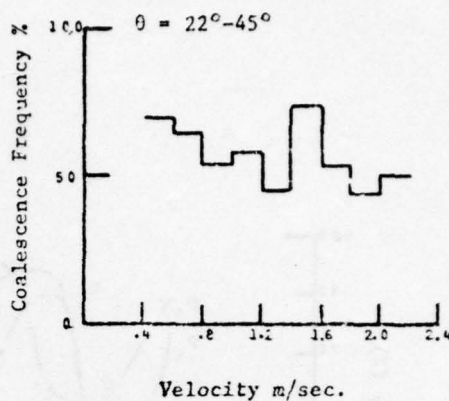
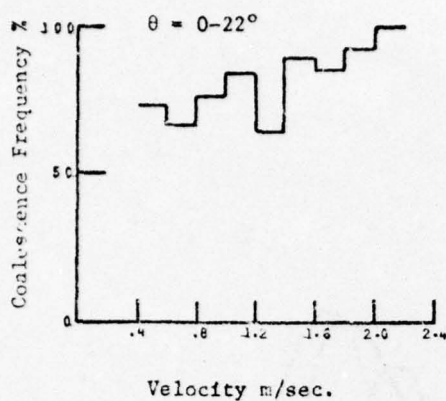


Fig. 2-4. % of coalescence frequency for different velocities (m/sec.) of small droplets for Various Contact angles.

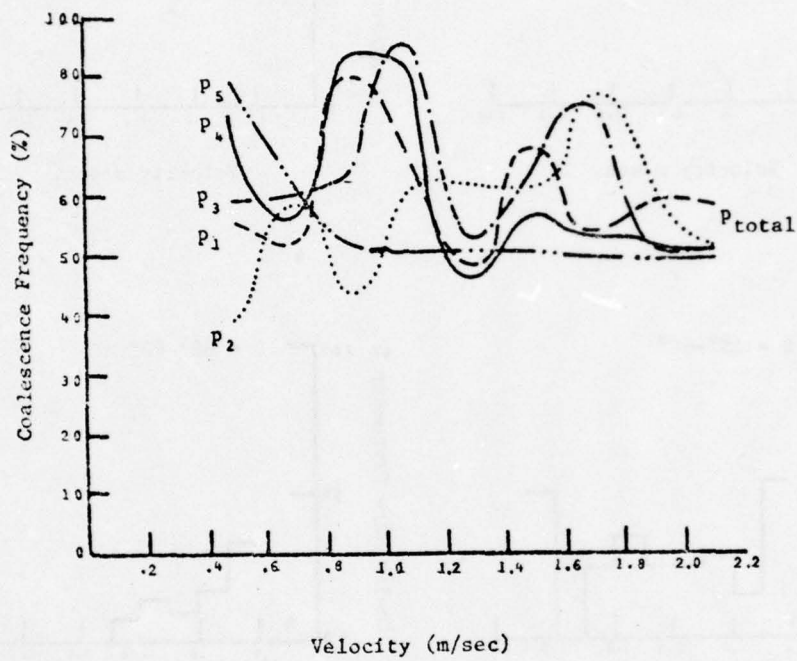


Fig. 2-5. Coalescence frequency as a function of impact speed for different  $p$  ratios.

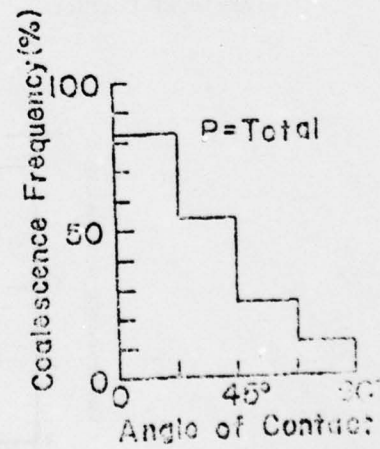
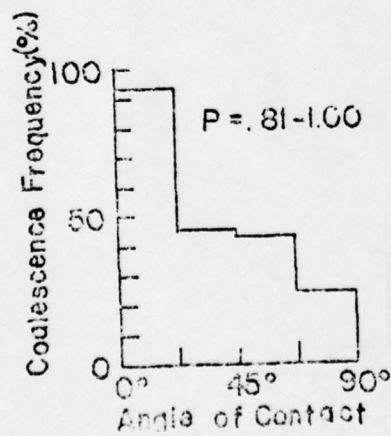
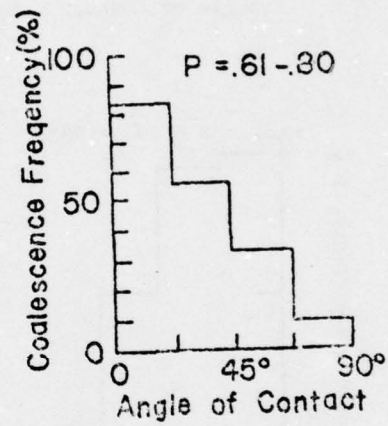
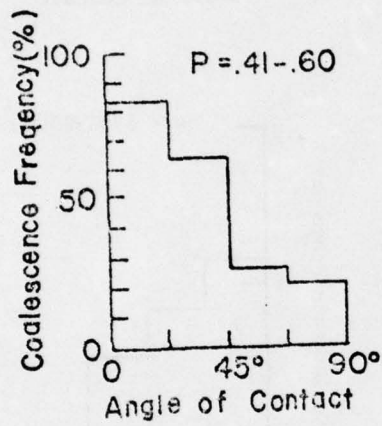
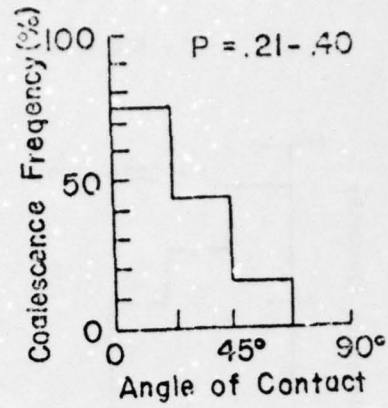
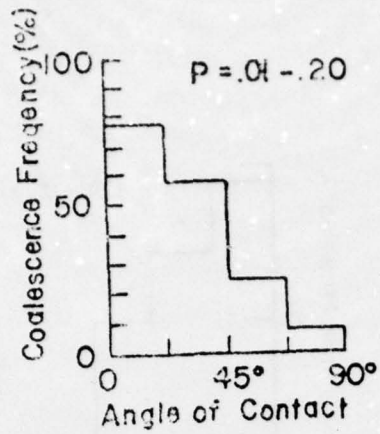


Fig. 2-6. Codealcescence frequency as a function of impact angle for different  $p$  ratios.

$P = 0.01-0.10$

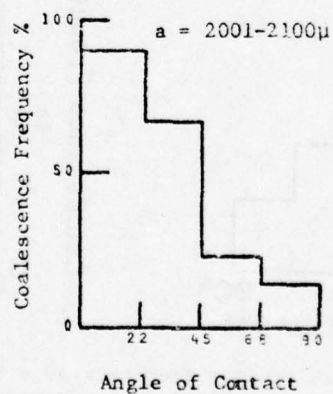
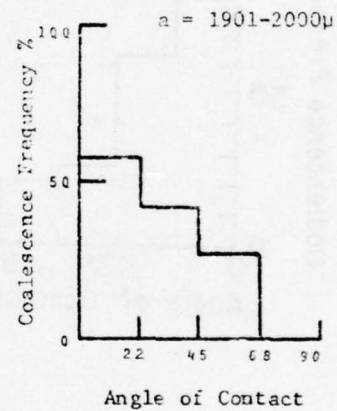
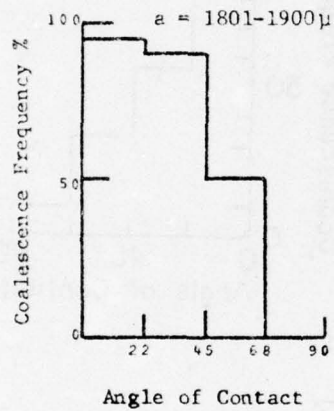
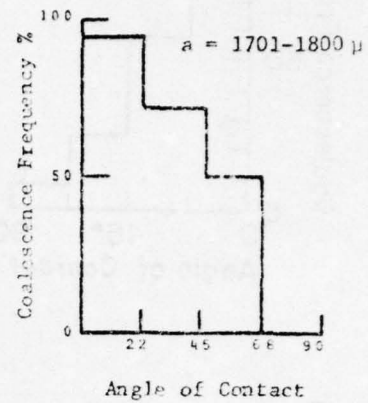
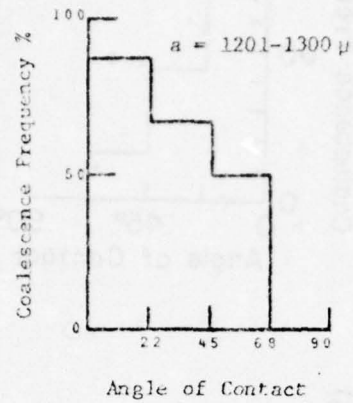


Fig. 2-7a. The dependence of the coalescence frequency on the impact angle for a variety of drop sizes and  $p$  ratios.

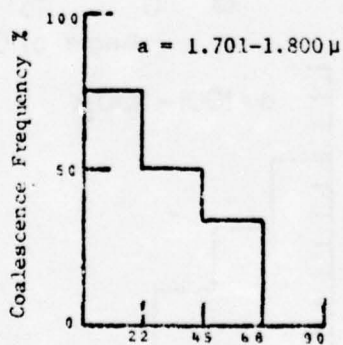
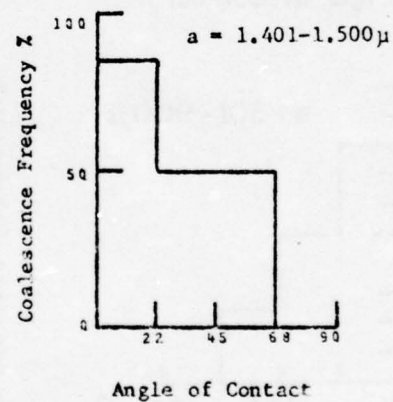
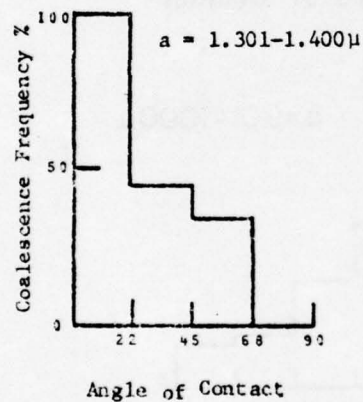
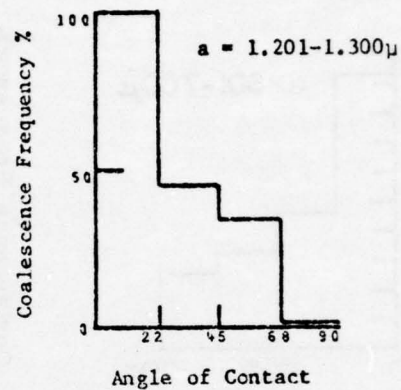
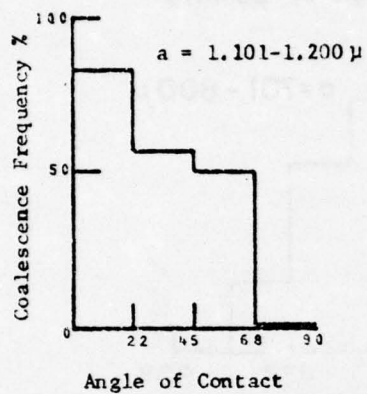
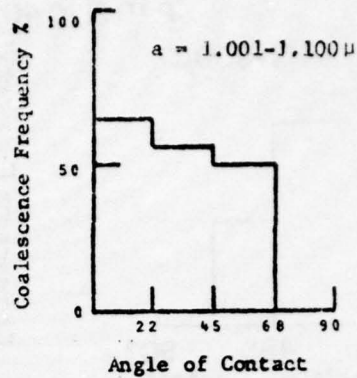
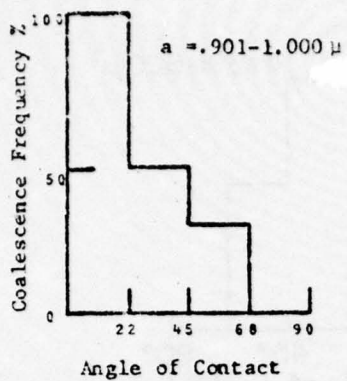


Fig. 2-7b. The dependence of the coalescence frequency on the impact angle for a variety of drop sizes and p ratios.

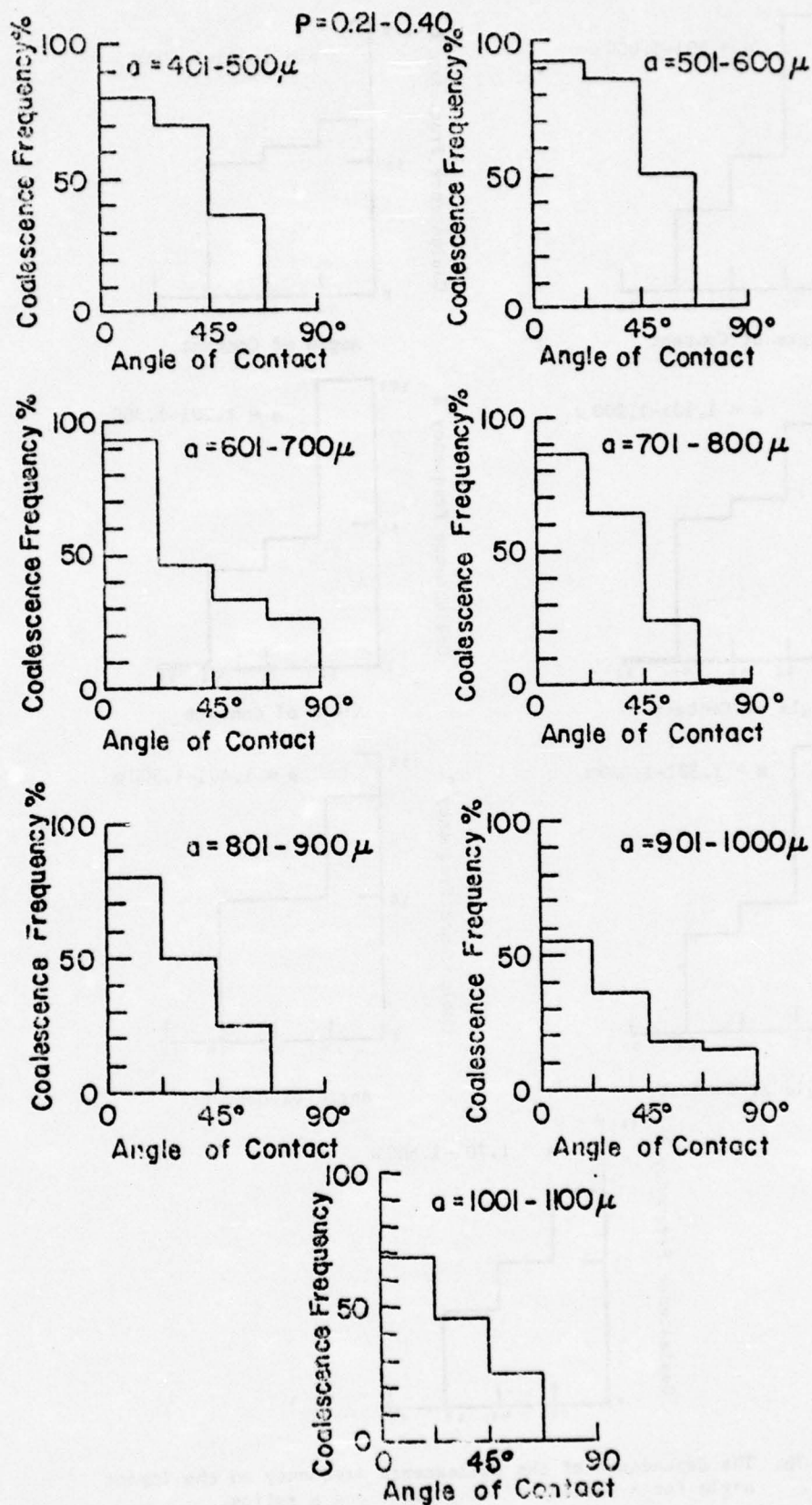
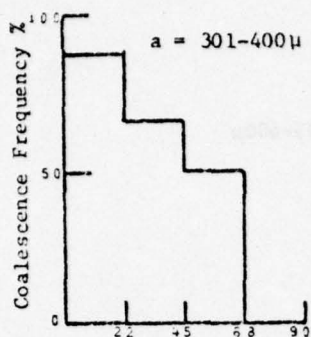
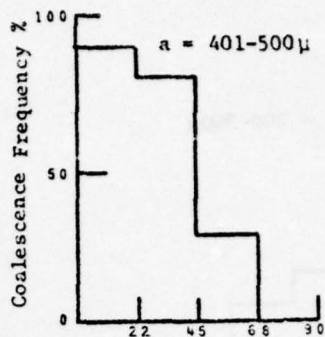


Fig. 2-7c. The dependence of the coalescence frequency on the impact angle for a variety of drop sizes and  $p$  ratios.

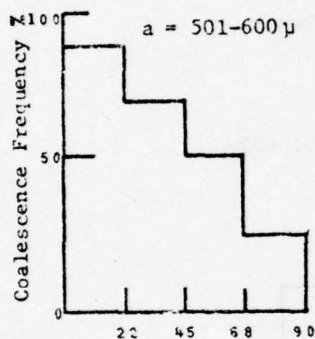
$P = 0.41-0.60$



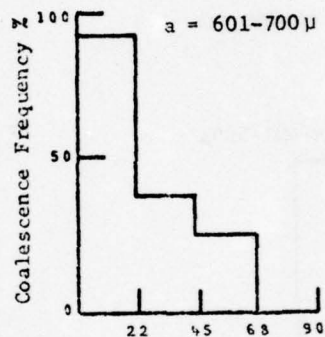
Angle of Contact



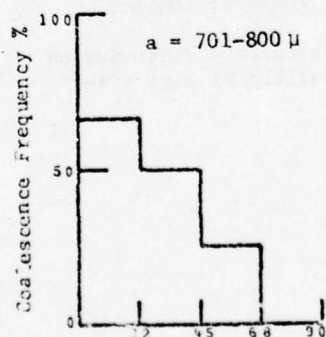
Angle of Contact



Angle of Contact



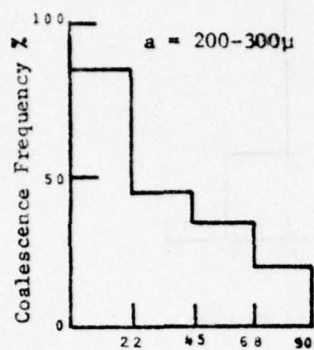
Angle of Contact



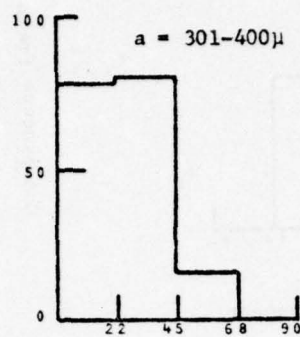
Angle of Contact

Fig. 2-7d. The dependence of the coalescence frequency on the impact angle for a variety of drop sizes and  $p$  ratios.

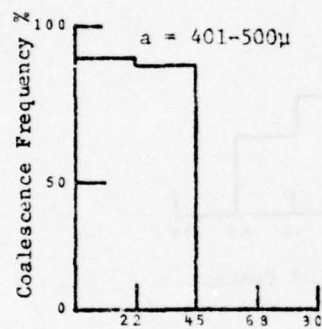
$P = 0.61-0.80$



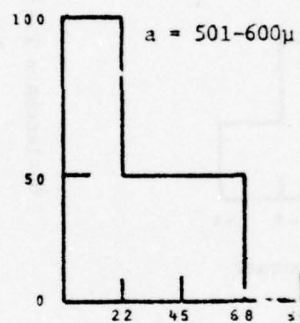
Angle of Contact



Angle of Contact



Angle of Contact



Angle of Contact

Fig. 2-7e. The dependence of the coalescence frequency on the impact angle for a variety of drop sizes and  $p$  ratios.

$P = 0.81-1.00$

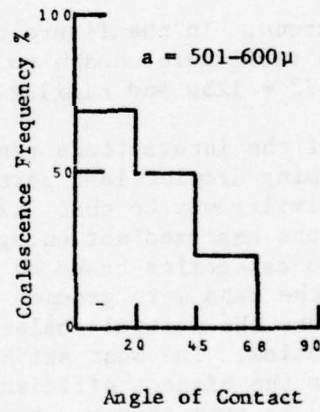
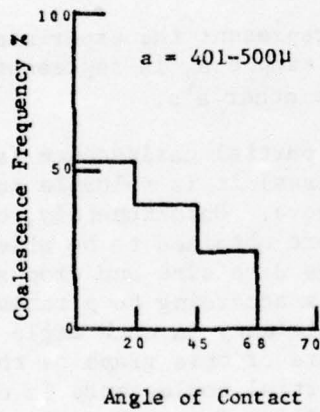
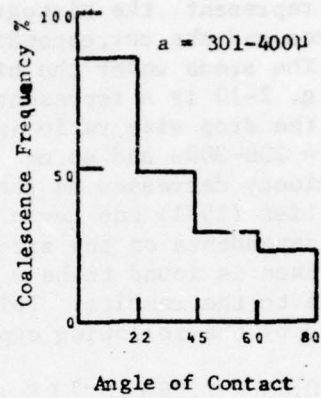
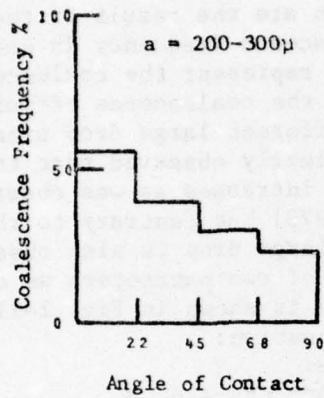


Fig. 2-7f. The dependence of the coalescence frequency on the impact angle for a variety of drop sizes and  $p$  ratios.

The projected area can be expressed as:

$$A = \pi R^2 [\sin^2 \theta_B - \sin^2 \theta_A]$$

where  $\theta_A$  and  $\theta_B$  are shown in Fig. 2-8 and R is the radius of the collector drop.

Figs. 2-9a-f represent the histograms which are the result of the product of the area and the corresponding coalescence frequency in each angle interval. The areas under the histograms represent the coalescence efficiencies. Fig. 2-10 is a representation of the coalescence efficiency as a function of the drop size ratio (p) for different large drop sizes. In the figure  $a_2 = 200-300\mu$  and so on. It is clearly observed that the coalescence efficiency decreases as the p ratio increases as was observed by Whelpdale and List (1971) and Levin et al (1973) but contrary to their results a strong dependence on the size of the large drop is also observed. Since the coalescence is found to be a function of two parameters we obtained a best fit surface to the results. This surface is shown in Fig. 2-11 and can be represented by the following empirical equation:

$$E = 0.65 - 2.08 \times 10^{-3} RR + 6.56 \times 10^{-4} p^2 R + 6.07 \times 10^{-7} p R^2 + 1.17 \times 10^{-2} p^2 - 9.3 \times 10^{-8} R^2 \quad (2-1)$$

where R is in microns. In the figure the dots represent the experimental values. The mean radii were chosen so that for exaple  $a_2$  is represented by a point at  $r = a_2/2 = 125\mu$  and similarly for the other  $a_i$ 's.

Since many of the interactions resulted in partial coalescence (events in which the incoming droplet lost part of its mass) it is valuable to analyze these data in a similar way to that discussed above. Unfortunately, out of the many photographs analyzed not enough data were obtained to be able and separate them into categories based on both large drop size and drop size ratio. Instead, the data were grouped in classes according to p ratios only. Fig. 2-12 represents the partial coalescence efficiency in each angle interval for different p ratios. The most striking feature of this graph is the fact that in most cases the highest efficiency for partial coalescence is observed between  $45^\circ$  and  $67.5^\circ$  even though a small probability for such occurances is found at other impact angles. The equation of best fit to this data can be expressed empirically by:

$$E_{\text{partial coalesce}} = 0.22 - 0.23p - 0.025p^2 \quad (2-2)$$

and Fig. 2-13 represents it in a graphical form.

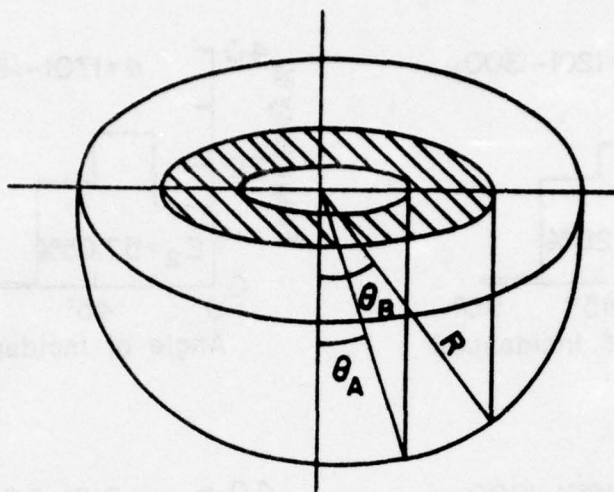


Fig. 2-8. The projected cross sectional area seen by the impacting droplets of a certain angle interval.

$P = 0.01 - 0.10$

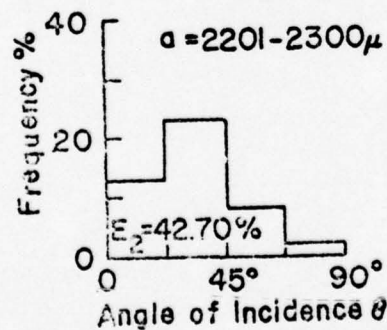
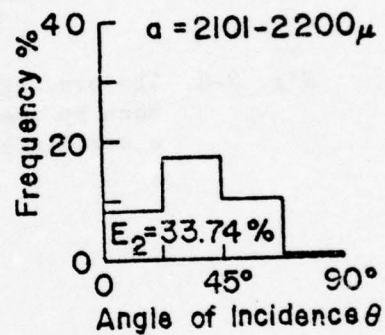
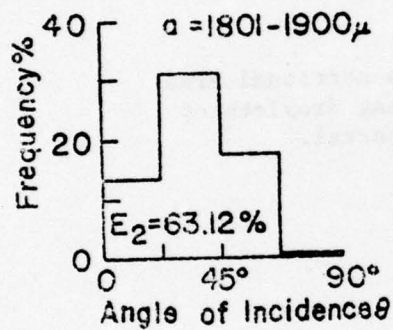
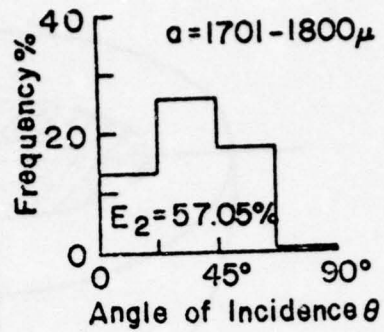
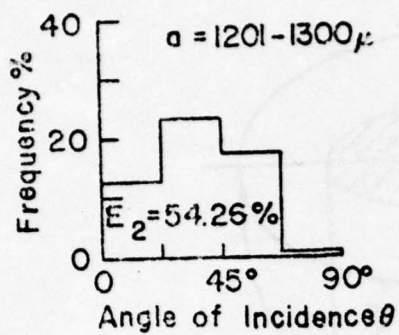


Fig. 2-9a. Coalescence efficiencies as a function of impact angle for different  $p$  ratios and sizes of large drops.

$P_1 = 0.11-0.20$

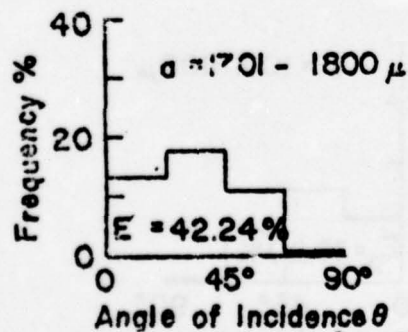
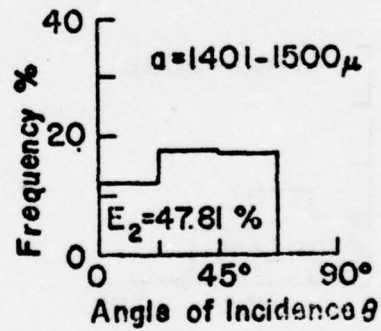
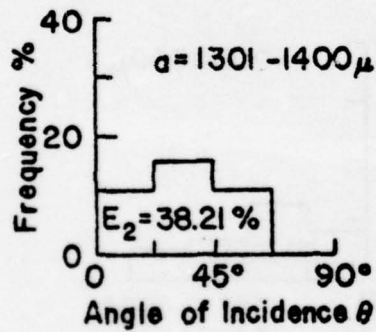
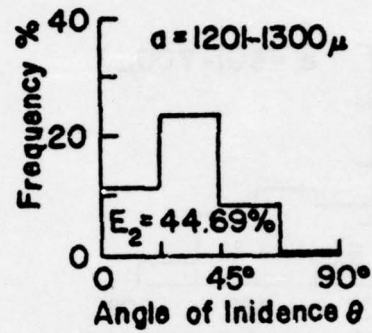
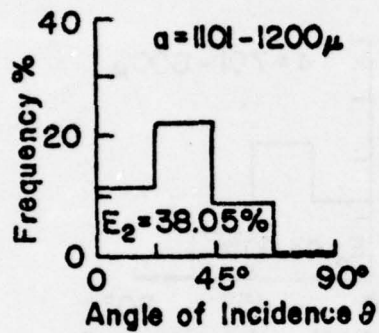
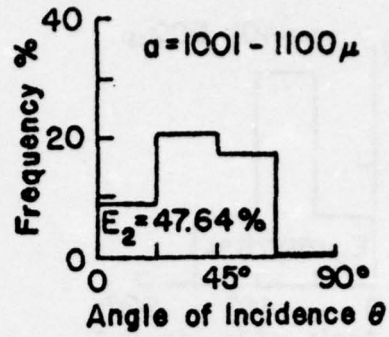
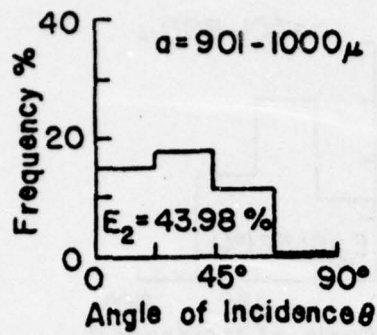


Fig. 2-9b. Coalescence efficiencies as a function of Impact angle for different  $p$  ratios and sizes of large drops.

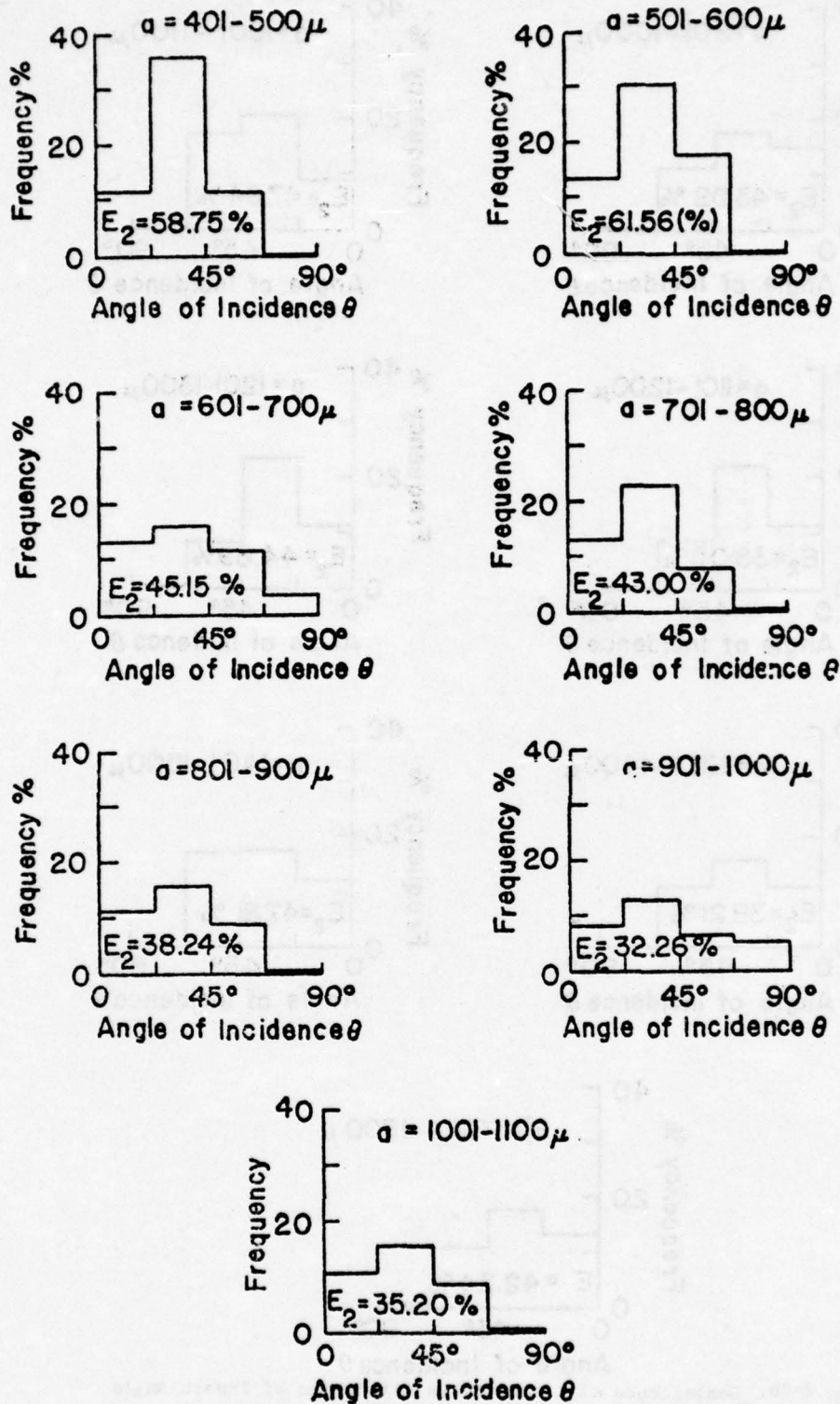


Fig. 2-9c, Coalescence efficiencies as a function of impact angle for different  $p$  ratios and sizes of large drops.

$P = 0.41 - 0.60$

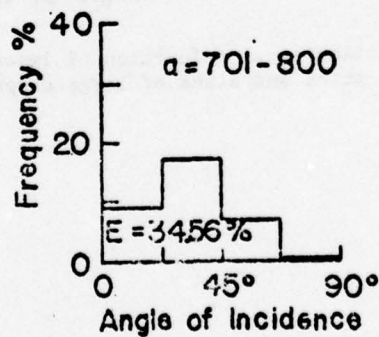
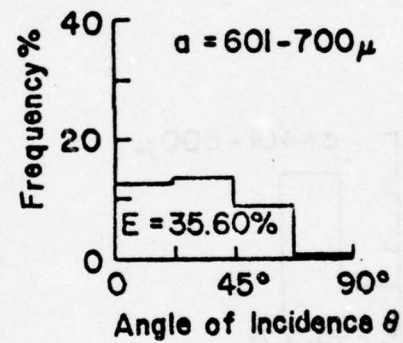
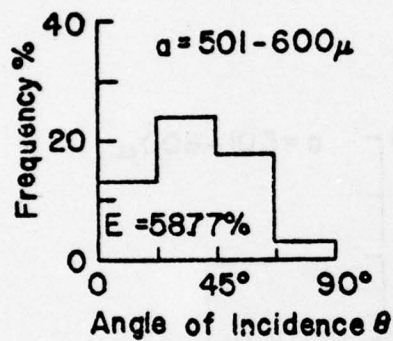
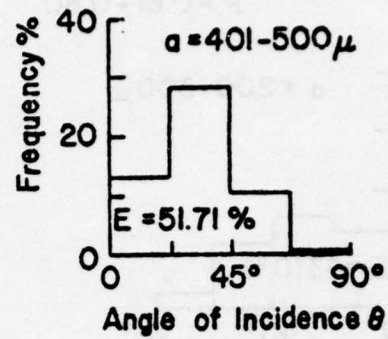
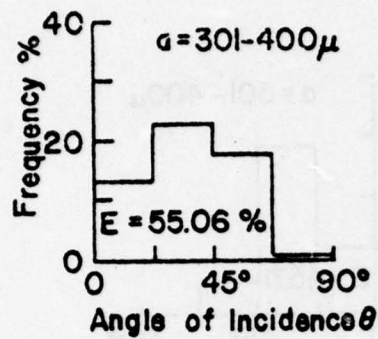


Fig. 2-9d, Coalescence efficiencies as a function of impact angle for different  $p$  ratios and sizes of large drops.

$p = 0.61 - 0.80$

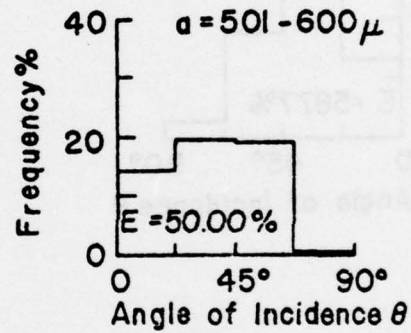
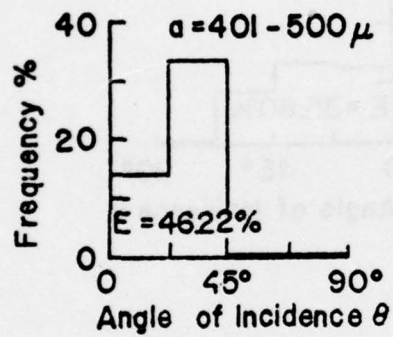
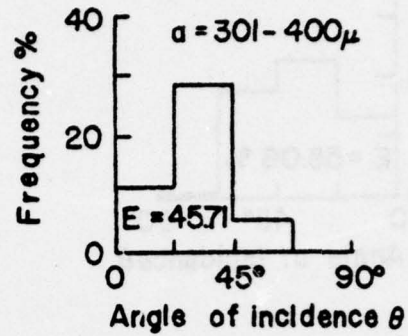
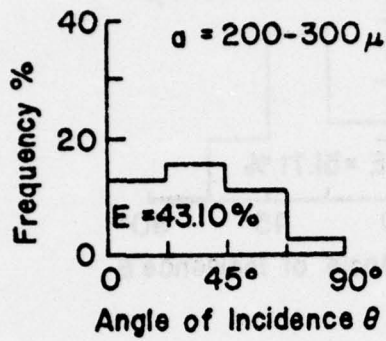


Fig. 2-9e. Coalescence efficiencies as a function of impact angle for different  $p$  ratios and sizes of large drops.

$p = 0.81 - 1.00$

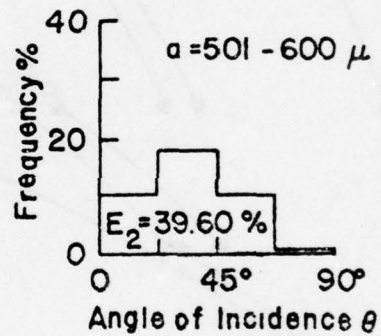
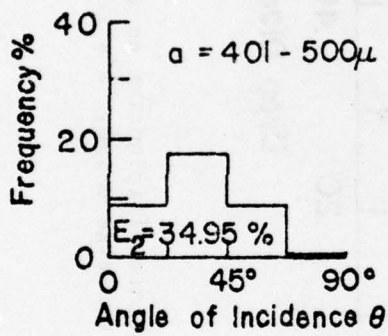
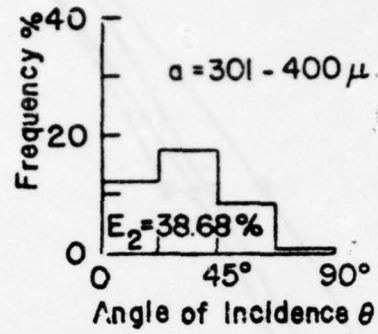
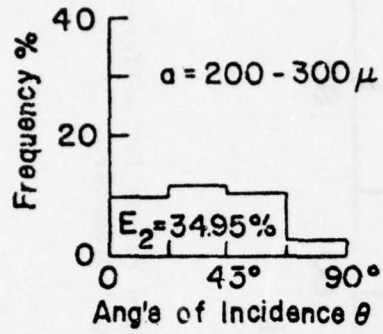


Fig.2-9f. Coalescence efficiencies as a function of impact angle for different  $p$  ratios and sizes of large drops.

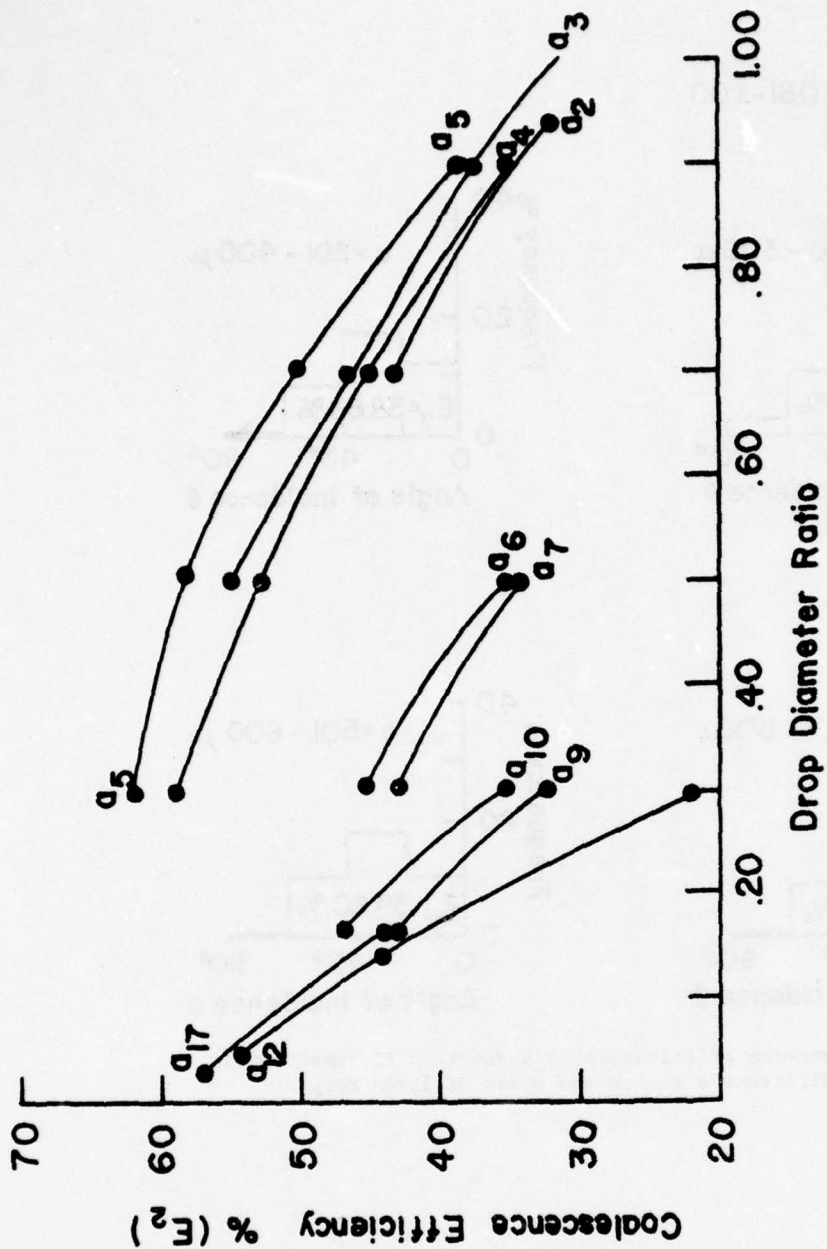


Fig. 2-10. Coalescence efficiencies as a function of p ratios for different sizes of large drops.  $a$ 's represent drops' diameter.

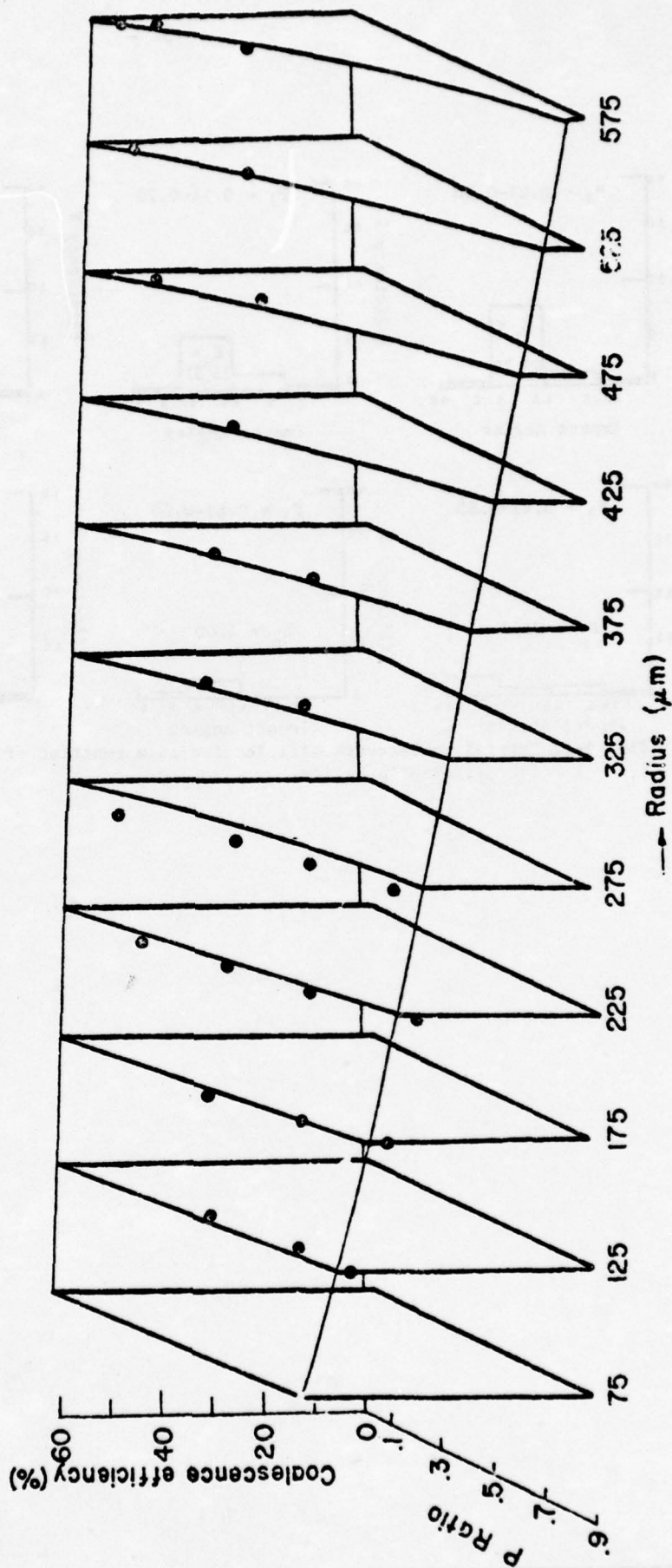


Fig. 2-11. A three dimensional representation of the coalescence efficiency as a function of p ratio and size of large drops. Dots represent experimental results.

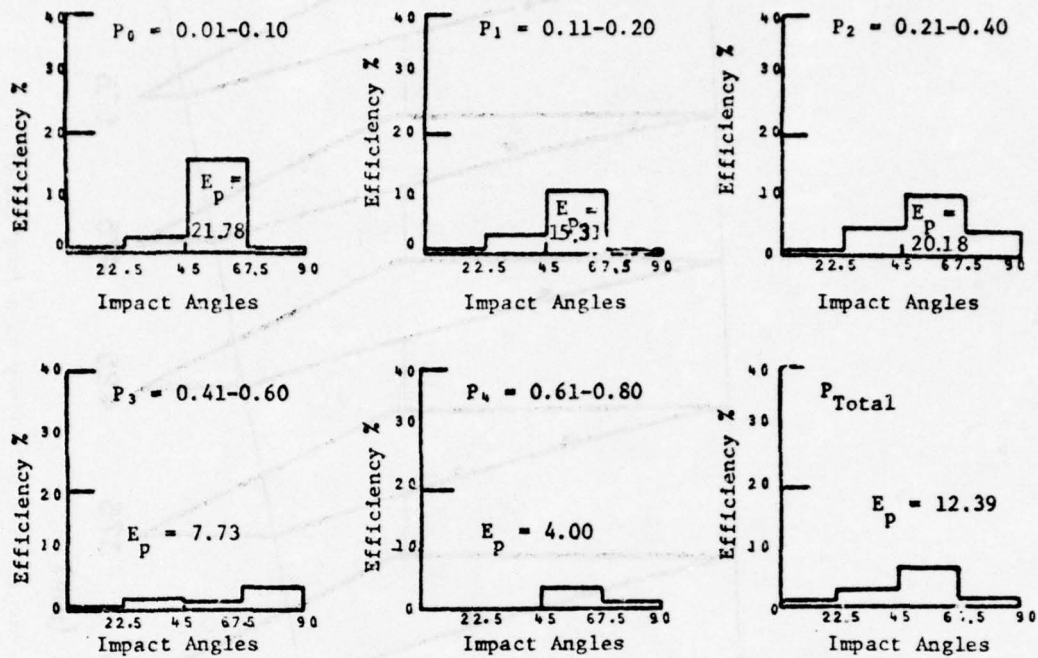


Fig. 2-12 Partial coalescence efficiencies as a function of impact angle for different  $p$  ratios.

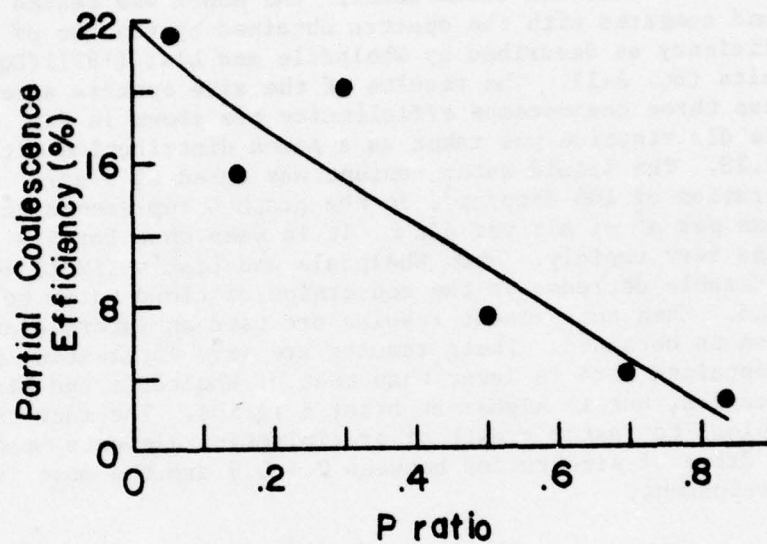


Fig. 2-13. Partial coalescence efficiency versus p Ratios. Dots represents experimental results and the curve is represented by Eq. 2-2.

## 2-5. THE EFFECTS ON THE DEVELOPMENT OF THE RAIN DROP SPECTRA

The above results are somewhat different than those found in the literature primarily due to their dependence on both radius and size ratio.

It is therefore important at this time to determine the effect such a difference can have on the development of rain in a cloud. For this purpose we used the stochastic numerical model of Scott and Levin (1975). This model treats the development of the drop spectra with 57 size classes as a function of time in an infinite cloud model. The model was tested with  $E_{\text{coalesce}} = 1$  and compared with the spectra obtained by the use of the coalescence efficiency as described by Whelpdale and List (1971) (Eq. 1-2) and by our results (Eq. 2-1). The results of the size spectra after 600 seconds for these three coalescence efficiencies are shown in Fig. 2-14. The initial size distribution was taken as a gamma distribution with radius dispersion of 0.28. The liquid water content was taken as  $3 \text{ gr/m}^3$  and initial concentration of  $100 \text{ drop/cm}^3$ . In the graph G represents the mass of water in grams per  $\text{m}^3$  of air per  $\Delta \ln r$ . It is seen that for  $E = 1$  the spectrum develops very rapidly. When Whelpdale and List's (1971) equation is used a considerable decrease in the conversion of cloud water to rain water is observed. When the present results are used an intermediate rate of autoconversion is obtained. These results are very interesting since the efficiency obtained here is lower than that of Whelpdale and List at least at low p ratios, but is higher at other p ratios. The fact that the present results lead to faster growth of precipitation elements means that interactions of drops of size ratios between 0.5-0.9 are the most important for the rain development.

## CHAPTER 3: THEORETICAL CONSIDERATIONS

### 3-1. INTRODUCTION

Unfortunately there is no theoretical explanation to the problem of coalescence. From the previous work in the literature and from our work described in Chapter 2 some general features are observed. These can be classified into effects or forces hindering coalescence and those that aid coalescence. In the following few pages we will discuss these effects or forces in order to justify some of the assumptions which will be made in the theoretical treatment that follows.

#### a. Effects that hinder coalescence

##### i. The air gap

If two rigid spheres were to approach each other the intervening air between them has no difficulty in escaping and clearing

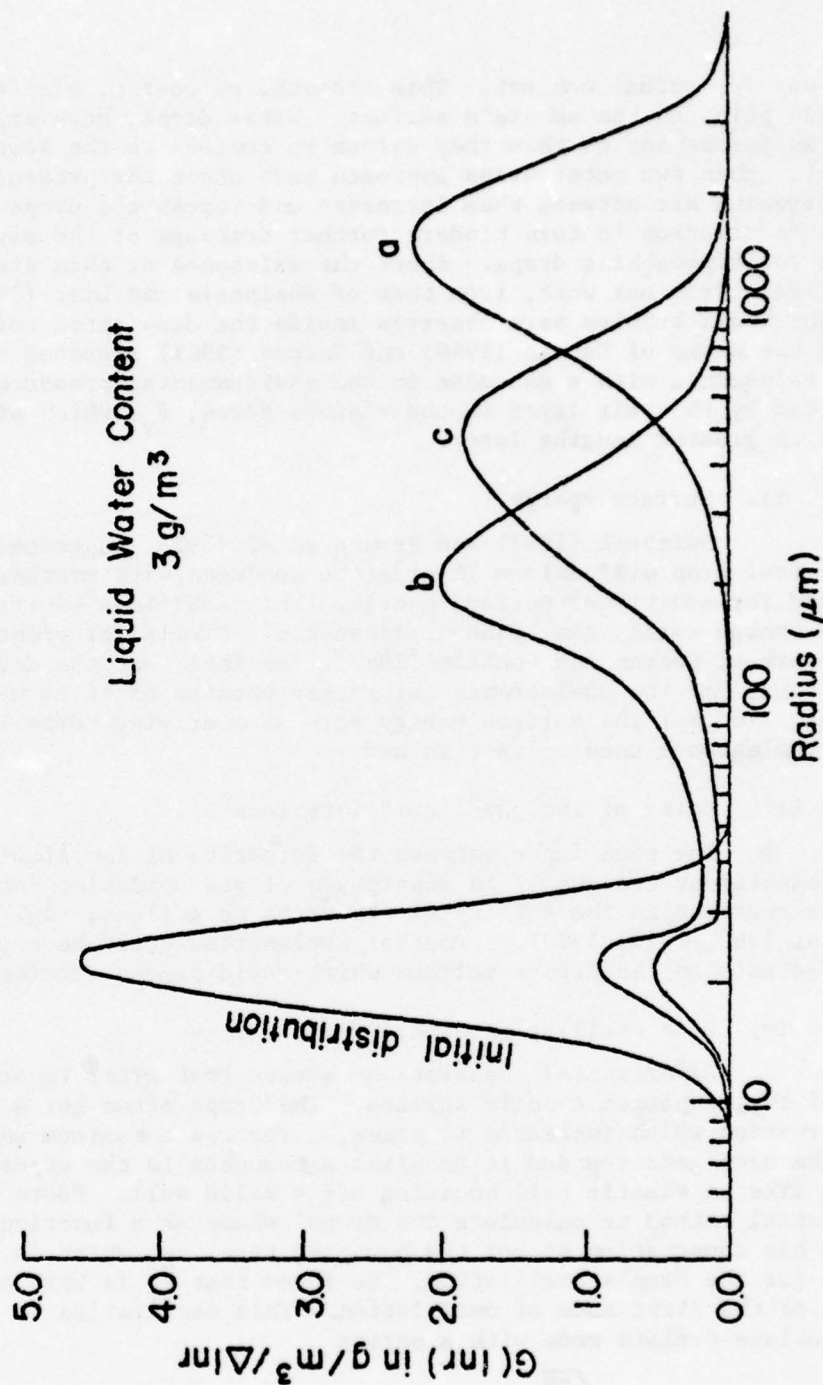


Fig. 2-14. The drop size spectra after 600 seconds for different  $E$  coalescence rates. (a)  $E = 1$ , (b)  $E$  as described by Eq. 2-2 and (c)  $E$  as described by Eq. 2-1.

the way for actual contact. This contact, of course, will occur at a single point on the sphere's surface. Water drops, however, are not rigid and as forces act on them they deform to conform to the lowest energy level. When two water drops approach each other the pressure in the intervening air between them increases and forces the drops to deform. This deformation in turn hinders further drainage of the air and slows down the approaching drops. About the existence of this air layer one can learn from our work, from that of Whelpdale and List (1971) and others in which air bubbles were observed inside the drop after coalescence. Also the works of Canals (1960) and Selman (1961) reported an increase in coalescence with a decrease in the environmental pressure. The force exerted by this air layer is the viscous force,  $F_v$ , which will be dealt with in greater lengths later.

ii. Surface energy

Swinbank (1947) and Browne et al (1954) suggested that if a spherical drop will deform in order to coalesce with another, there is a need for additional surface energy. This additional surface energy, even though small, can hinder coalescence. Similar arguments appear in the work of Cotton and Gokhale (1967). We feel that the deformation does not occur for the coalescence but rather because of it as will be seen later. In fact the surface energy acts as a driving force in completing the coalescence once contact is made.

iii. Aging of the gas-liquid interface

The time lapse between the formation of the liquid surface and the experiment can result in adsorption of gas molecules into the surface and a decrease in the ability of the drops to coalesce (eg. Charles and Mason, 1960, Park, 1970). Another explanation could be the presence of surfactants on the drop's surface which could prevent coalescence.

iv. Drop oscillation after impact

Experimental observations showed that after impact drops behave as if they impacted a solid surface. The drops often get a disk like deformation which increases in sizes, reaches a maximum and then decreases. As the drop gets rounded it acquires a momentum in the opposite direction, just like an elastic ball bouncing off a solid wall. Foote (1975) used a numerical method to calculate the drops' shape as a function of time. From his computation he got the bouncing time,  $t_B$ , which is the characteristic time for the drop's oscillation. He found that  $t_B$  is very similar to the time of the first mode of oscillation. This oscillation is referred to as the oblate-prolate mode with a period

$$\tau_R = \pi \sqrt{\frac{\rho R}{2\sigma}} \quad (3-1)$$

where  $\sigma$  is the surface tension,  $R$  is the radius of the drop and  $\rho$  its density. It therefore means that after  $\tau_R$  from the initial point of collision if no coalescence occurs the drops will move apart. In other words according to Foote the impact can be divided into two processes. The first is the impact with the solid like air layer and the second is the drainage of the air film. This drainage competes with the oscillation of the drops. If the drainage is faster than  $\tau_R$ , coalescence will occur. Otherwise a bounce will result.

v. The electrical double layer

Due to the polar nature of the water molecules they tend to arrange themselves at the water - air interface with their oxygen atoms pointing outward. This arrangement creates an electrical double layer at the interface which acts as a negatively charged surface at small distances. Hence when two drops approach each other the electrical double layers on both surfaces repulse each other. This force might be important at very small distances of separation and will be discussed later on.

b. Effects that assist coalescence

i. Electrical effects

Many investigators reported on the effects of electrical charges and electric fields on the coalescence of drops. Most find that below a certain charge, bouncing occurs as if no charge was present. However, when the charge exceeds about  $10^{-3}$  esu the coalescence and partial coalescence probabilities increase (e.g. Jayaratne and Mason, 1964, Telford and Thorndike, 1961, Wheldpale and List, 1971 and others).

Electrical forces can affect coalescence in the following ways: (1) Decrease the deformation and so decrease the viscous force,  $F_v$ . (2) Increase (or decrease) the attractive forces. (3) Cause elongation of the close surfaces and thereby increase the probability for initial contact.

ii. Oscillations on the deformed surfaces

If waves or disturbances exist on the approaching deformed surfaces they can assist in the coalescence process by decreasing the distance of separation. If peaks of such waves are opposite each other they can actually start the coalescence process even though the average separation distance is large. In other words the minimum distance of separation is the determining factor in the coalescence and not the average distance.

iii. Internal circulation

As the drops fall in free fall in the atmosphere an internal circulation within them is developed as a result of the stresses exerted on their surfaces by the air flow. This internal circulation enhances the drainage of the air film between the drops due to the fact that the air velocity at the air-water interface within this region does not vanish. Foote (1975) has shown that coalescence between two equal size large drops occurred only when internal circulation was included.

iv. Van der Waals force

This attractive force could act between the approaching drops at very small separation distances. However, calculations show that for distances larger than  $0.1\mu$  it could be neglected (Whelpdale and List, 1971).

c. The shape of the deformation and its size

In our previous discussion we mentioned that the deformation of the approaching surfaces resembles two parallel disks. This is, of course, an approximation. Allan et al (1961), Lindblad (1964) and others have observed a dimple like deformation. Burrill and Woods (1969) have observed two such dimples. Attempts to describe this deformation as a function of time were also made (e.g. Burrill and Woods, 1969). Charles and Mason (1960) developed an equation for the viscous force under any symmetric deformation.

Despite all these attempts to describe the forces under different deformations, the most commonly used is the disk like deformation (e.g. Plumlee, 1964, Foote 1975). The justification for the flat deformation is based on the facts that some experimental observations can be explained by this assumption (MacKay and Mason, 1963) and some theoretical analysis (Frankel and Mysels, 1961) show agreement to within 2% with experiments when this assumption is used. In the present work the disk-like deformation is assumed especially for the computations of the viscous force,  $F_v$ .

In addition to the shape of the deformation, its size is also of great importance. Derjaguin and Kussakov (1939) suggested that the radius of deformation is proportional to the square of the radius of the drop itself and is a constant throughout the interaction. However, their results only apply to slowly moving drops.

At higher velocities the deformation is a function of time as was shown by Plumlee (1964) and by Foote (1975).

In the present work we used two models to describe the deformation. One in which the deformation is constant during the interaction and the other where it increases as the separation distance decreases.

d. The coalescence distance

The coalescence distance is defined as the observed minimum distance between the drops' surfaces before coalescence occurs. Observations of the coalescence distance are very difficult to obtain. Lindbald (1964) observed it to be less than  $1450 \text{ \AA}$  while Allan et al (1961) reported that the coalescence distance was about  $900 \text{ \AA}$ . Whelpdale and List (1971) obtained by energy consideration a coalescence distance of between  $0.1\text{-}1\mu$ . Sartor and Albott (1972) computed the coalescence distance by observation of the air bubble trapped during the coalescence. They obtained about  $0.16\mu$  for the coalescence distance. Based on all these observations we decided to use a coalescence distance of  $0.1\mu$ .

3-2. HEAD ON COALESCENCE

a. The Model

In this model the coalescence of two liquid drops is investigated. The Model is primarily aimed at describing the effect of the different forces on the approach of an upward moving droplet toward a suspended drop, as was discussed in the experimental section of the report. However, as will be shown later, the results can be applicable to a variety of other type of experiments, e.g. interactions at relatively high impact velocities such as impact of two drops of different sizes at free fall, impact into a liquid surface and others. It is not applicable, however, to cases where a drop is placed at rest on a flat liquid surface or to cases where interactions of two large drops occur at free fall.

The model assumes that the origin of the coordinate system rests at the center of the large drop and that it rests with respect to the surrounding air. The smaller drop moves vertically upward at a velocity  $\Delta V_T$  which is the difference in the terminal velocities of the drops. Since the model describes the approach of the two drops it is possible to determine whether coalescence occurs. In the next chapter the same method will be used to determine conditions for coalescence in non-head-on interactions. From all these coalescence efficiencies for different drop sizes will be determined. In order to develop the equation of motion we first have to find an expression describing the forces acting on the drops. The viscous force, the force of the electrical double layer, Van der Waals force and electrical forces all depend on the shape of the drops. Hence, the approach of the drops also depends on their shape.

To our knowledge there is no way in which the shape of approaching liquid drops can be expressed mathematically. All the expressions found deal with a quasi stationary problem in which the drops are almost at rest with respect to each other. For this reason we chose two simple deformations

to express the changes that take place on the surfaces of the approaching drops. However, the equations we will propose can be easily changed when a better expression for the deformation is found.

b. The Forces and the deformation. The forces acting on a droplet which moves upward toward the center of a larger suspended drop are:

i. The viscous force  $F_V$ . This force arises as a result of the resistance of air to the motion of the drop. At large distances of separation, this force depends on the size of the smaller drop, on its velocity, and on its instantaneous deformation. At small distances of separation,  $F_V$  depends on the deformation of the two drops and on the distance between them.

ii. The gravitation force,  $F_g$ . This force acts in a direction so as to prevent the upward motion of the droplet.

iii. The electrical double layer force,  $F_{dl}$ . This repulsive force results from the electrical dipoles which align themselves along the water-air interface. They are arranged so that at small distances of separation the water surfaces act as two negatively charged surfaces. This force depends on the size of the two drops and their distance of separation.

iv. The London-Van-der-Waals force,  $F_{LV}$ . This attractive force depends on the deformation of the drops and the distance between them.

Let  $D$  be the instantaneous minimum distance between the two drops. We are interested in effects which take place at distances larger than  $10^{-6}$  cm since it is widely reported that coalescence occurs at distances of the order of  $10^{-5}$  cm (the mean free path of air molecules at room temperatures). According to Adamson (1967),  $F_{dl}$  and  $F_{LV}$  per unit area are given by

$$F_{dl} = (8.9 \cdot 10^{-7} / D^2) (\text{dynes/cm}^2) \quad (3-2)$$

$$F_{LV} = (10^{-13} / 6\pi D^3) (\text{dynes/cm}^2) \quad (3-3)$$

so that

$$\frac{F_{dl}}{F_{LV}} = 54\pi 10^6 D \quad (3-4)$$

which implies that  $F_{dl}$  and  $F_{LV}$  are equal when  $D = 10^{-6} / 54\pi = 5.9 \cdot 10^{-9}$  cm so that for any  $D$  larger than  $10^{-6}$  cm,  $F_{LV} \ll F_{dl}$ , so that  $F_{LV}$  can be neglected.

The three forces  $F_v$ ,  $F_g$  and  $F_{dl}$  are all repulsive forces in the present situation. Qualitatively, the behavior of the small drop and the forces on it can be described as follows: the small drop moves upward at an initial velocity  $v_0$  which decreases as it approaches the larger drop. Where no coalescence occurs the small drop stops, the pressure between the drops decreases and the deformation of the drops decreases as well. This decrease in the viscous force may result in oscillations about the equilibrium spherical shape of the drops which may enhance the probability for coalescence. On the other hand, since at that point  $F_g$  and  $F_{dl}$  still act, the drops are forced apart. These last two effects compete with each other and, hence, there is a need to treat them both simultaneously. In this report we deal only with the motion of the small drop to the point at which it stops and neglect the effect of the oscillations.

The equation of motion of the small drop can be written as:

$$m_s \ddot{r} = F_{dl} + F_g + F_v$$

Since  $F_v$  and  $F_{dl}$  strongly depend on the shape of the approaching surfaces, we first have to discuss the deformation of the drops.

v. The Deformation. The deformation of the drop depends on its size, on the distribution of pressures around it, and on its surface tension. It is an impossible task to evaluate the pressure distribution of the approaching drops at each point. As a reasonable approximation it is usually assumed that the approaching surfaces are planes (even though it is believed that the larger drops tend to get a dimple-like deformation). Frankel and Mysels (1962) showed that the approximation of a planar deformation of a drop approaching a water surface gives reasonable results to within 2% error.

We assume a planar deformation proportional to the radius of the smaller drop. Two deformation are attempted:

$$\text{I. } R_D = \alpha R_s \quad (3-5)$$

$$\text{II. } R_D = \beta R_s / D \quad (3-6)$$

where  $D$  is the distance between the deformed surfaces,  $R_D$  is the radius of deformation and  $R_s$  is the radius of the small drop.  $\alpha$  and  $\beta$  are constants. Since the deformation of the large drop is a direct result of the approach of the small drop, we assume that  $R_D$  is the same for both drops.

vi. The Viscous Force. This force acts mainly due to the fact that the deformed surfaces approach each other. We can therefore use the force

between two planes of radius  $R_D$  moving toward each other at a velocity  $V$  (see Landau and Lifshitz, 1959):

$$F_V = \frac{3\pi\eta R_D^4}{2} \frac{V}{D^3} \quad (3-7)$$

It is interesting to note that this was the starting point for many previous works (e.g. Charles and Mason, 1960). However, they assumed that  $F_V$  in addition to  $R_D$  are constant and so arrived at the Stefan-Reynolds equation:

$$t - t_o = \frac{3\pi\eta R_D^4}{4F_V} \left[ \frac{1}{D^2} - \frac{1}{D_o^2} \right]$$

However the assumption of a constant viscous force  $F_V$  is unreasonable as will be shown later. In the present work, contrary to most other works, we are not assuming the quasi-stationary conditions and the equations are solved without neglecting the inertial force  $mD$ . Foote (1971) has also considered inertial forces but only with respect to the plane of deformation and not with respect to the other drop.

vii. The Electrical Double Layer Forces. When a planar deformation is considered it is reasonable to assume that only the deformed portion of the drop contributes to the electrical double layer force, and according to Adamson (1967) it can be expressed as follows:

$$F_{dl} = \frac{8.9 \cdot 10^{-7} \pi R_D^2}{D^2} \text{ dynes} \quad (3-8)$$

viii. The force of gravity. If the radius of the small droplet is  $R_s$  the force of gravity on it would be

$$F_g = \frac{4}{3} \pi R_s^3 g \quad (3-9)$$

This force can enhance coalescence or inhibit it depending on the interaction. In the case where a small droplet impacts the lower hemisphere of a large drop, the force of gravity tends to oppose coalescence. In impact of drops onto flat liquid surfaces it assists in the coalescence. In all cases tested here where the impact speed was comparable to the relative terminal velocities of drops between 20-2000 $\mu$  the effect of gravity was very small and could be neglected.

c. The equation of motion

The model deals with a small drop moving upward toward a large drop. The forces  $F_V$ ,  $F_{dl}$  and  $F_g$  all act downward. It can be easily shown that the connection between  $r$  and  $D$  can be written as:

$$r = D + \sqrt{R_L^2 - R_D^2} + \sqrt{R_s^2 - R_D^2} \quad (3-10)$$

where  $r$  is the distance between the centers of the drops and  $R_L$  is the radius of the large drop. The equation of motion of the small droplet can now be written as

$$m_s \frac{d^2 r}{dt^2} = \Sigma F \quad (3-11)$$

where

$$\begin{aligned} \Sigma F &= F_V + F_{DL} + F_{LV} + F_g \\ &= \frac{3\pi\eta R_D^4}{2D^3} \frac{dD}{dt} + \frac{8.9 \times 10^{-7}\pi R_D^2}{D^2} + \\ &\quad + \frac{10^{-13}}{6D^3} R_D^2 \pm \frac{4\pi R_s^3}{3} g \end{aligned} \quad (3-12)$$

and where  $\eta$  is the viscosity of air,  $D$  is the distance between the approaching surfaces and  $m_s$  is the mass of the small droplet.

It is worthwhile at this stage to change the dependent variable from  $r$  to  $D$ . By the use of Eq. (3-10) we can show

$$\frac{d^2 r}{dt^2} = v^2 \frac{d^2 r}{dD^2} + \frac{d^2 D}{dt^2} \frac{dr}{dD} \quad (3-13)$$

where  $v \equiv \frac{dD}{dt}$

is the relative velocity of the deformed surfaces.

If we use the first deformation criterion:

$$\begin{aligned} R_D &= \alpha R_s \\ \text{we get} \quad \frac{d^2 r}{dt^2} &= \frac{d^2 D}{dt^2} \end{aligned}$$

so that the equation of motion becomes

$$\frac{d^2 D}{dt^2} = \frac{1}{m_s} \Sigma F \left( \frac{dD}{dt}, D \right) \quad (3-14)$$

If the second deformation is used namely

$$R_D = \frac{\beta R_s}{D}$$

than we get

$$\frac{dr}{dD} = 1 + \frac{\beta^2 R_s^2}{D^3} \left( \frac{1}{\sqrt{R_L^2 - R_D^2}} + \frac{1}{\sqrt{R_s^2 - R_D^2}} \right) \quad (3-15)$$

$$\frac{d^2 r}{dD^2} = - \frac{3\beta^2 R_s^2}{D^4} \left( \frac{1}{\sqrt{R_L^2 - R_D^2}} + \frac{1}{\sqrt{R_s^2 - R_D^2}} \right) - \frac{\beta^4 R_s^4}{D^6} \left( \frac{1}{(R_L^2 - R_D^2)^{3/2}} + \frac{1}{(R_s^2 - R_D^2)^{3/2}} \right) \quad (3-16)$$

and the equation of motion looks like

$$\frac{d^2 D}{dt^2} = \frac{1}{m_s} \Sigma F \left( \frac{dD}{dt}, D \right) - v^2 \frac{d^2 r}{dD^2} \Big/ \frac{dr}{dD} \quad (3-17)$$

substitution of Eqs. (3-15) and (3-16) into (3-17) gives the equation of motion without  $r$ .

The order of the above differential equations can be reduced by the use of

$$\frac{d^2 D}{dt^2} = v \frac{dv}{dD}$$

Using this relationship we get for  $R_D = \alpha R_s$

$$\frac{dv}{dD} = \frac{1}{m_s v} \Sigma F(v, D) \quad (3-18)$$

and for  $R_D = \frac{\beta R_s}{D}$

$$\frac{dv}{dD} = \left( \frac{1}{m_s v} \Sigma F(v, D) - v \frac{d^2 r}{dD^2} \right) \Big/ \frac{dr}{dD} \quad (3-19)$$

This equation is applicable for  $v \neq 0$

Both equations were solved numerically by the use of a forth order Runge-Kutta method. For small values of  $v$  it was required to substantially reduce the step size in order to achieve better accuracy. A great

improvement was obtained by substituting

$$u = \frac{m_s}{2} \left( \frac{dD}{dt} \right)^2 \quad (3-20)$$

With this substitution we obtain:

$$\text{for } R_D = \alpha R_s$$

$$\frac{du}{dD} = \Sigma F(u, D) \quad (3-21)$$

$$\text{for } R_D = \frac{\beta R_s}{D}$$

$$\frac{du}{dD} = (\Sigma F(u, D) - 2u \frac{d^2 r}{dD^2}) / \frac{dr}{dD} \quad (3-22)$$

where both  $\frac{d^2 r}{dD^2}$  and  $\frac{dr}{dD}$  can be substituted from Eqs. (3-15) and (3-16),

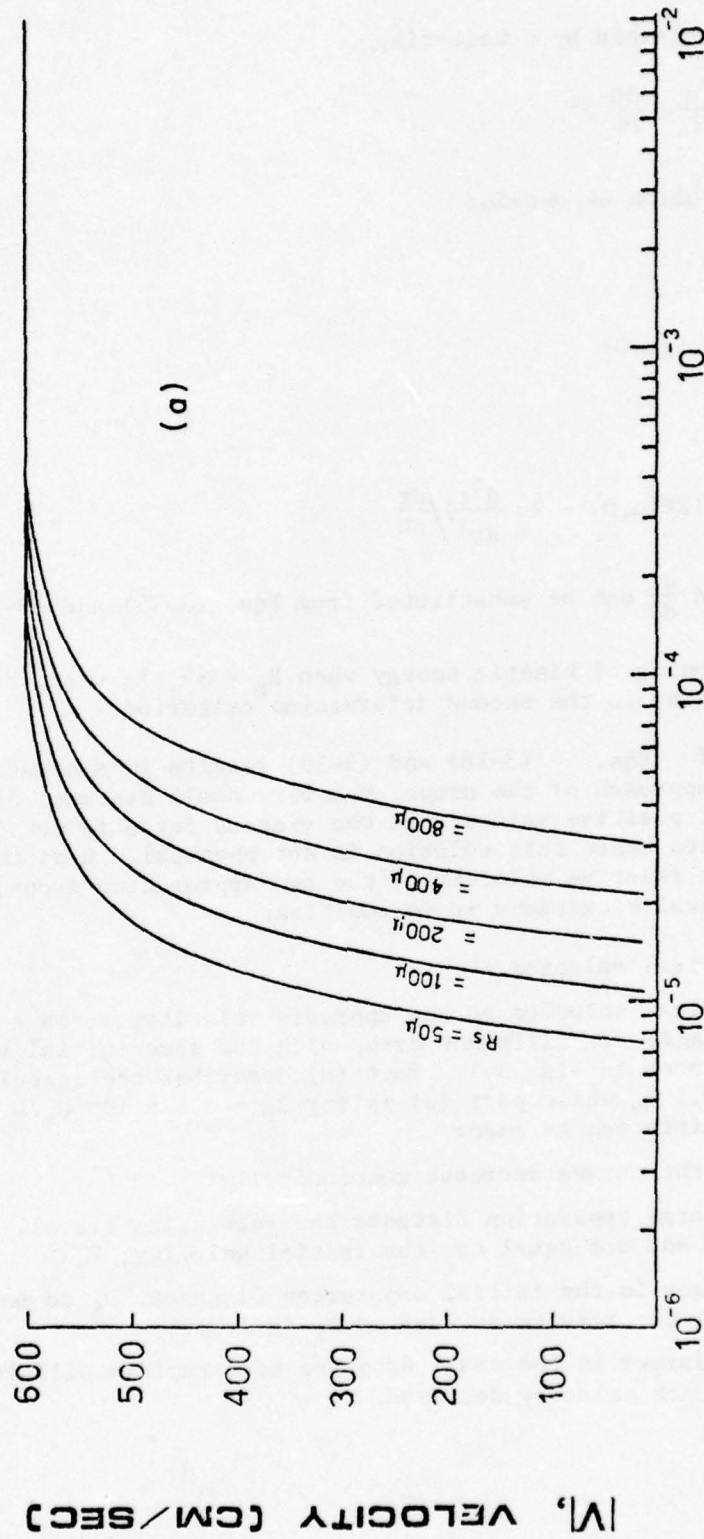
$u$  has the meaning of kinetic energy when  $R_D = \alpha R_s$  is used, but it has no simple meaning in the second deformation criterion.

A solution of Eqs. (3-18) and (3-19) results in a negative  $v$  which implies an approach of the drops. At a very small distance of separation,  $D$ ,  $v$  may get positive values, but the viscous force is not defined for such a situation hence this solution is not physical.  $u$  on the other hand describes the relative velocity of the two approaching drops, hence for all real physical situations it is positive.

#### d. The numerical solution

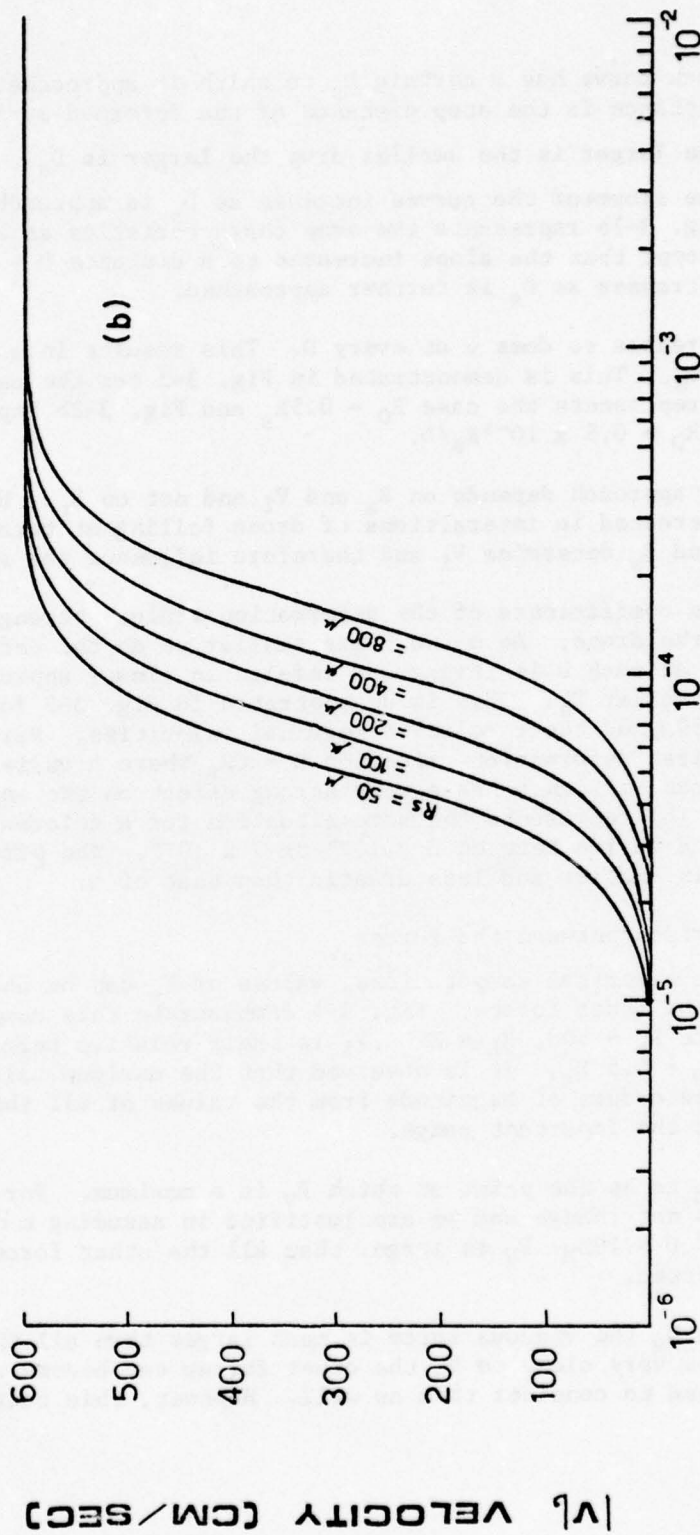
The numerical solution to the approach velocity,  $v$ , as a function of separation distance for different drops with the same initial velocity (-600 cm/sec) is shown in Fig. 3-1. Part (a) describes the velocity for deformation  $R_D = 0.5 R_s$  while part (b) is for  $R_D = 0.5 \times 10^{-5} R_s/D$ . The following observations can be made:

- (1) All the curves decrease monotonically
- (2) At large separation distance the velocities are all the same and are equal to the initial velocity,  $V_i$ .
- (3) Changes in the initial separation distance,  $D_i$  do not alter the results as long as  $D_i$  is large.
- (4) The larger is the small drop the more rapidly will its approach velocity decrease.



### D, DISTANCE OF SEPARATION (CM)

Fig. 3-1a. The dependence of the approach velocity of the deformed surfaces on the distance between the surfaces for different  $R_L$  when the deformation  $R_D = 0.5R_S$ . Here  $R_L = 250 \mu$ ,  $v_0 = -600 \text{ cm-sec}^{-1}$  and large  $D_0$ .



### $D$ , DISTANCE OF SEPARATION (CM)

Fig. 3-1b. The same as in part a except  $R_D = \frac{0.5 \times 10^{-5} R_s}{D}$ .

- (5) Each curve has a certain  $D_s$  to which it approaches. This distance is the stop distance of the deformed surfaces.
- (6) The larger is the smaller drop the larger is  $D_s$ .
- (7) The slopes of the curves increase as  $D_s$  is approached. Fig. 3-1b represents the same characteristics as above except that the slope increases to a distance  $D > D_s$  and decreases as  $D_s$  is further approached.

As  $|V_i|$  increases so does  $v$  at every  $D$ . This results in a decrease in the value of  $D_s$ . This is demonstrated in Fig. 3-2 for the case  $R_s = 50\mu$ . Again Fig. 3-2a represents the case  $R_D = 0.5R_s$  and Fig. 3-2b represents the deformation  $R_D = 0.5 \times 10^{-5} R_s/D$ .

The head-on approach depends on  $R_s$  and  $V_i$  and not on  $R_L$ . However, since we are interested in interactions of drops falling at terminal velocities,  $R_L$  and  $R_s$  determine  $V_i$  and therefore influence the approach.

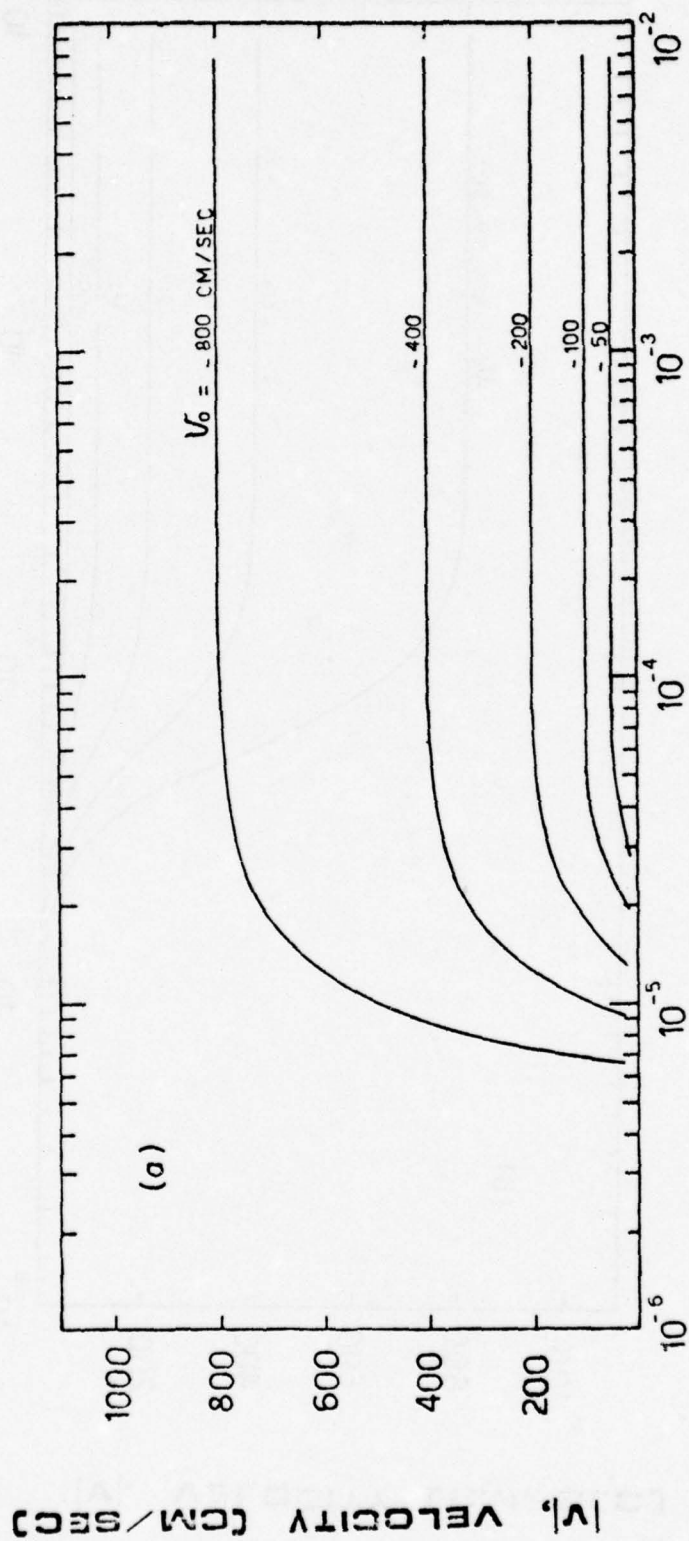
$\alpha$  and  $\beta$ , the coefficients of the deformation radius, strongly influence the approach of the drops. As  $\alpha$  and  $\beta$  get smaller so do the deformations and the velocity at each  $D$  is larger and results in closer approach of the drops and a smaller  $D_s$ . This is demonstrated in Fig. 3-3 for the case  $R_s = 50\mu$ ,  $R_L = 250\mu$  and their relative terminal velocities. Part (a) represents the first deformation criterion  $R = \alpha R_s$  where  $\alpha$  varies between 0.3 to 0.7. As can be seen  $\alpha$  has a very strong effect on the approach of the drops. Part (b) represents the same situation for a deformation  $R_D = \beta R_s/D$  where  $\beta$  varies between  $3 \times 10^{-6}$  to  $7 \times 10^{-6}$ . The effect of  $\beta$  on the approach is smaller and less drastic than that of  $\alpha$ .

#### e. A comparison between the forces

From the numerical computations, values of  $F_v$  can be obtained and compared to the other forces. Fig. 3-4 demonstrate this comparison for the case where  $R_s = 50\mu$ ,  $R_L = 250\mu$ ,  $V_i$  is their relative terminal velocities and  $R_D = 0.5 R_s$ . It is observed that the maximum value of  $F_v$  is larger by a few orders of magnitude from the values of all the other forces throughout the important range.

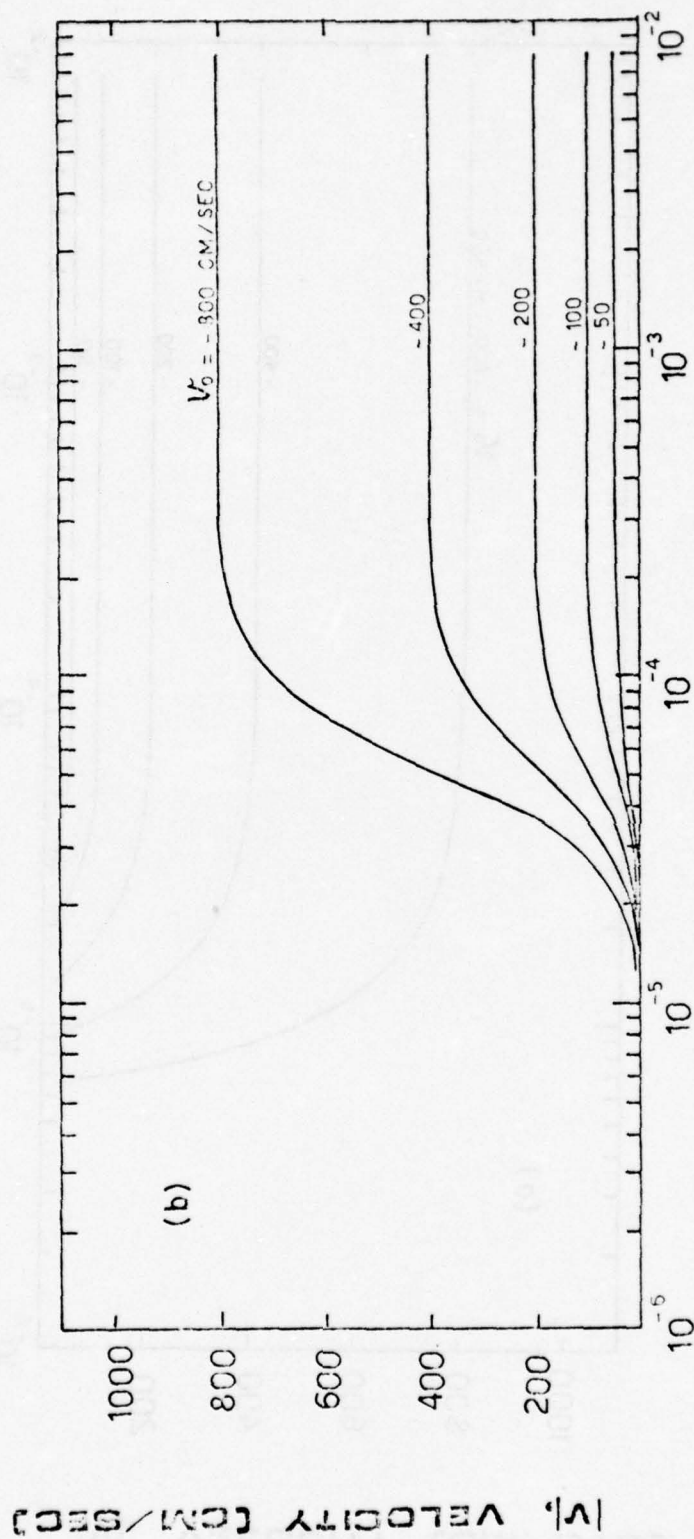
We define  $D_M$  to be the point at which  $F_v$  is a maximum. For  $D > 10 D_M$  the velocity does not change and we are justified in assuming  $m\ddot{r} = 0$ . In the range  $D_M < D < 10D_M$   $F_v$  is larger than all the other forces and so they can be neglected.

For  $D$  around  $D_M$  the viscous force is much larger than all the other forces. As  $D$  gets very close to  $D_s$  the other forces can become important and there is a need to consider them as well. However, this range is very



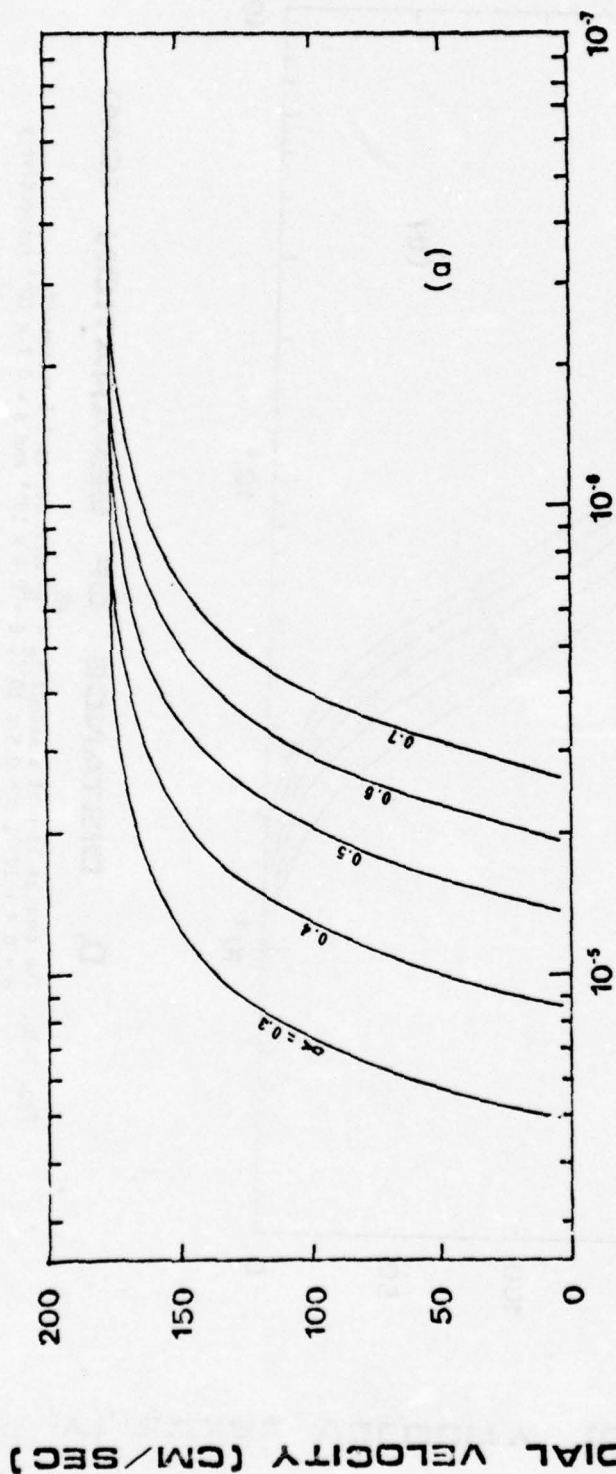
## D, DISTANCE OF SEPARATION (CM)

Fig. 3-2a. The dependence of approach velocity on the distance of separation for different initial velocities. Here  $R_D = 0.5R_S$ ,  $R_S = 50\mu$  and  $R_L = 250\mu$ .



### D, DISTANCE OF SEPARATION [CM]

Fig. 3-2b. The same as in part a except  $R_0 = \frac{0.5 \times 10^{-5} R_s}{D}$ .



**D, DISTANCE OF SEPARATION (CM)**

Fig. 3-3a. The dependence of the approach velocity on the deformation constant  $\alpha$ .  
 $R_D = \alpha R_S$ ,  $R_S = 50\mu$ .

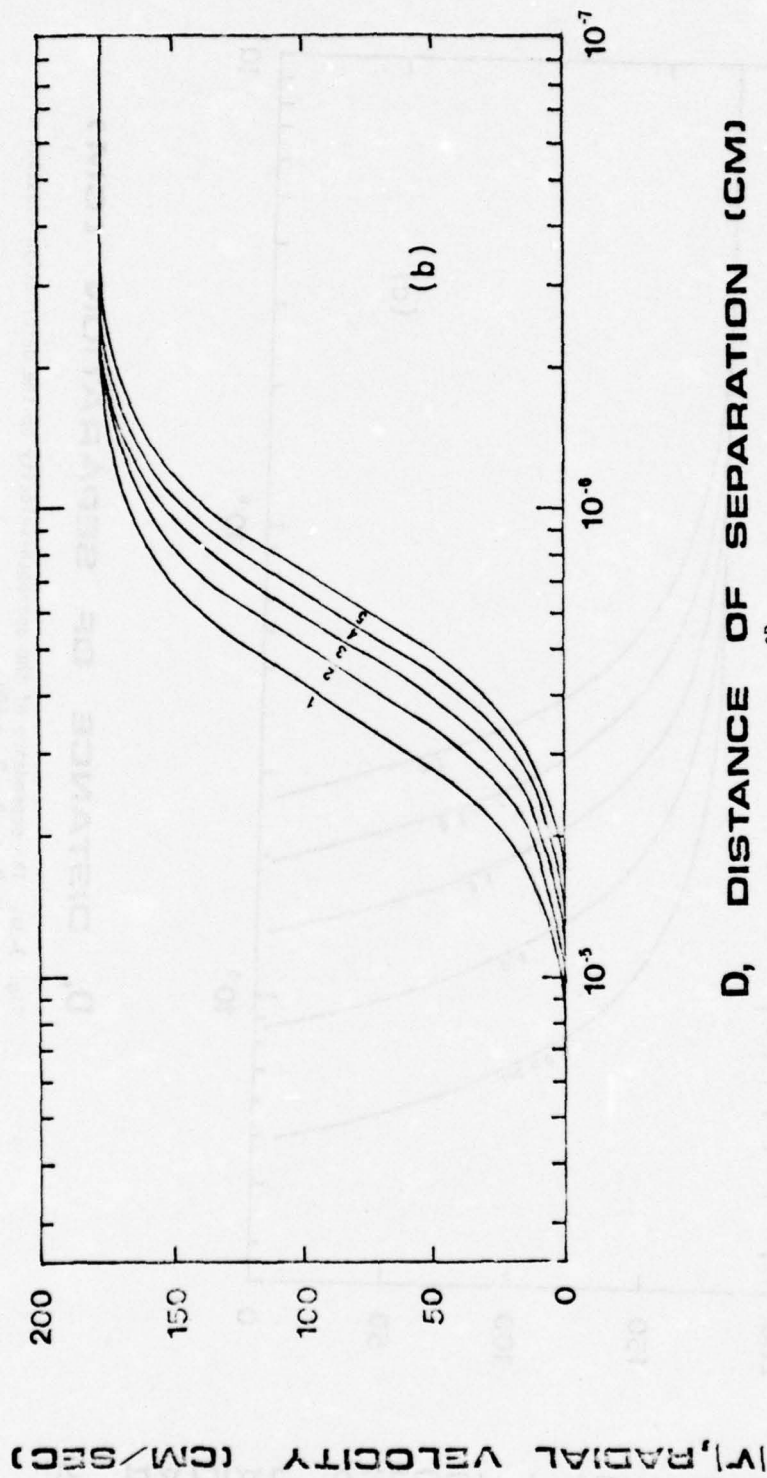


Fig. 3-3b. The same as in part a except  $R_0 = \frac{\beta R_s}{D}$  when curves 1-5 represent,  $\beta = 0.4 \times 10^{-5}$ ,  $\beta = 0.5 \times 10^{-5}$ ,  $\beta = 0.6 \times 10^{-5}$  and  $\beta = 0.7 \times 10^{-5}$  respectively.

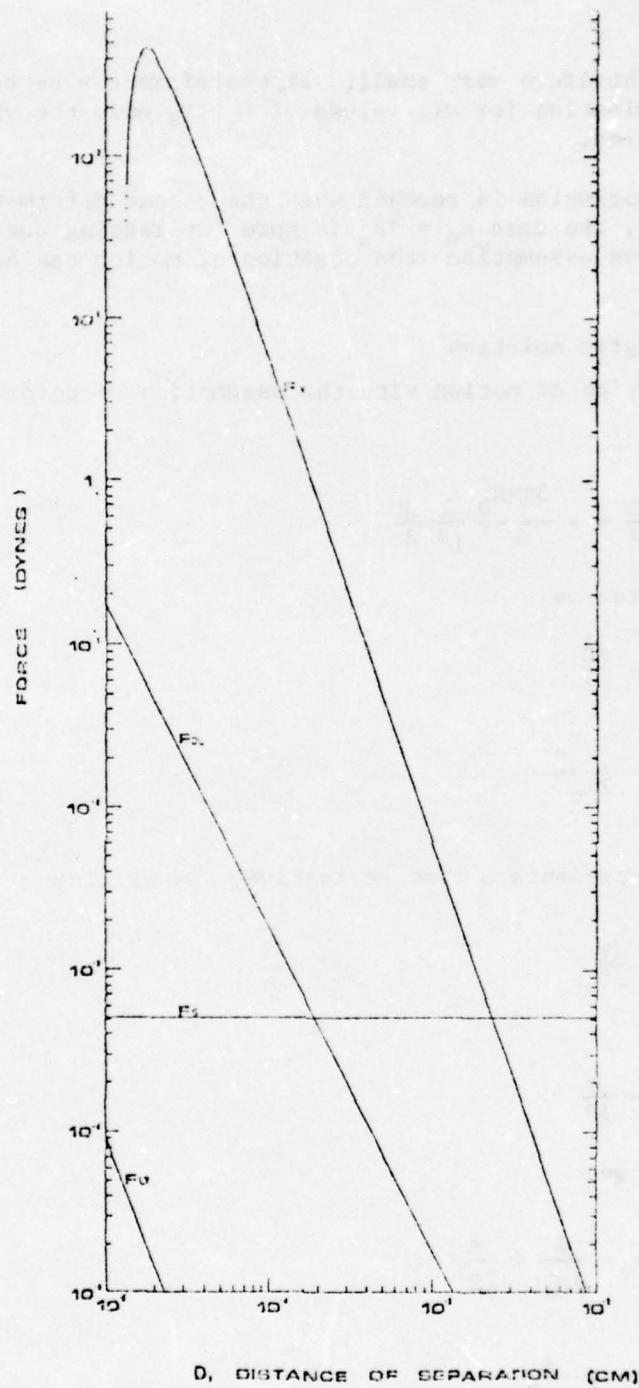


Fig. 3-4. A comparison of the forces as a function of the distance of separation.

close to  $D_s$  and therefore very small. It, therefore, can be concluded that to a first approximation for all values of  $D > D_s$  only the viscous force has to be considered.

A similar conclusion is reached when the second deformation criterion is used. However, the case  $R_D = \alpha R_s$  is more interesting due to the fact that with the above assumptions the equation of motion can be solved analytically.

f. The analytic solution

The equation of motion with the assumption of deformation  $R_D = \alpha R_s$  can be written:

$$m_s \frac{d^2 D}{dt^2} = - \frac{3\pi\eta R_D^2}{2} \frac{1}{D^3} \frac{dD}{dt} \quad (3-23)$$

and can be rewritten as

$$m\ddot{D} = - \frac{AD}{D^3} \quad (3-24)$$

$$\text{where } A = \frac{3\pi\eta(\alpha R_s)^4}{2m_s} \quad (3-25)$$

and where a dot represents a time derivative. By writing

$$\ddot{D} = v \frac{dv}{dD}$$

we get

$$\frac{dv}{dD} = - \frac{A}{D^3}$$

By integration we get

$$v = v_0 - \frac{A}{2D_0^2} + \frac{A}{2D^2} \quad (3-26)$$

If we define

$$W_1 = v_0 - \frac{A}{2D_0^2} \quad (3-27)$$

we can re-write Eq. (3-26) as

$$v = W_i + \frac{A}{2D^2} \quad (3-28)$$

Since we deal with approaching surfaces the equation had a meaning only if

$$D > \sqrt{-\frac{A}{2W_i}}$$

$W_i$  has the meaning of the velocity that the small drop was to have at infinity in order to reach point  $D_i$  at a velocity  $V_i$ .

The analytic solution provides a better understanding of the approach problem, for example:

$$(1) \text{ If } D_o \gg \sqrt{-\frac{A}{2v_o}}$$

then

$$v = v_o + \frac{A}{2D^2} \quad (3-29)$$

Here  $D_o$  does not appear at all and therefore it implies that in this case the approach does not depend on  $D_o$ .

$$(2) \text{ For } D \gg \sqrt{-\frac{A}{2v_o}} \text{ the velocity is almost constant } v \approx v_o.$$

(3) The value of  $D_s$  can be found. We know that

$$\lim_{D \rightarrow D_s} v = 0$$

Therefore

$$D_s = \sqrt{-\frac{A}{2W_i}} \quad (3-30)$$

If we now define  $D_N = D/D_s$  and  $V_N = v/W_i$  we get a relation between a normalized velocity and normalized distance

$$V_N = 1 - \frac{1}{D_N^2} \quad (3-31)$$

Fig. 3-5 represents Eq. (3-31).

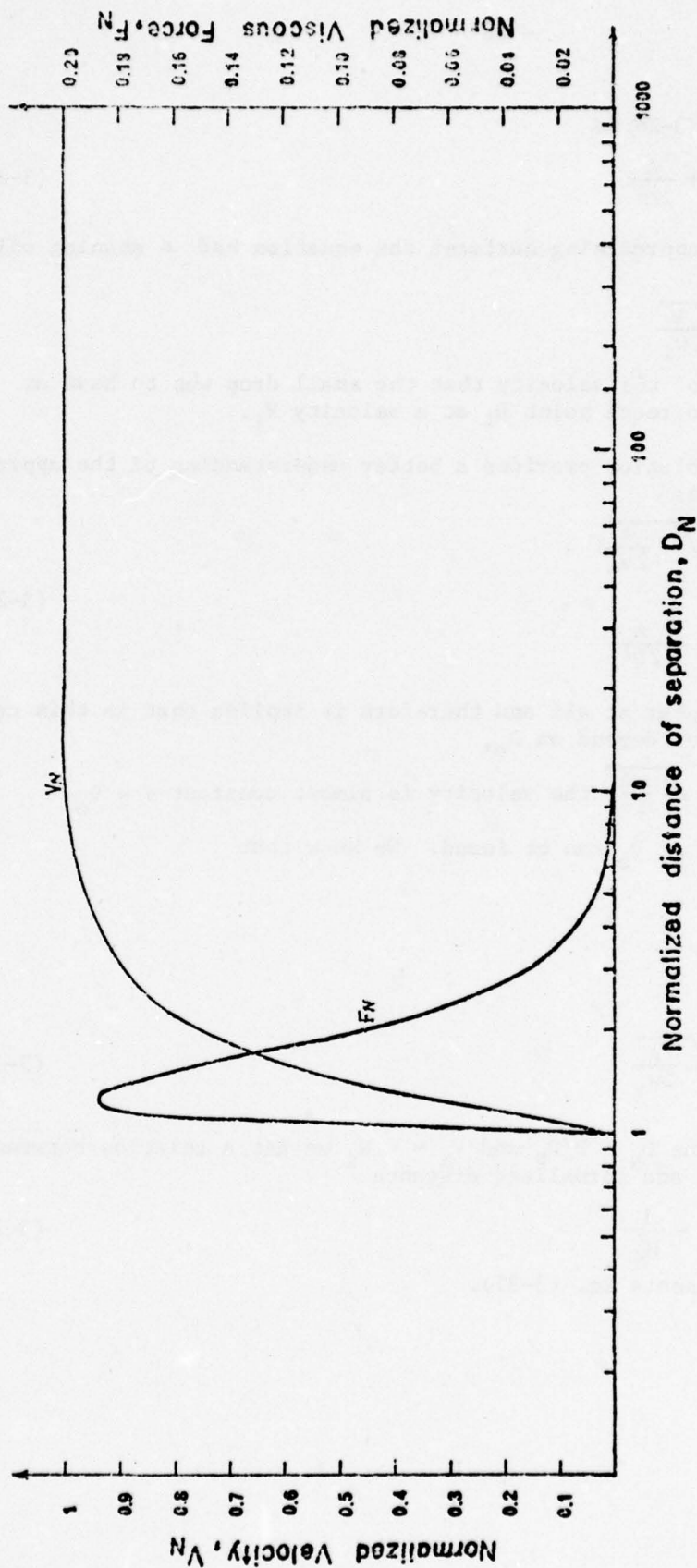


Fig. 3-5. Normalized velocity and viscous force as a function of the normalized distance of separation.

g. The viscous force

Substitution of Eqs. (3-25) and (3-28) into Eq. (3-6) gives

$$F_V(D) = (-m_s AW_i) \frac{1}{D^3} - \frac{m_s^2}{2} \frac{1}{D^5}$$

It is therefore easy to see that

$$F_V(D_N) = - \frac{m_s AW_i}{D_s^3} \left( \frac{1}{D_N^3} - \frac{1}{D_N^5} \right) \quad (3-32)$$

The coefficient  $\left( - \frac{m_s AW_i}{D_s^3} \right)$  is the viscous force that would have acted between the drops at a distance  $D_s$  if the drop did not lose part of its speed. If we define a normalized viscous force

$$F_N = \frac{F_V}{\left( - \frac{m_s AW_i}{D_s^3} \right)} \quad (3-33)$$

we get

$$F_N = \frac{1}{D_N^3} - \frac{1}{D_N^5} \quad (3-34)$$

This equation is also represented in Fig. 3-5.  $F_V$  becomes maximum at

$$D_M = \sqrt{\frac{5}{3}} D_s = 1.291 D_s$$

At that point  $F_V$  is:

$$F_{V_{\max}} = - \frac{2}{5} \left( \frac{3}{5} \right)^{3/2} \frac{m_s AW_i}{D_s^3}$$

when  $F_V$  is a maximum  $V = 2/5$ . As the two drops approach each other and get very close to  $D_s$ , the viscous force decreases rapidly.

h. The approach time

It is sometimes interesting to calculate the time it takes for the droplet to approach to within a distance  $D$  from another drop under the action of its inertial and viscous forces.

The time can be found by:

$$t = \int_{D_0}^D \frac{dD}{v}$$

Substitution of V from Eq. (3-28) and integration results:

$$t = \frac{D_0 - D}{-W_1} + \tau \ln \frac{D + D_s}{D - D_s} - \tau \ln \frac{D_0 + D_s}{D_0 - D_s} \quad (3-35)$$

where  $\tau$  is a time constant defined as:

$$\tau = \frac{D_s}{2(-W_1)}$$

According to this equation the drop gets closer to  $D$  but reaches it only after infinite time. However, one has to remember that the analytic solution is not applicable at distances close to  $D_s$ , since at this distance other forces have to be considered.

i. The range in which the analytic solution is valid

(a) For the analytic solution to be physically valid  $F_{V_{\max}} \gg F_g$  and also  $F_{V_{\max}} \gg F_{DL}(D_M)$ . For these conditions we find

$$-W_1 \geq 5.4 \sqrt[5]{R_s}$$

and

$$-W_1 \geq 0.0103 \frac{1}{R_s}$$

(3-36)

respectively. For the range  $20\mu \leq R_s < 2000\mu$  it is enough that  $W_1 > 5.15$  cm/sec for these conditions to be fulfilled.

(b) Lets assume that there is a range  $[D_1, D_0]$  in which the analytic solution is valid and lets try and find it.

For large  $D$  the velocity  $v \approx v_0$  if within the range  $D$  to  $D_M$  there was no appreciable lose of velocity. For large  $D$   $F_{DL} \ll F_g$  and hence  $D_0$  will be determined by:

$$g \left( \frac{D_0 - 1.291 D_s}{-W_1} \right) \leq 100 W_1$$

If  $D_0 \gg D_s$  then in c.g.s. units

$$D_0 \leq 0.1 W_1^2 \quad (3.37)$$

For cases of meteorological interest  $W_1$  is of the order of tens or hundreds cm-sec<sup>-1</sup> and  $D_0$  is of the order of microns and therefore fulfills the required conditions.

(c)  $D_1$  has to fulfill the following conditions:

$$F_V(D_1) \gg F_g$$

and also

$$F_V(D_1) \gg F_{DL}(D_1)$$

So it is possible to numerically find for every case the lower point,  $D_1$ , for which the analytic solution is physically correct. In order to get an estimate of  $D_1$  we can look at  $D = 1.005 D_s$  where the drop loses 99% of its initial velocity. It is easy to show that:

$$F_V(1.005 D_s) \gg F_g$$

when  $-W_1 \geq 17.2 \sqrt[5]{R_s}$

and  $F_V(1.005 D_s) \gg F_{DL}(1.005 D_s)$

when  $-W_1 \geq 0.1018 \frac{1}{R_s}$

These conditions are stronger than those expressed in Eq. (3-36).

For the range  $20 < R_s < 2000 \mu$   $F_V(1.005 D_s) \gg F_g$  for all  $R_s$  if  $-W_1 \geq 12.6$  cm/sec and  $F_V(1.005 D_s) \gg F_{DL}(1.005 D_s)$  for  $-W_1 \geq 51$  cm/sec.

From all these we can conclude that the analytic solution is valid for most cases considered where the impact velocity is higher than 51 cm/sec and is fairly good for even lower values of  $W_1$ . However, for lower impact speeds and impact at angles different from head-on a numerical solution is needed.

#### CHAPTER 4: NON-HEAD-ON APPROACH OF TWO DROPS

In this chapter we follow the motion of two drops as they approach in a non-head on collision course. From considerations of this approach it is possible to draw conclusions regarding the coalescence itself.

##### a. The equations of motion

The origin of the coordinate system was centered at the center of mass of the large drop with the assumption that the coordinate system is inertial. The equations of motion of the small drop in polar coordinates are:

$$m_s \frac{d}{dt}(r^2 \dot{\theta}) = r F_t \quad (4-1)$$

$$m_s \ddot{r} - m_s r \dot{\theta}^2 = F_R \quad (4-2)$$

where  $r$  is the distance between the centers of the two masses,  $m_s$  the mass of the smaller drop and  $F_t$  and  $F_R$  are the tangential and radial forces, respectively. In our calculations here we assume: (1) That the planes of deformations on the two drops are parallel. This assumption causes the forces  $F_V$ ,  $F_{DL}$  and  $F_{LV}$  to act radially. In order to get  $F_V$  we substitute in Eq. 3-12 the relative velocity of the deformation planes,  $v \equiv dD/dt$  in the radial direction. (2) Since in the tangential direction the drop looks spherical  $F_R \gg F_t$  and hence  $F_t$  will be neglected.

Here we have to define a few terms:

Impact velocity  $V_1$  - is the relative velocity of the drops before impact.

Impact trajectory - is the line drawn before impact from the center of the small drop in the direction of motion.

Impact point A - The intersection of the impact trajectory with a sphere of radius equal to the sum of the radii of the drops and centered on the center of the large drop (see Fig. 4-1).

Impact angle  $\theta_1$  - is the angle between the direction of the impact velocity of the small drop and the line connecting the impact point with the center of the large drop.

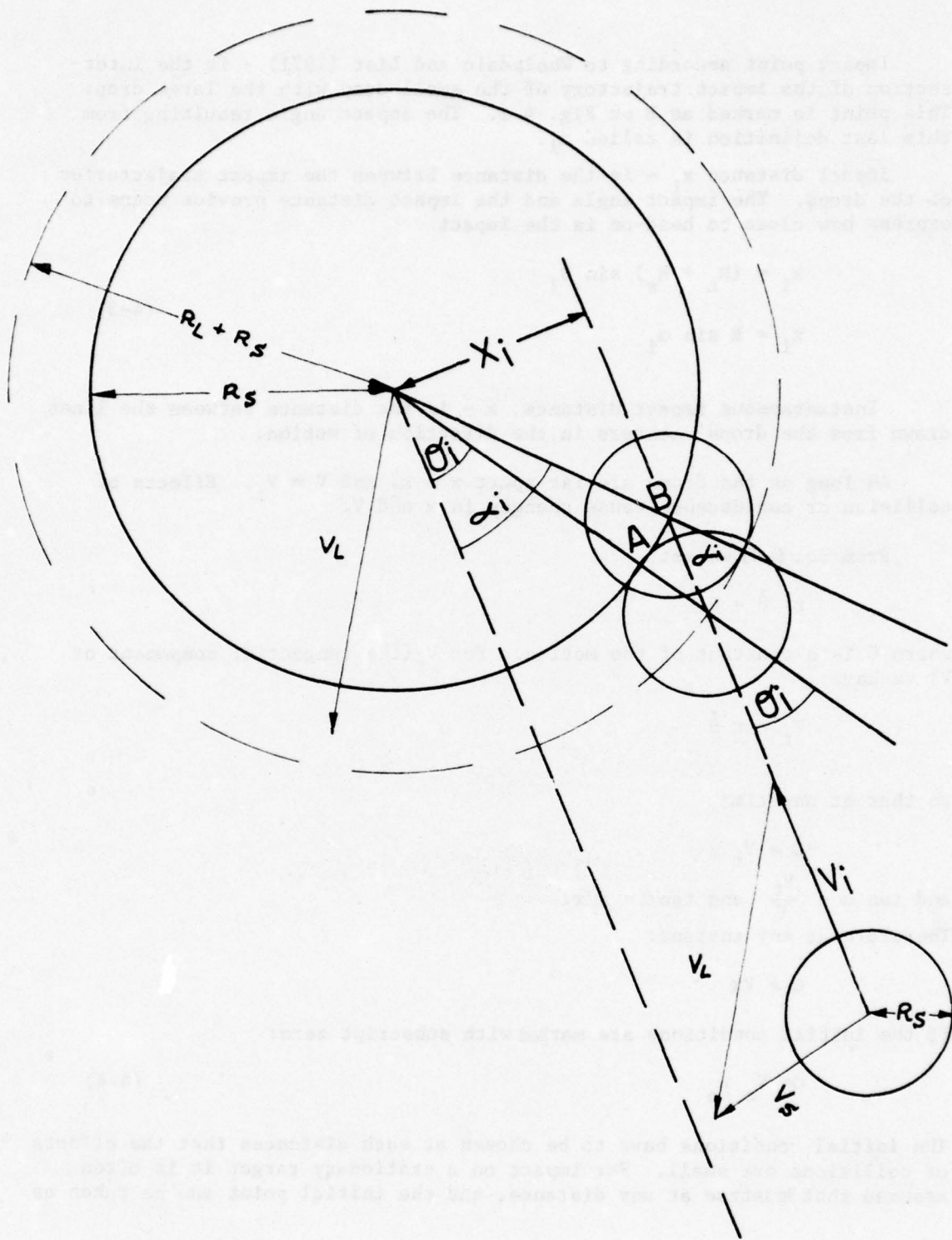


Fig. 4-1. An illustration of the geometry of a non-head-on collision.

Impact point according to Whelpdale and List (1971) - is the intersection of the impact trajectory of the small drop with the large drop. This point is marked as B on Fig. 4-1. The impact angle resulting from this last definition is called  $\alpha_i$ .

Impact distance  $x_i$  - is the distance between the impact trajectories of the drops. The impact angle and the impact distance provide means to express how close to head-on is the impact

$$\begin{aligned} x_i &= (R_L + R_s) \sin \theta_i \\ x_i &= R \sin \alpha_i \end{aligned} \quad (4-3)$$

Instantaneous impact distance,  $x$  - is the distance between the lines drawn from the drops' centers in the direction of motion.

As long as the drops are far apart  $x = x_i$  and  $V = V_i$ . Effects of collision or coalescence cause changes in  $x$  and  $V$ .

From Eq. (4-1) we get

$$r^2 \dot{\theta} = C$$

where  $C$  is a constant of the motion. For  $V_t$  (the tangential component of  $V$ ) we have:

$$V_t = r \dot{\theta}$$

so that at any time

$$C = V_t r$$

and  $\tan \alpha = \frac{V_t}{V}$  and  $\tan \alpha = x/r$ .

Therefore at any instant:

$$C = Vx$$

If the initial conditions are marked with subscript zero:

$$C = V_0 x_0 \quad (4-4)$$

The initial conditions have to be chosen at such distances that the effects of collisions are small. For impact on a stationary target it is often assumed that it is true at any distance, and the initial point can be taken as

$x_0 = x_1$  and  $V_0 = V_1$ . Under these conditions

$$C = V_1 x_1 \quad (4-5)$$

we now get

$$m_s r \dot{\theta}^2 = m_s \frac{c^2}{r^3} = \frac{m_s (V_0 x_0)^2}{r^3}$$

and substituting into Eq. 4-2 we get

$$m_s \ddot{r} = F_R + \frac{m_s (V_0 x_0)^2}{r^3} \quad (4-6)$$

where

$$F_R = F_V + F_{DL} + F_{LV}$$

The gravitational force,  $F_g$ , is not necessarily in the radial direction, however it can be generally neglected.

Eqs. (4-1) and (4-2) can be divided to a tangential equation whose solution is:

$$V_t(r) = \frac{V_0 x_0}{r} \quad (4-7)$$

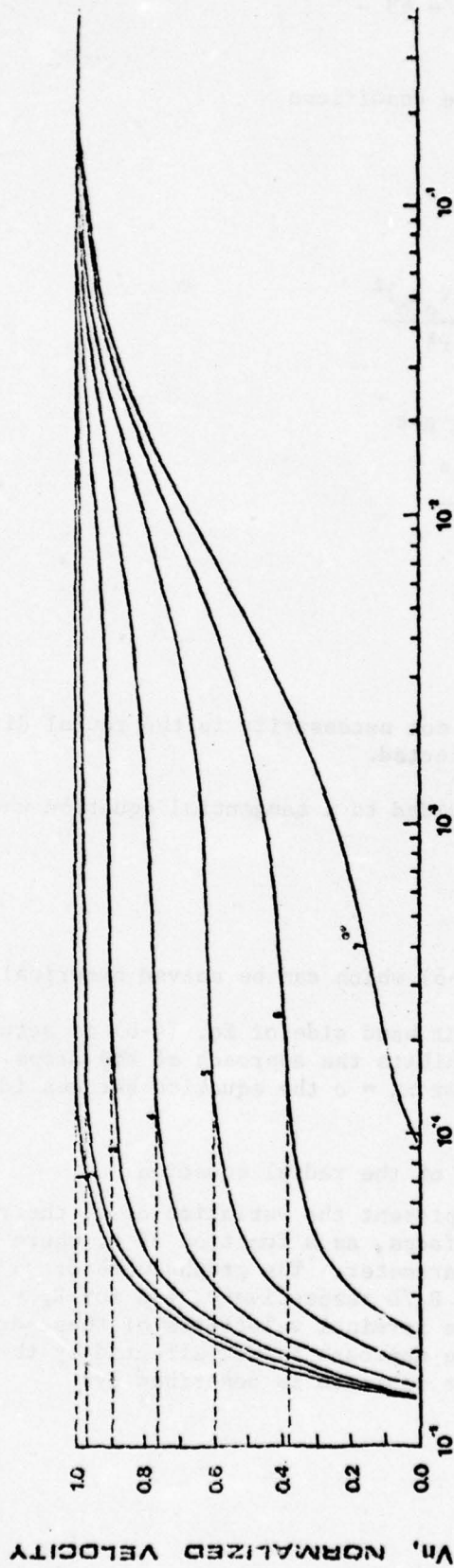
and to a radial equation (Eq. 4-6) which can be solved numerically.

The second term on the right hand side of Eq. (4-6) is actually the centrifugal force,  $F_c$ , which inhibits the approach of the drops.  $F_c$  increases as  $x_0$  gets larger. For  $x_0 = 0$  the equation becomes identical to a head-on collision.

b. The numerical solution of the radial equation

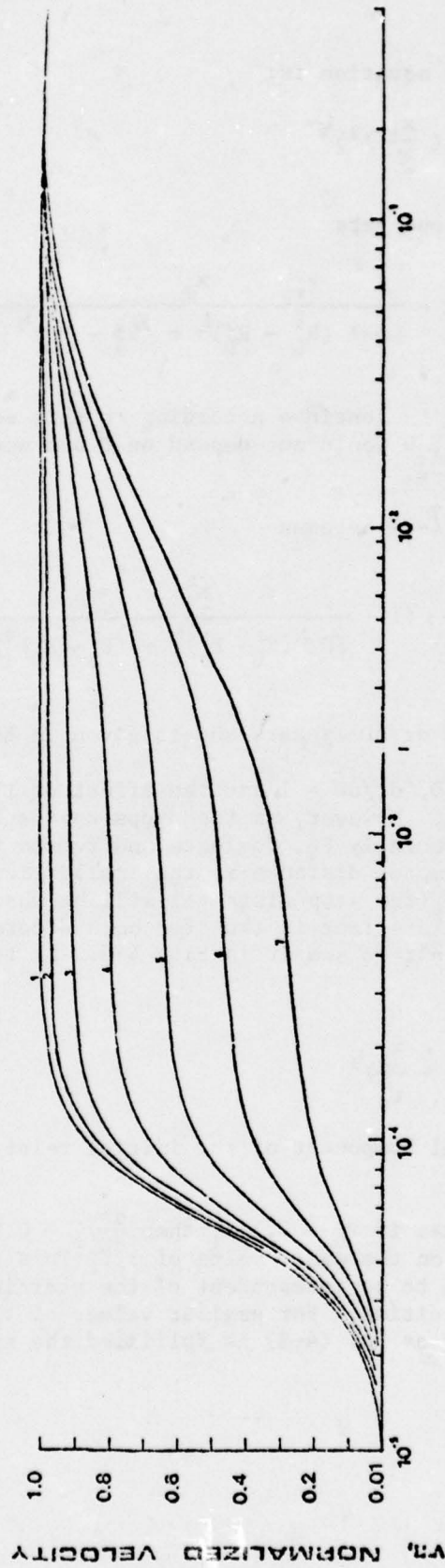
Figs. (4-2) and (4-3) present the variation of  $v$ , the relative velocity of the deformation surfaces, as a function of  $D$ , where the impact distance is taken as a parameter. The graphs were drawn for  $R_D = 0.5 R_s$  and  $R_D = 0.5 \times 10^{-5} R_s/D$  respectively, and for  $R_s = 50\mu$ ,  $R_L = 250\mu$  and  $V_1$  as the relative terminal velocities of these drops. Initially (high values of  $D$ ) the approach is not affected by the presence of  $F_V$ ,  $F_{DL}$  and  $F_{LV}$ . So that the approach is describes by:

$$m_s \ddot{r} = \frac{m_s}{r^3} (V_1 x_1)^2$$



D, DISTANCE OF SEPARATION (CM)

Fig. 4-2. The dependence of the normalized velocity on the distance of separation for  $R_D = 0.5 R_S$  in a non-head-on coalescence. Here  $R_S = 50\mu$ ,  $R_I = 250\mu$  and the relative terminal velocity was chosen as the initial velocity at large  $r_0$ . The curves represent the following: 1.  $x_i = 0$ ,  $\theta_i = 0$ ; 2.  $x_i = 67\mu$ ,  $\theta_i = 1/14\pi$ ; 3.  $x_i = 130\mu$ ,  $\theta_i = 1/7\pi$ ; 4.  $x_i = 187\mu$ ,  $\theta_i = 3/14\pi$ ; 5.  $x_i = 234\mu$ ,  $\theta_i = 2/7\pi$ ; 6.  $x_i = 270\mu$ ,  $\theta_i = 5/14\pi$ ; and 7.  $x_i = 292\mu$ ,  $\theta_i = 3/7\pi$ .



D, DISTANCE OF SEPARATION (CM)

Fig. 4-3. The same as Fig. 4-2 except  $R_D = \frac{0.5 \times 10^{-5} R}{D}$ .

The solution to the above equation is:

$$\frac{dr}{dt} = V_i \left( 1 - \left( \frac{x_i}{r} \right)^2 \right)^{\frac{1}{2}} \quad (4-8)$$

When  $R_D = \alpha R_s$ ,  $v = dr/dt$  one gets

$$v(D) = V_i \left( 1 - \frac{x_i^2}{[D + (R_L^2 - R_D^2)^{\frac{1}{2}} + (R_s^2 - R_D^2)^{\frac{1}{2}}]^2} \right)^{\frac{1}{2}} \quad (4-9)$$

If the approach were to continue according to this equation then for small  $D$  ( $D \ll (R_L^2 - R_D^2)^{\frac{1}{2}}$ ),  $v$  would not depend on  $D$  but would approach the horizontal line in Fig. 4-2.

For  $R_D = \frac{\beta R_s}{D}$ , Eq. (4-8) becomes

$$v(D) = \frac{V_i}{(dr/dD)} \left( 1 - \frac{x_i^2}{[D + (R_L^2 - R_D^2)^{\frac{1}{2}} + (R_s^2 - R_D^2)^{\frac{1}{2}}]^2} \right)^{\frac{1}{2}} \quad (4-10)$$

In Eq. (4-10) a term  $dr/dD$  appears and is given in Eq. (3-15).

For large values of  $D$ ,  $dr/dD \approx 1$  and the effect of the radius of deformation,  $R_D$ , is small. However, as the drops approach each other, the other forces, and especially  $F_v$ , dominate and reduce the value of  $|v|$ . The larger is the impact distance  $x_i$  the smaller is  $|v|$  (for the same  $D$ ), and the larger  $D_s$  (the stop distance) will be when the drops stop their approach ( $v = 0$ ). This fact is true for both deformations even though it might be difficult to see it in Fig. 4-3. At the initial point Eq. (4-8) looks like:

$$\left( \frac{dr}{dt} \right)_0 = V_i \left( 1 - \frac{x_i^2}{r_0^2} \right)^{\frac{1}{2}}$$

when  $(dr/dt)_0$  is the radial component of the initial relative velocity of the centers of the drops.

It is easy to see that if  $r_0 > 7.1 x_i$  then  $\left( \frac{dr}{dt} \right)_0 > 0.99 V_i$  and  $(dr/dt)_0$  does not depend on  $x_i$  or on the exact value of  $r_0$ . This is sufficient conditions for the motion to be independent of the starting place, however, it is not a necessary condition. For smaller values of  $r_0$ ,  $(dr/dt)_0$  will depend on  $r_0$ , but as long as Eq. (4-8) is fulfilled the approach will still

be independent of  $r$ . In fact numerical tests indicate that the approach of the drops is not affected by the initial separation,  $r_0$ , as long as  $F_V(r_0)$  is small.

Fig. 4-4 represents the radial force  $F_R(=F_V)$  and the centrifugal force,  $F_C$ , as a function of distance,  $D$ , for  $R_S = 50\mu$  and  $R_L = 250\mu$  interacting at their relative terminal velocity  $V_i$ .

The deformation was taken as  $R_D = 0.5 R_S$  and the impact angle  $\theta_i = 45^\circ$ . The other force  $F_g$ ,  $F_{LV}$  and  $F_{DL}$  are much smaller and could not be drawn on this scale. The curves indicate that down to a distance,  $D$ , of a few microns  $F_C$  dominates. However, at smaller separation distances the viscous force dominates. Since  $F_g$  is small and can be neglected (under the present case of relatively high velocities) the solutions can be applied to different interactions irrespective of their impact direction.

The approach of the drops in head on collision was independent of the size of the larger drop,  $R_L$ , except when  $V_i$  was computed. In the general case  $R_L$  affects the centrifugal force through  $V_i$ :

$$F_C = \frac{m_s (V_i x_i)^2}{[D + (R_L^2 - R_D^2)^{1/2} + (R_S^2 - R_D^2)]^3} \quad (4-11)$$

It indicates that as  $R_L$  decreases the radial velocity will vanish when the drops are further apart.

#### c. Summary

The relative velocity of the deformation planes of the drops can be divided into tangential and radial components. The tangential velocity does not change appreciably during the approach while the radial velocity decreases sharply. If no coalescence occurs when  $v = 0$ , the small drop will move sideways at a velocity equal to its tangential velocity at that point.

The larger is  $x_i$  the smaller is  $v$  and the lower is the probability that the interaction will result in coalescence.

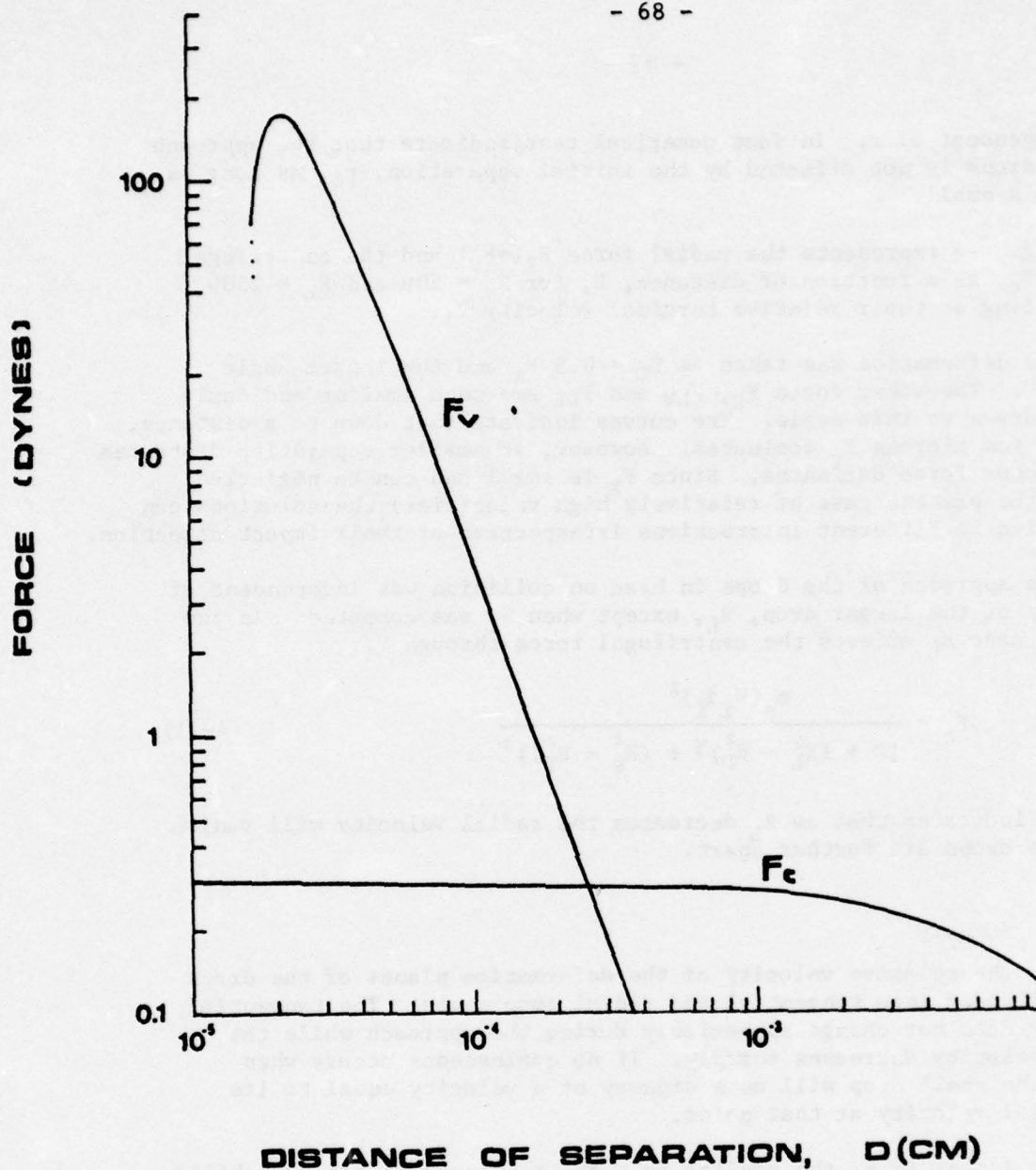


Fig. 4-4. The viscous and the centrifugal forces as a function of the distance of separation. Here  $R_s = 50\mu$ ,  $R_L = 250\mu$ ,  $R_D = 0.5R_s$  and the initial velocity was taken as the relative terminal velocity.

## CHAPTER 5. THE COALESCENCE PROBLEM AND THE COALESCENCE EFFICIENCY

The problem of coalescence concerns with the question of whether two colliding drops will coalesce, even temporarily, or will bounce off each other. This chapter offers a criterion for answering this question, for determining the regions of coalescence and bouncing from the approach of two drops, for determining critical contact angles and for determining impact distances and coalescence efficiencies.

### 5-1. An answer to the coalescence problem

Experimental and theoretical considerations suggest that the maximum separation distance needed before coalescence can take place is about  $0.1\mu$ . We therefore take this distance as the necessary distance to which the drops have to approach. If the approach velocity of the two deformed surfaces,  $v$ , vanishes at a distance larger than  $0.1\mu$ , bouncing results. If, on the other hand,  $v$  has a value greater than zero at  $D_s = 0.1\mu$  the interaction results in coalescence.

According to the above criterion a computer program was developed into which the initial conditions of the motion and the drops' sizes were fed and which provided the answer to the coalescence problem for each pair of drops.

### 5-2. Regions of bouncing and coalescence

Since the radial component of the velocity is smaller for larger impact angles, the distance,  $D_s$ , at which  $v = 0$  is larger. This implies that head-on collisions that result in separation will not coalesce at larger impact angles. These cases can be studied from the results of Chapter 3.

The more complicated problem is the determination of the angle below which coalescence occurs and above which bouncing takes place.

#### i. Regions of bouncing and coalescence in $(R_s, |V_i|)$ plane

In the analytic case we obtained

$$D_s = \frac{3}{4} \alpha^2 \left( \frac{\eta R_s}{-W_i} \right)^{1/2}$$

when  $W_i$  is given in Eq. (3-27). For known  $\alpha$  and  $\eta$  and large  $D_0$  we can write

$$D_s = D_s(R_s, V_i) = \frac{3}{4} \alpha^2 \left( \frac{\eta R_s}{-V_i} \right)^{1/2}$$

Fig. 5-1 describes schematically  $D_s$  versus  $R_s$  and  $|V_i|$  and the intercept of the function with the plane  $D_s = 0.1\mu$ . This intercept is a straight line which can be described in the  $V_i - R_s$  plane as

$$|V_i| = (1.78 \times 10^{10} \eta \alpha^4) R_s \quad (5-1)$$

Fig. 5-2 describes this equation for a few values of  $\alpha$ . For each  $\alpha$  there is a curve which divides the plane into two regions. Above the curve all interactions result in coalescence. Below it all interactions result in separation.

For the cases where an analytic solution cannot be obtained, a computer program was developed which provides the appropriate curves for different  $\alpha$ .

For the deformation  $R_D = \alpha R_s$  a full correspondence with Fig. 5-2 was obtained. For  $R_D = \beta R_s / D$  the curves presented in Fig. 5-3 were obtained when  $R_L = 1000\mu$ . With both deformations straight lines near the origin were obtained and their slope was found to increase monotonically with the deformation constant.

For every  $|V_i|$  the point  $(|V_i|, R_s)$  on the curve gives the critical  $R_s$  above which coalescence takes place and below which bouncing occurs. In the same way for each  $R_s$  there is a  $|V_i|$  above which coalescence takes place. This result explains the experimental fact that in head-on collisions at low velocities, coalescence occurs (Rayleigh, 1882, Park, 1970 and Nelson and Gokhale, 1973).

#### ii. Regions of bouncing and coalescence in the $(p, R_L)$ plane

If one is interested in initial velocities which are equal to the relative terminal fall velocities of the drops, it is possible to express  $D_s$  in terms of  $R_L$  and  $R_s$  or  $p$  and  $R_L$  or even  $p$  and  $R_s$ . The intercept of the function  $D_s$  with the plane  $D_s = 0.1\mu$  divides the plane into regions of coalescence and bouncing.

Fig. 5-4 and 5-5 describe these curves in the plane  $(p, R_L)$  for the deformations  $R_D = \alpha R_s$  and  $R_D = \beta R_s / D$ , respectively. Each deformation coefficient produces a curve which divides the plane into a coalescence region, below the curve, and bouncing above it.

If one looks at a region of coalescence and reduces the size of the large drop, without changing  $p$ , there will come a point at which bouncing will start. This phenomenon was observed by many investigators. For example Telford and Thondike (1961) reported that drops smaller than  $35\mu$  diameter did not coalesce. Levin et al (1973) reported that bouncing occurred for all drops smaller than  $30-40\mu$  radius. We see that the present work predicts a critical radius which depends on the  $p$  ratio.

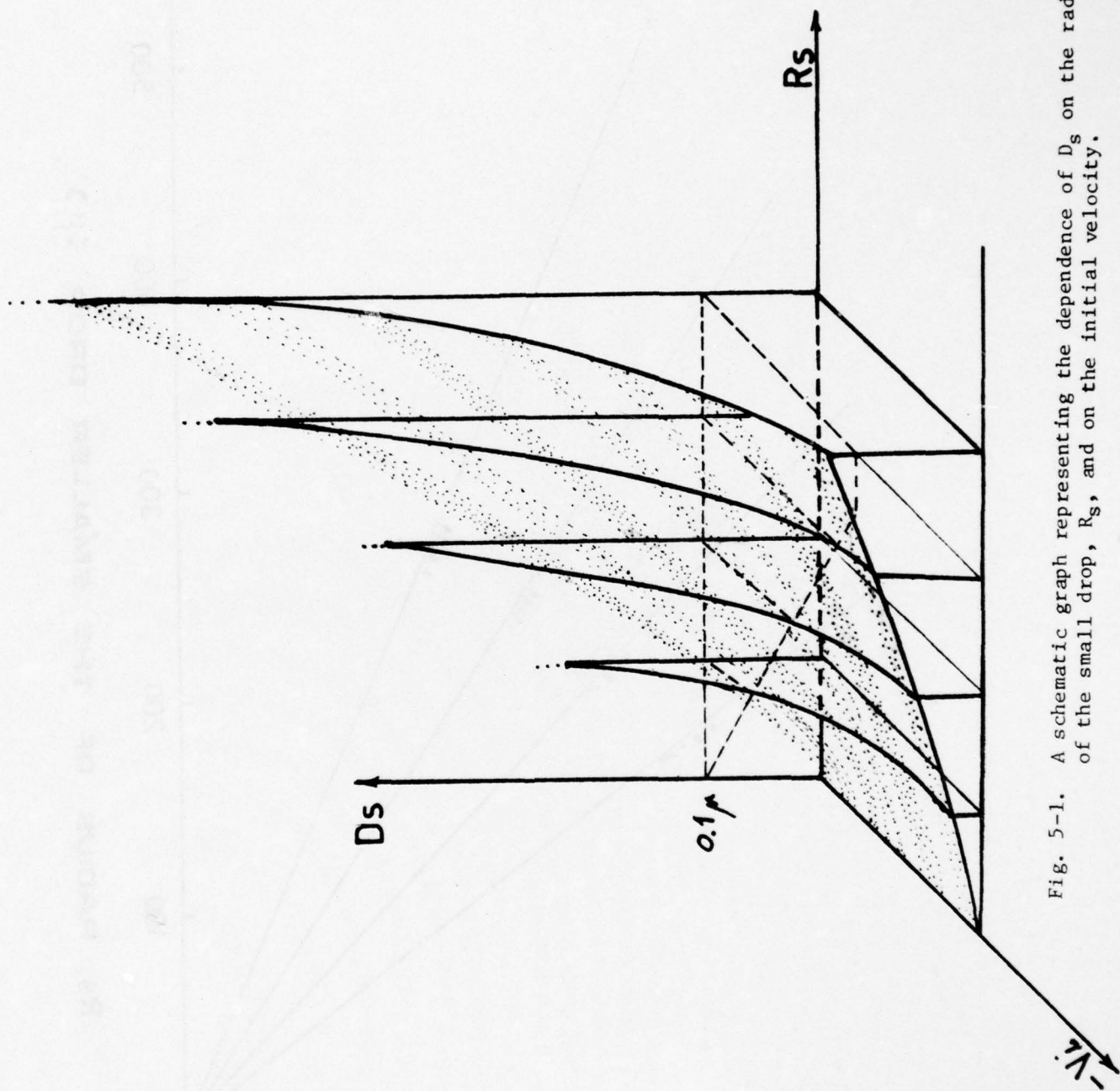


Fig. 5-1. A schematic graph representing the dependence of  $D_s$  on the radius of the small drop,  $R_s$ , and on the initial velocity.

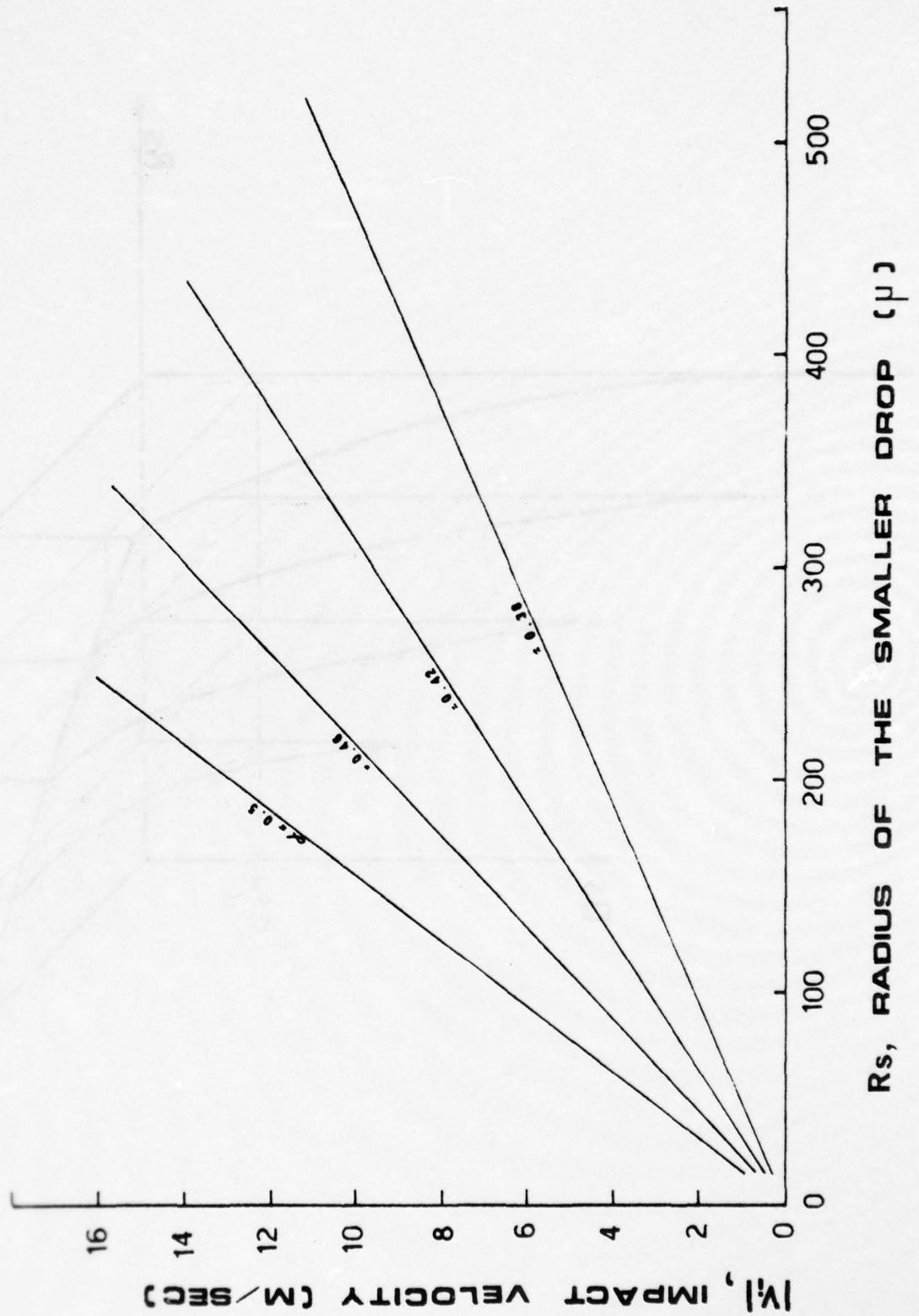


Fig. 1. Regions of bouncing and coalescence in the  $(|v_i|, R_s)$  plane. Here  $R_D = \alpha R_s$ .

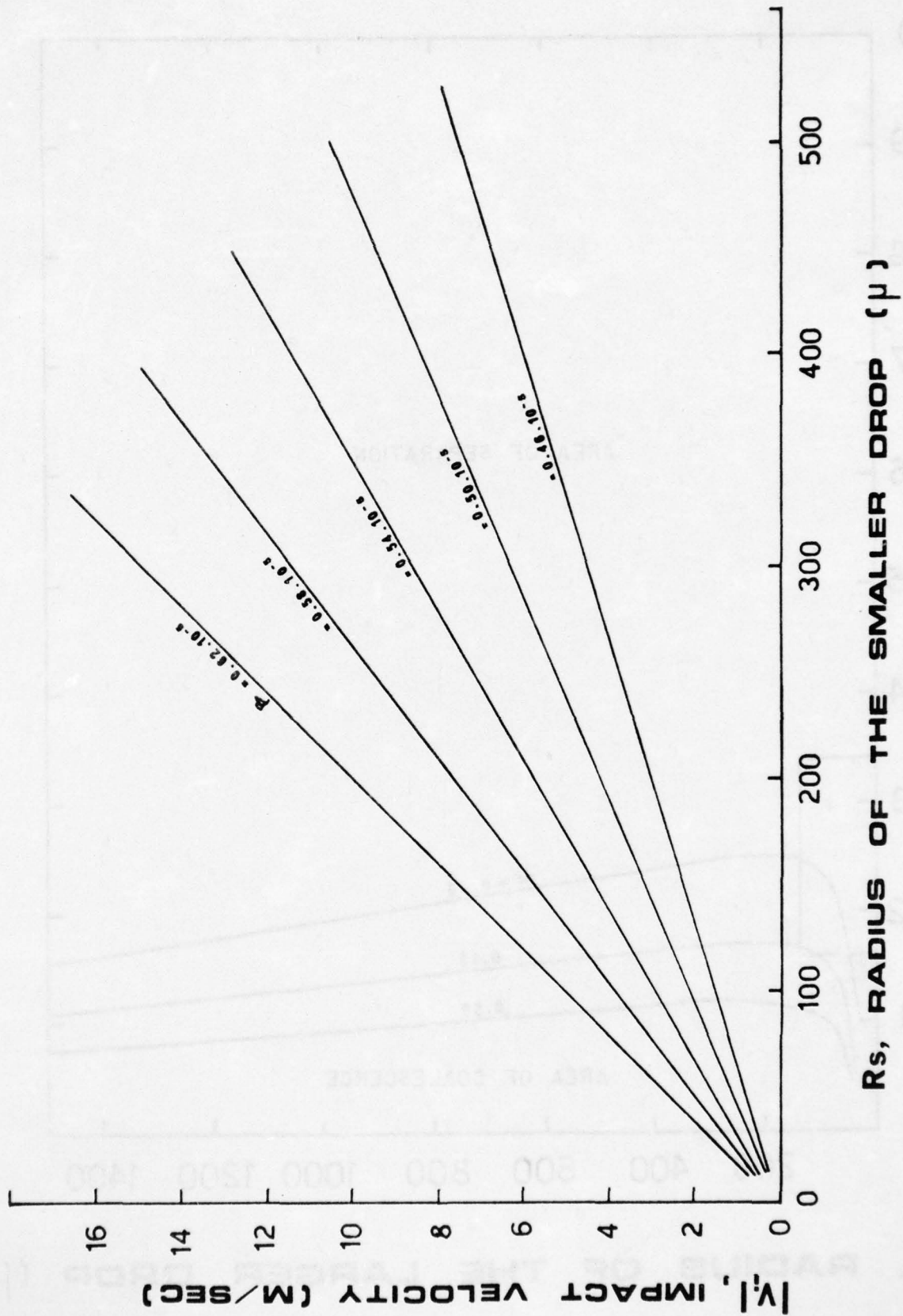


Fig. 5-3. Regions of bouncing and coalescence in the  $(|V_I|, R_s)$  plane. Here  $R_D = \frac{\beta R_s}{D}$ .

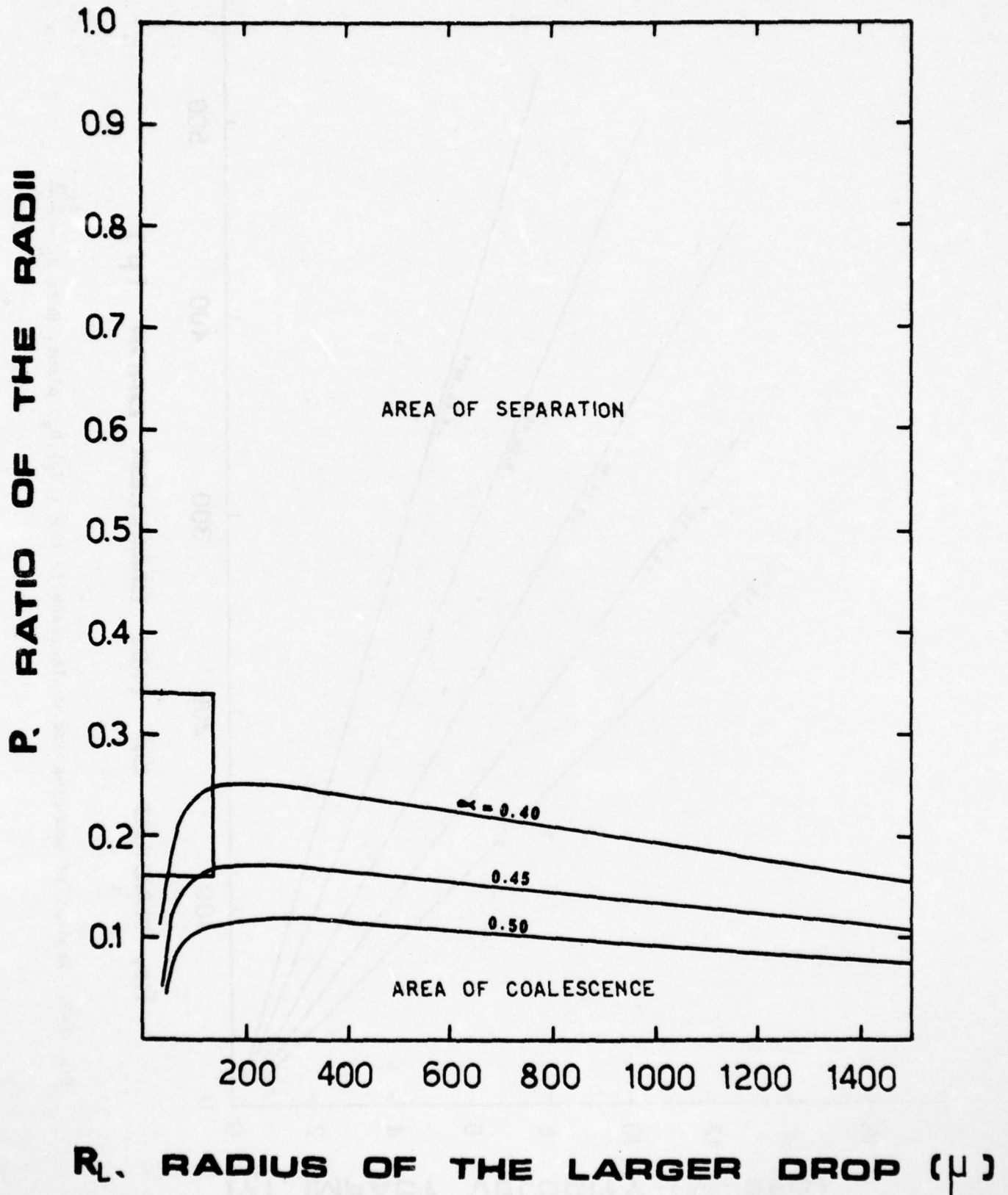


Fig. 5-4. Regions of bouncing and coalescence in the  $(p, R_L)$  plane for  $R_D = \alpha R_S$ . The enclosed area is enlarged in Fig. 5-6.

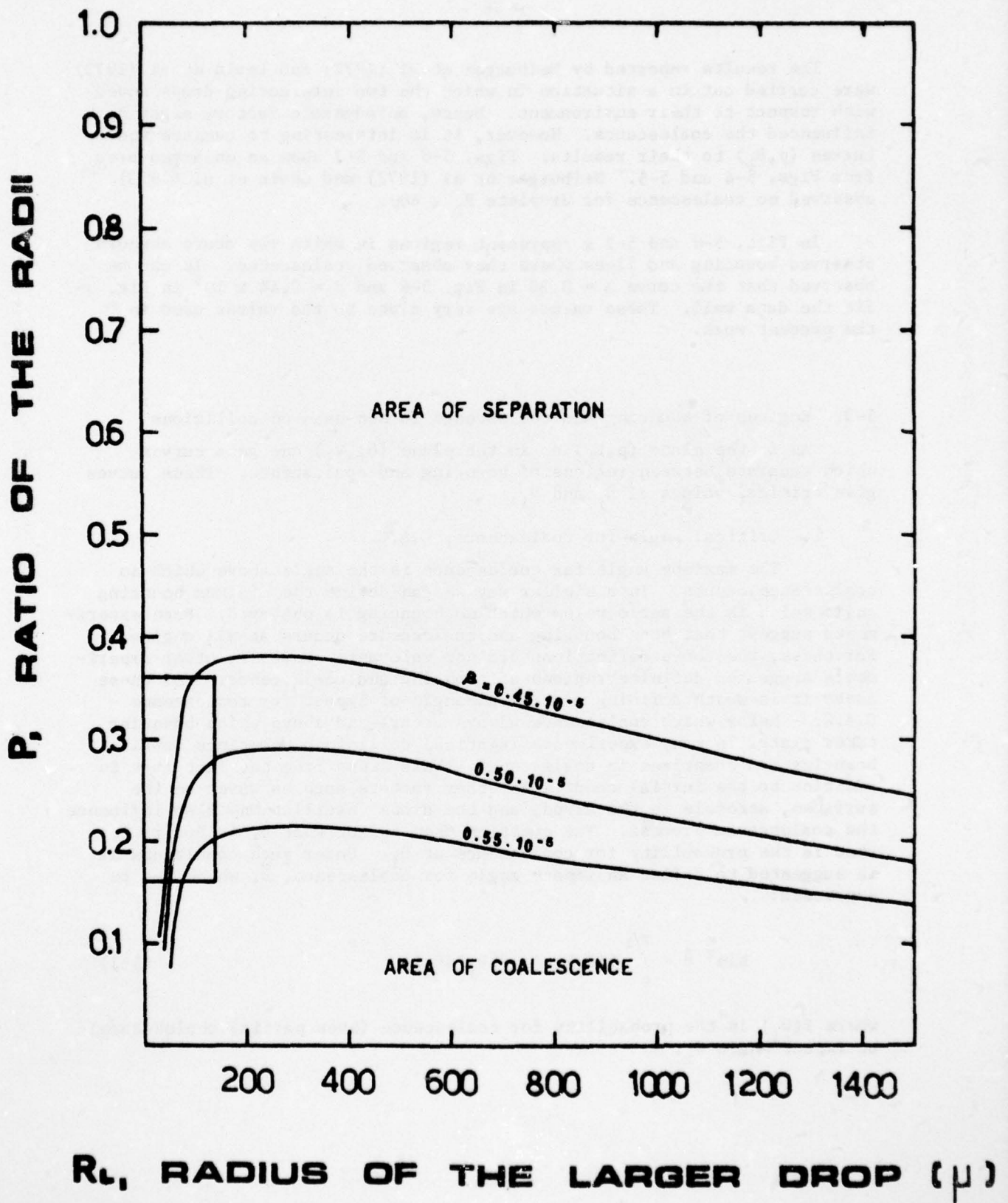


Fig. 5-5. The same as in Fig. 5-4 but for  $R_D = \frac{BR_s}{D}$ . The enclosed area is enlarged in Fig. 5-7.

The results reported by Neiburger et al (1972) and Levin et al (1973) were carried out in a situation in which the two interacting drops moved with respect to their environment. Hence, aerodynamic factors might have influenced the coalescence. However, it is interesting to compare the curves  $(p, R_L)$  to their results. Figs. 5-6 and 5-7 show an enlarged area from Figs. 5-4 and 5-5. Neiburger et al (1972) and Levin et al (1973) observed no coalescence for droplets  $R_L \leq 40\mu$ .

In Figs. 5-6 and 5-7 x represent regions in which the above authors observed bouncing and lines where they observed coalescence. It can be observed that the curve  $\alpha = 0.38$  in Fig. 5-6 and  $\beta = 0.44 \times 10^5$  in Fig. 5-7 fit the data well. These values are very close to the values used in the present work.

### 5-3. Regions of bouncing and coalescence in non-head-on collisions

As in the plane  $(p, R_L)$  so in the plane  $(\theta_i, V_i)$  one gets curves which separate between regions of bouncing and coalescence. These curves give critical values of  $\theta_i$  and  $V_i$ .

#### i. Critical angle for coalescence, C.A.C.

The maximum angle for coalescence is the angle above which no coalescence occurs. In a similar way we can define the minimum bouncing angle which is the angle below which no bouncing is observed. Some experiments suggest that both bouncing and coalescence occurs at all angles. For these, the above definitions are not relevant. However, other experiments suggested definite regions of bouncing and coalescence. For these cases it is worth defining a critical angle of impact for coalescence - C.A.C. - below which coalescence always occurs and above which bouncing takes place. In many experiments identical collisions sometimes result in bouncing and sometimes in coalescence. This stems from the fact that in addition to the initial conditions other factors such as waves on the surfaces, aerosols in the drops, and the drops' oscillations also influence the coalescence process. The question then is not what  $\theta_i$  is but rather what is the probability for coalescence at  $\theta_i$ . Under such conditions it is suggested to define an impact angle for coalescence,  $\bar{\theta}$ , which can be expressed:

$$\sin^2 \bar{\theta} = \int_0^{\pi/2} f(\theta_i) \sin(2\theta_i) d\theta_i \quad (5-2)$$

where  $f(\theta_i)$  is the probability for coalescence (even partial coalescence) at impact angle  $\theta_i$ .

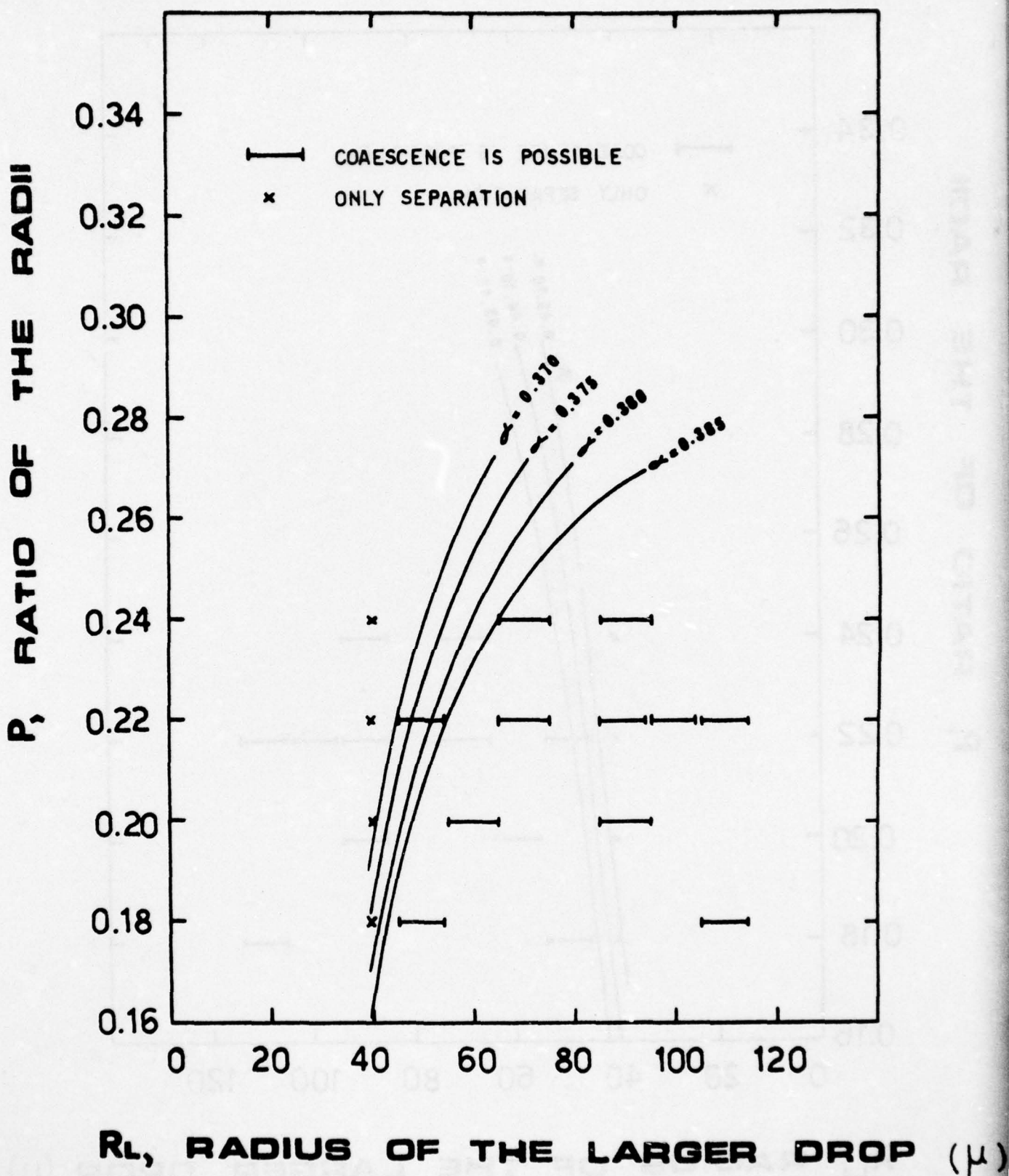


Fig. 5-6. Regions of coalescence and bouncing in the  $(p, R_L)$  plane for  $R_D = \alpha R_s$ .  
x and — represent bouncing and coalescence, respectively in the data of Levin et al (1973).

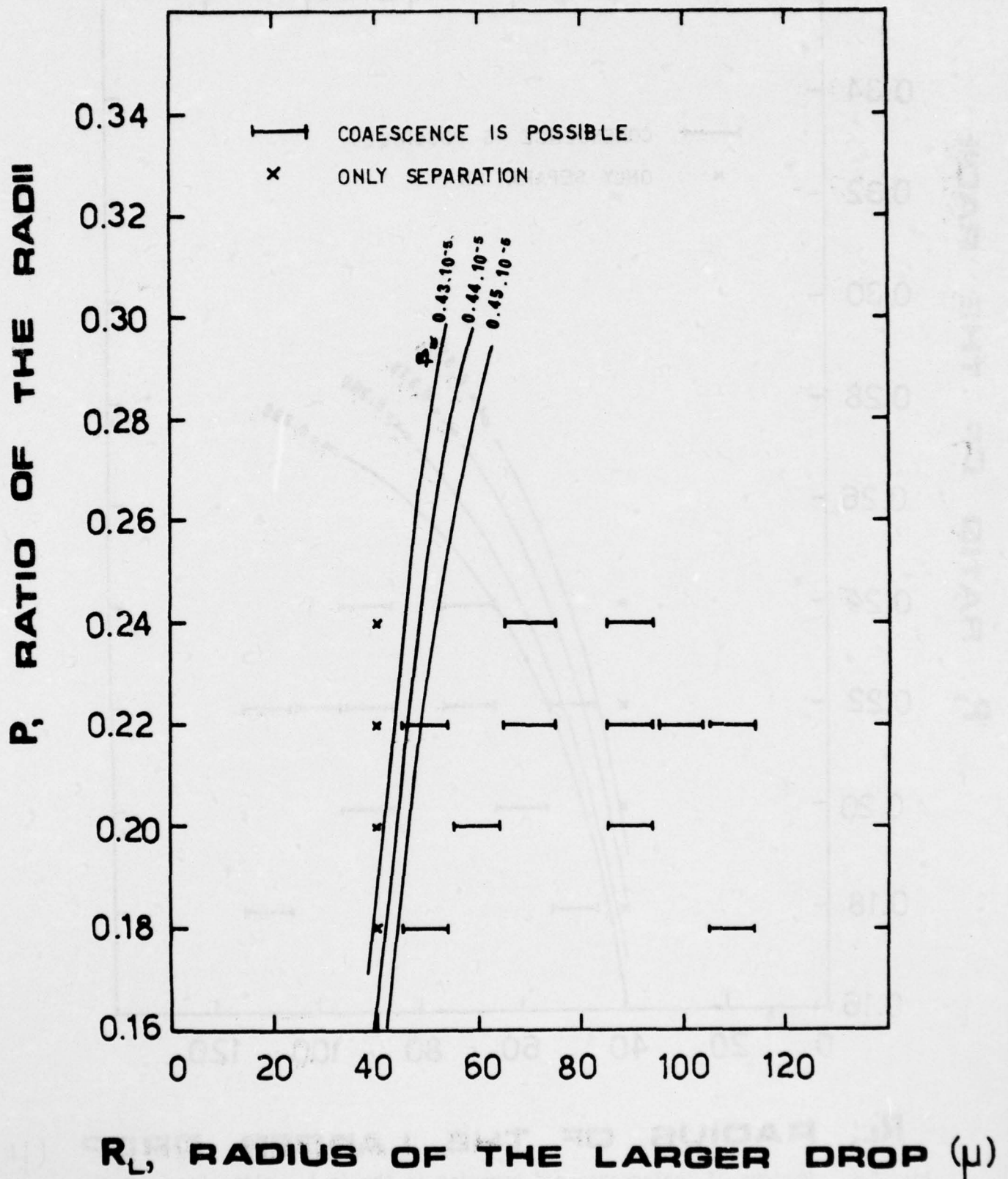


Fig. 5-7. The same as Fig. 5-6 except for  $R_D = \frac{\beta R_s}{D}$ .

$\sin^2 \bar{\theta}$  is the collection efficiency or the coalescence efficiency in cases of impact on a stationary target. If a critical impact angle for coalescence exists than

$$f(\theta_i) = \begin{cases} 1 & \theta_i \leq \theta_c \\ 0 & \theta_i > \theta_c \end{cases}$$

and

$$\sin^2 \bar{\theta} = \int_0^{\theta_c} \sin \theta_i d\theta_i$$

It seems that a critical impact angle for coalescence, CAC, actually exist, but that disturbances smear it out. The smaller these disturbances are the closer the impact angle for coalescence comes to CAC.

ii. Available data on the critical impact angles

a. Impact on a stationary target

Jayarathne and Mason (1964) investigated impacts of drops on horizontal surfaces and found critical angles below which coalescence occurred and above which bouncing was observed. They also investigated impacts of drops on curved surfaces. For drops larger than  $120\mu$  they observed, as before, regions of coalescence and bouncing. However, for small drops they found four regions of impact angles in which coalescence and bouncing occurred starting with coalescence at head-on collisions.

Whelpdale and List (1971) presented their results in the form of histograms from which it can be seen that coalescence occurs at low impact angles and bouncing occurs at higher angles. They estimated that:

$$\theta_c = \arcsin \frac{1}{1+p} \quad (5-3)$$

b. Impact of two moving drops

Park (1970), Nelson and Gokhale (1973) and others have observed that coalescence usually occurs at head-on collisions and bouncing at large impact angles. Many have observed that in the intermediate angles partial coalescence usually occurred.

Park (1970) also observed that the critical impact angles decrease as the impact velocity decreases. A number of different values of CAC appear in the literature and they vary from experiment to experiment (e.g.  $30^\circ$  according to Ryley and Woods, 1965, 1966 and  $60^\circ$  according to Tubman, 1968).

iii. Critical impact angle for coalescence, CAC, from the present model

In this section the CAC for impact on a stationary target is computed.

In the model as  $\theta_i$  increases so do  $x_i$  (Eq. 4-3)  $F_i$  (Eq. 4-11) and  $D_s$ . If there is a  $\theta_i$  for which  $D_s = 0.1\mu$  than for lower  $\theta_i$   $D_s > 0.1\mu$  and coalescence will occur. For larger  $\theta_i$   $D_s > 0.1\mu$  and bouncing will occur. This  $\theta_i$  is the CAC. A computer program was developed which provided the CAC for given initial conditions ( $R_L$ ,  $R_S$ ,  $V_i$  and  $\eta$ ).

Jayarathne and Mason (1964) and Park (1970) reported that CAC is a monostonic increasing function of the impact speed. Whelpdale and List (1971) found similar dependence for high impact speeds. However, for lower impact speeds it is difficult to conclude about the dependence of  $\theta_i$  on  $V_i$  from their results since both increasing and decreasing trends are observed (see Fig. 5-9). In the present model we obtain a monotonically increasing functions of  $\theta_i$  with  $V_i$  as is shown in Fig. 5-8 for  $R_L = 250\mu$ ,  $R_S = 50\mu$  and  $R_D = 25\mu$ . This figure was drawn for  $R_D = 0.5 R_S$ . For  $R_D = 0.5 \times 10^{-5} R_S/D$  a similar graph is obtained but with different values. According to Whelpdale and List (1971) CAC is a monotonically decreasing function of  $p$  (Eq. 5-3). This tendency is also obtained here (see Fig. 5-8).

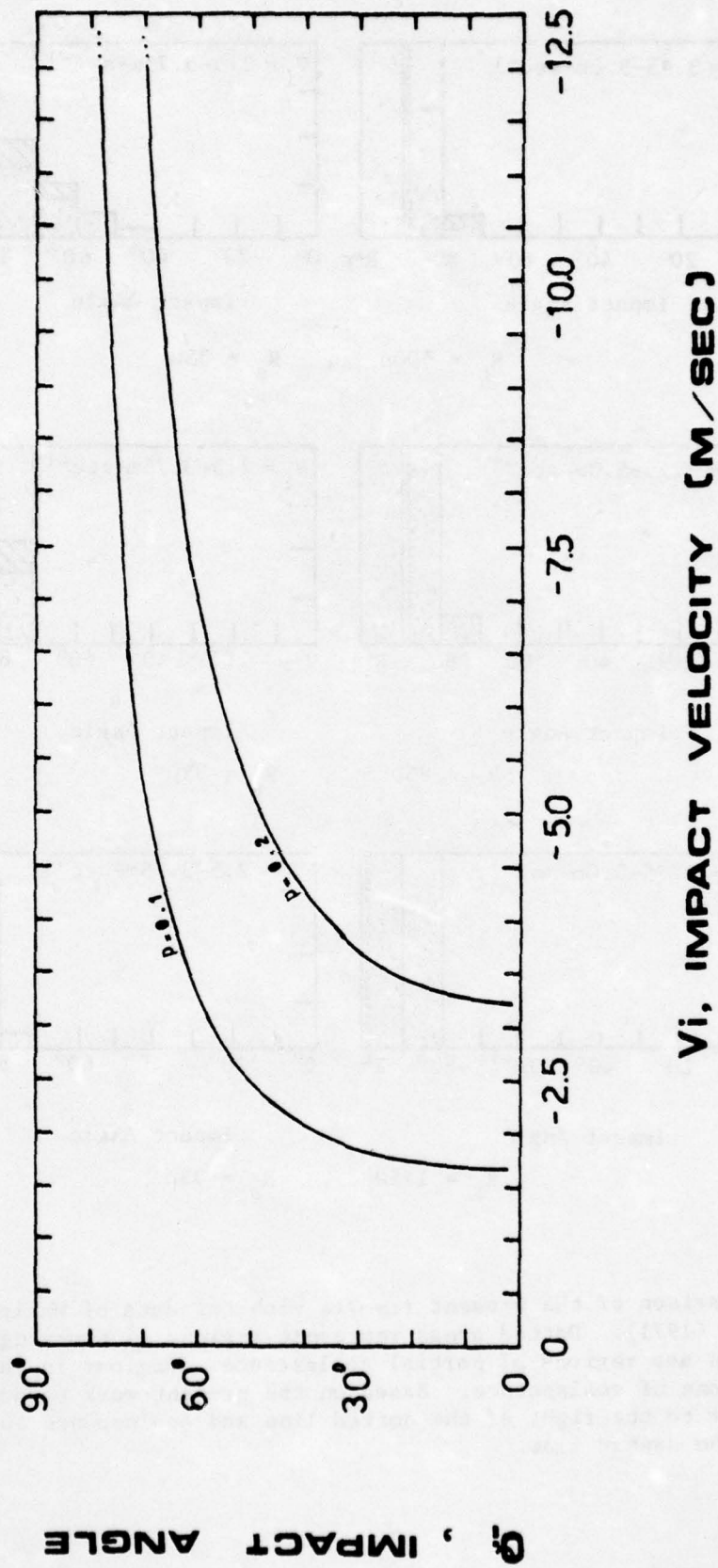
Whelpdale and List (1971) presented their results in histograms which display the frequency of coalescence for each  $\Delta\alpha_i = 10^\circ$ , where  $\alpha_i$  is defined in Chapter 4 section a. Their results relate to three values of  $R_L$  and four values of  $V_i$  (see Fig. 5-9).

For each  $V_i$  there is a CAC within a range of angles which we can call the critical range. The smallest angle in this range (marked by a dashed line) is the angle below which only coalescence occurs. The largest angle in this range (marked by a dotted line) is the one above which only bouncing takes place. Since Whelpdale and List (1971) did not provide a velocity spectrum for each case it is difficult to compare the results of the present model to their results. However, the use of the two deformations ( $R_D = 0.5 R_S$  and  $R_D = 0.5 \times 10^{-5} R_S/D$ ) results in CAC which falls within the critical range shown in Fig. 5-9. In fact the results of the present model fit better as the impact speed becomes higher.

iv. Critical impact velocity

Available data

Tverskaya (1954) observed two critical impact velocities. At lower velocities all interactions resulted in coalescence while at higher velocities only partial coalescence was observed. Impacts with velocities of values in the intermediate range resulted in both coalescence and partial coalescence.



**$V_i$ , IMPACT VELOCITY (M/SEC)**

Fig. 5-8. Regions of bouncing and coalescence in the  $(\theta_i, V_i)$  plane for two different  $p$  ratios.

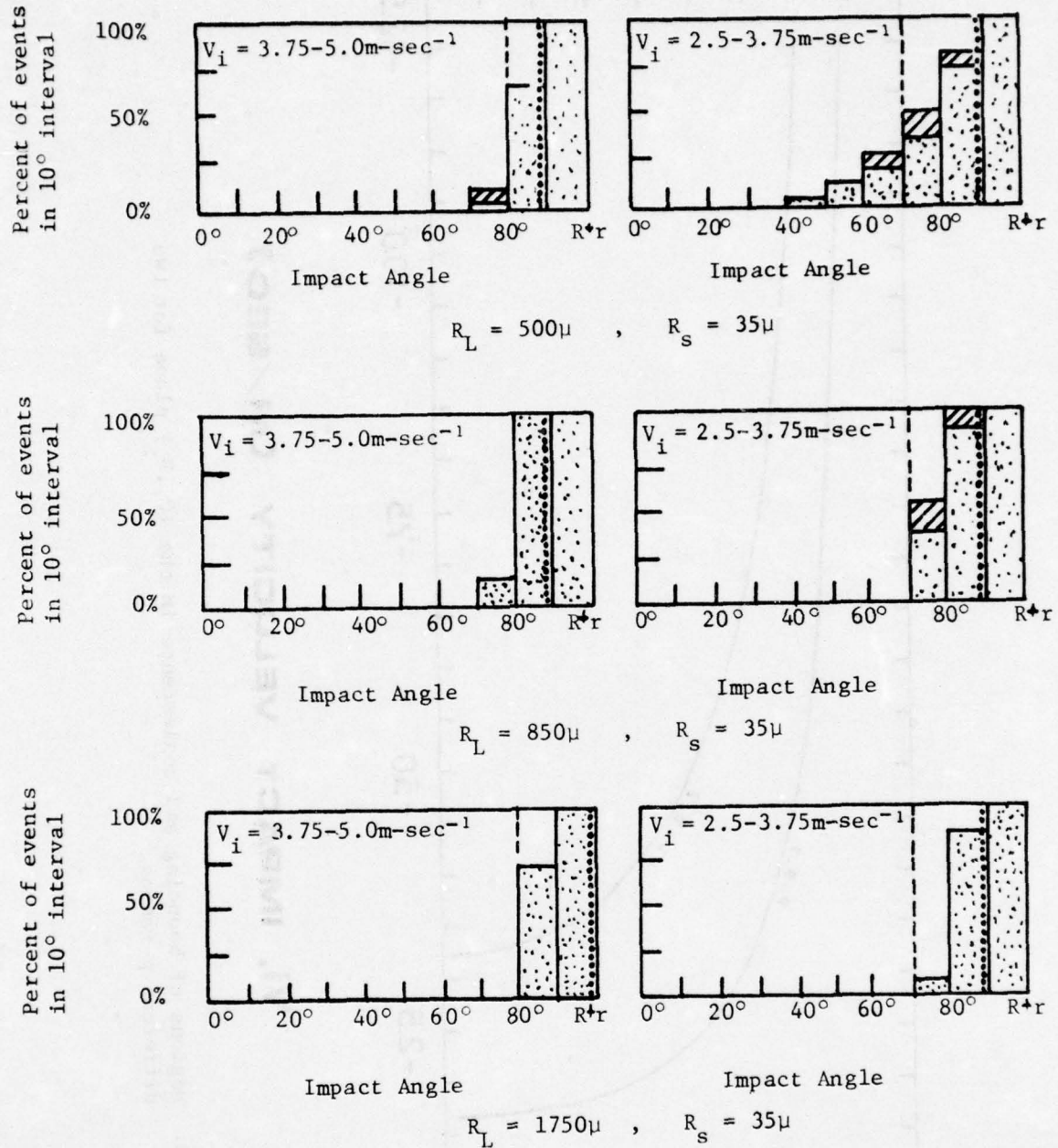


Fig. 5-9. Comparison of the present results with the data of Whelpdale and List (1971). Dotted areas represent regions of bouncing. Dashed areas are regions of partial coalescence. Regions in white are regions of coalescence. Based on the present work bouncing will occur to the right of the dotted line and coalescence to the left of the dashed line.

Prokhorov (1949), (1954) found that all interactions resulted in coalescence except the ones at very low impact speeds. Similarly, Canlas (1960) found that bouncing occurred at low impact speeds. As the impact velocity increased and passed a critical value all interactions resulted in partial coalescence. When the impact speed increased even further a second critical velocity was reached beyond which interactions resulted in coalescence. Similar results were reported by Schotland (1960).

Sartor and Abbott (1972) in an experiment with two falling drops observed a critical velocity below which bouncing occurred and above which coalescence took place. They also observed a lower critical velocity below which coalescence occurred.

The relation between  $\theta_c$  and  $V_c$  in the  $(\theta_i, V_i)$  plane

As was pointed out before, the curve in Fig. 5-8 divides the plane into regions of coalescence and bouncing. For each  $V_i$  the point on the curve gives  $\theta_i = \theta_c$  the critical angle. Similarly, each  $\theta_i = \theta_c$  on the curve gives  $V_i = V_c$ , critical velocity. If  $R_L$  is kept constant and  $R_S$  is changed we obtain a curve (in the  $(\theta_i, V_i)$  plane) which cuts the  $V_i$  axis at different points, this is the critical velocity at head-on-collision. We see that the model gives the critical velocities for each impact angle.

#### 5-4. Coalescence efficiency

In this section a method is suggested by which the coalescence efficiency and collection efficiency can be computed.

##### 1. Definitions

Coalescence distance,  $x_c$ , - the maximum impact distance in which coalescence occurs.

If a CAC exists than  $x_c$  can be written

$$x_c = (R_L + R_S) \sin \theta_c \quad (5-4)$$

collision distance,  $y_c$ , - the maximum impact distance in which collision occurs.

The relation between the collection efficiency  $E$  and  $x_c$  is:

$$E = \frac{x_c^2}{(R_L + R_S)^2} \quad (5-5)$$

The connection between the collision efficiency,  $E_1$  and  $y_c$  is

$$E_1 = \frac{y_c^2}{(R_L + R_s)^2} \quad (5-6)$$

The relation between the coalescence efficiency,  $E_2$ , and  $x_1$  is:

$$E_2 = \frac{x_c^2}{y_c^2} \quad (5-7)$$

It is easy to see that the relation between these equations is:

$$E = E_1 E_2$$

If there is no definite CAC we can define

$$\bar{x} \equiv (2 \int_0^{R_s + R_L} f(x_1) x_1 dx_1)^{1/2}$$

where  $f(x_1)$  is the probability that an impact from an impact distance  $x_1$  results in coalescence. It follows that

$$\bar{x} = (R_L + R_s) \sin \bar{\theta}$$

and

$$E = \frac{\bar{x}^2}{(R_L + R_s)^2}, \quad E_2 = \frac{\bar{x}^2}{y_c^2}$$

## ii. Available data

The available data from the literature points out to a variety of values of coalescence efficiencies ranging from zero to unity. However many of the experiments expressed their results in terms of full coalescence versus partial coalescence and bouncing. Even the experimental part reported on at the beginning of this report separates the two events. However, in the present theoretical model the coalescence is defined as any bridging of the surfaces of drops regardless of whether it results in full or partial coalescence.

iii. Coalescence efficiency for impacts on a stationary target

We will define  $E_{2R}$  as the coalescence efficiency of drop impacting on stationary targets. In this case  $E_1 = 1$  (see the experiments of Whelpdale and List, 1971, Levin and Machnes, 1976, and Chapter 2 of this report). Hence we get:

$$E_{2R} \approx E = \frac{x_c^2}{(R_L + R_S)^2} \quad (5-8)$$

The computer program which provides  $\theta_c$  and  $x_c$  also computes  $E_{2R}$ .

We are interested in values of  $E_{2R}$  for impacts at the relative terminal fall velocities of the drops. Tables 5-1 and 5-2 present  $E_{2R}$  as a function of  $R_L$  and  $p$  for the deformations  $R_D = 0.5 R_S$  and  $R_D = 0.5 \times 10^{-5} R_S/D$ , respectively.

Figs. 5-10 and 5-11 presents  $E_{2R}$  as a function of  $R_L$  and  $p$  for the above deformations. For clarity, part (a) of the figures was plotted for small  $R_L$  and part (b) for large values of  $R_L$ . Fig. 5-12 shows the relation of  $E_{2R}$  with  $p$  as was suggested by Whelpdale and List (1971):

$$E_{2R} = \frac{1}{(1 + p)^2} \quad (5-9)$$

The figure also presents the results from the present model with both deformations for the drop size ( $R_S = 35\mu$ ) used by Whelpdale and List.

As was already pointed out, Eq. (5-9) has two main draw backs: i. There is no dependence of  $E_{2R}$  on  $R_L$  (see Levin and Machnes, 1976, and Chapter 2 of this report). ii. The lowest value of  $E_{2R}$  according to this equation is 0.25 while other experiments (Levin et al, 1973) found regions of  $E_{2R} = 0$ . Figs. 5-10 and 5-11 show that the present model does not have these limitations. In these figures  $E_{2R}$  is a monotonic decreasing function of  $p$  to the point at which  $E_{2R} = 0$ .  $E_{2R}$  remains zero for larger values of  $p$  (it should be remembered that the assumption in the model makes it most applicable for small values of  $p$ ). Both Whelpdale and List (1971), and the experimental results reported in this report suggest similar dependence of  $E_{2R}$  on  $p$ .

Fig. 5-13 describes  $E_{2R}$  as a function of  $R_L$  and  $p$  in a three dimensional graph. Here we see that  $E_{2R}$  increases as  $R_L$  increases up to about  $100\mu$  and then decreases slowly. The intercept of the function  $E_{2R} = E_{2R}(p, R_L)$  with the plane  $(p, R_L)$  gives the same curves as in Fig. 5-3 and 5-4 which were

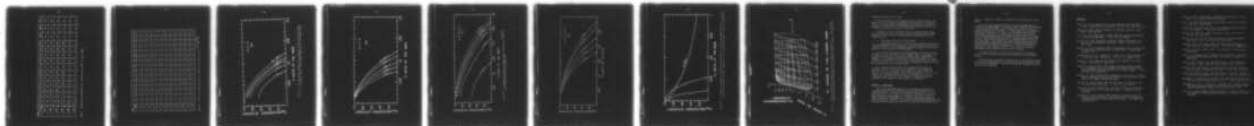
AD-A032 010

TEL-AVIV UNIV (ISRAEL) DEPT OF GEOPHYSICS AND PLANET--ETC F/G 4/1  
EXPERIMENTAL AND THEORETICAL INVESTIGATION OF THE COALESCENCE 0--ETC(U)  
MAY 76 Z LEVIN, B MACHNES, N ARBEL

DA-ERO-124-74-G-0058

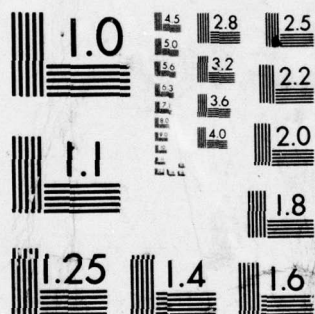
UNCLASSIFIED

2 OF 2  
AD  
A032010



END

DATE  
FILMED  
1-77



MICROCOPY RESOLUTION TEST CHART  
NATIONAL BUREAU OF STANDARDS-1963-A

$\frac{RL}{P}$	20 $\mu$	40 $\mu$	60 $\mu$	80 $\mu$	100 $\mu$	150 $\mu$	200 $\mu$	250 $\mu$	300 $\mu$	350 $\mu$	500 $\mu$	750 $\mu$	1000 $\mu$	1250 $\mu$	1500 $\mu$
0.025	0	0	.63	.83	.89	.93	.94	.95	.95	.95	.95	.94	.93	.92	.90
0.050	0	0	.47	.67	.74	.79	.82	.82	.83	.83	.82	.78	.72	.67	.59
0.075	0	0	.10	.38	.49	.56	.60	.61	.62	.61	.60	.49	.35	.21	.01
0.100	0	0	0	0	.12	.23	.29	.31	.31	.30	.27	.05	0	0	0
0.125	0	0	0	0	0	0	0	0	0	0	0	0	0	0	0
0.150	0	0	0	0	0	0	0	0	0	0	0	0	0	0	0

Table 1. Coalescence efficiencies as a function of  $R_L$  and  $p$  for  $R_D = 0.5R_g$ .

$\frac{R_L}{p}$	20 $\mu$	40 $\mu$	60 $\mu$	80 $\mu$	100 $\mu$	150 $\mu$	200 $\mu$	250 $\mu$	300 $\mu$	350 $\mu$	500 $\mu$	750 $\mu$	1000 $\mu$	1250 $\mu$	1500 $\mu$
0.025	0	0	.74	.89	.93	.96	.98	.98	.98	.98	.98	.98	.98	.98	.98
0.050	0	0	.69	.84	.90	.93	.95	.95	.96	.96	.96	.95	.95	.94	.93
0.075	0	0	.61	.79	.84	.89	.91	.92	.92	.92	.92	.91	.89	.87	.74
0.100	0	0	.51	.71	.78	.84	.86	.87	.87	.87	.87	.85	.81	.78	.58
0.125	0	0	.39	.62	.71	.77	.80	.81	.81	.81	.81	.76	.71	.66	.36
0.150	0	0	.25	.52	.62	.70	.73	.73	.73	.73	.73	.66	.56	.49	.09
0.175	0	0	.08	.40	.51	.60	.64	.65	.65	.65	.63	.53	.41	.28	0
0.200	0	0	0	.26	.40	.49	.53	.64	.54	.53	.51	.38	.22	.01	0
0.225	0	0	0	.10	.25	.36	.41	.42	.41	.40	.37	.19	0	0	0
0.250	0	0	0	0	.09	.21	.26	.27	.26	.25	.21	0	0	0	0
0.275	0	0	0	0	0	.04	.09	.10	.08	.06	.02	0	0	0	0
0.300	0	0	0	0	0	0	0	0	0	0	0	0	0	0	0

Table 2. Coalescence efficiencies as a function of  $R_L$  and  $p$  for  $R_D = \frac{0.5 \times 10^{-5} R_g}{D}$ .

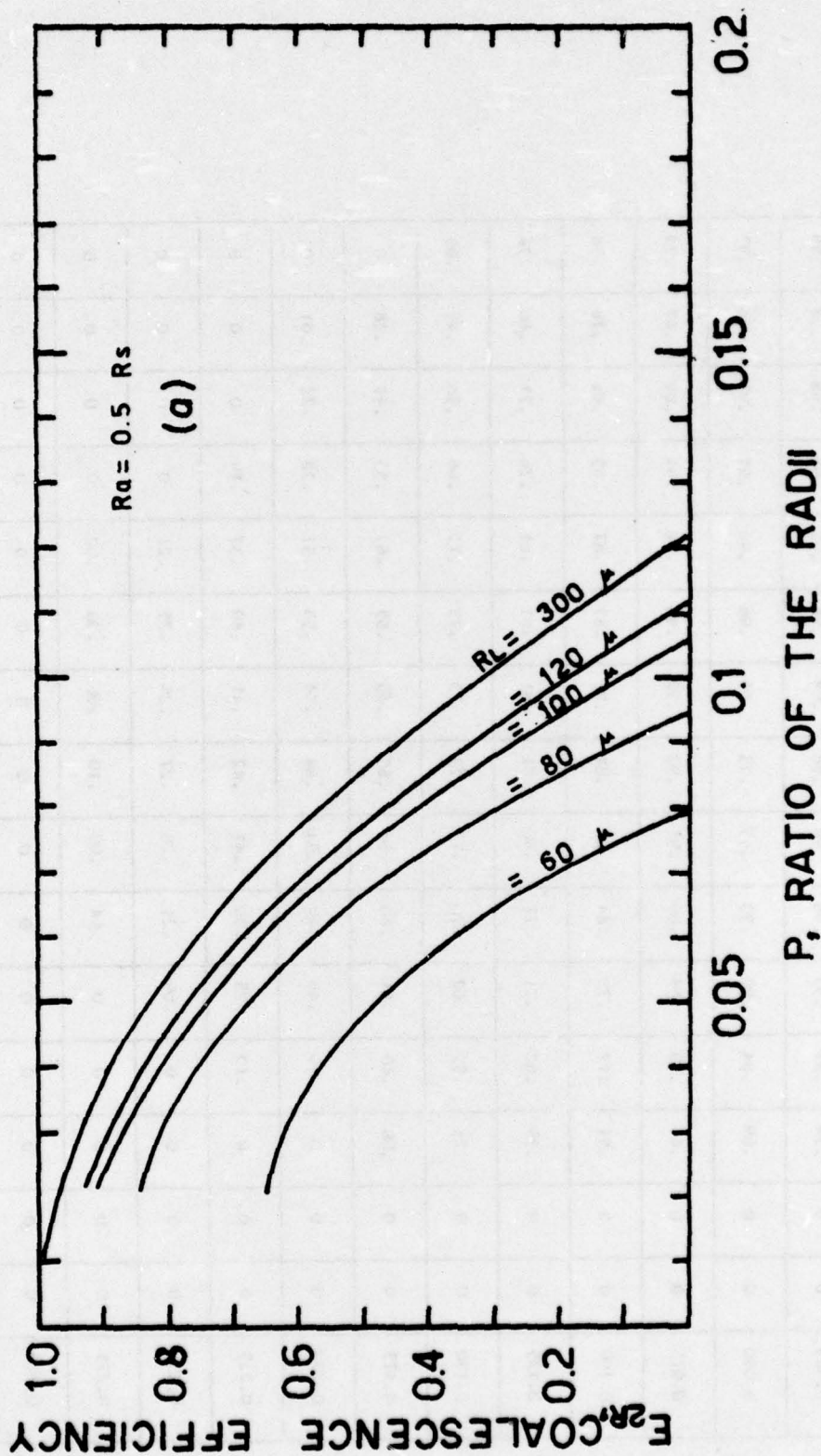
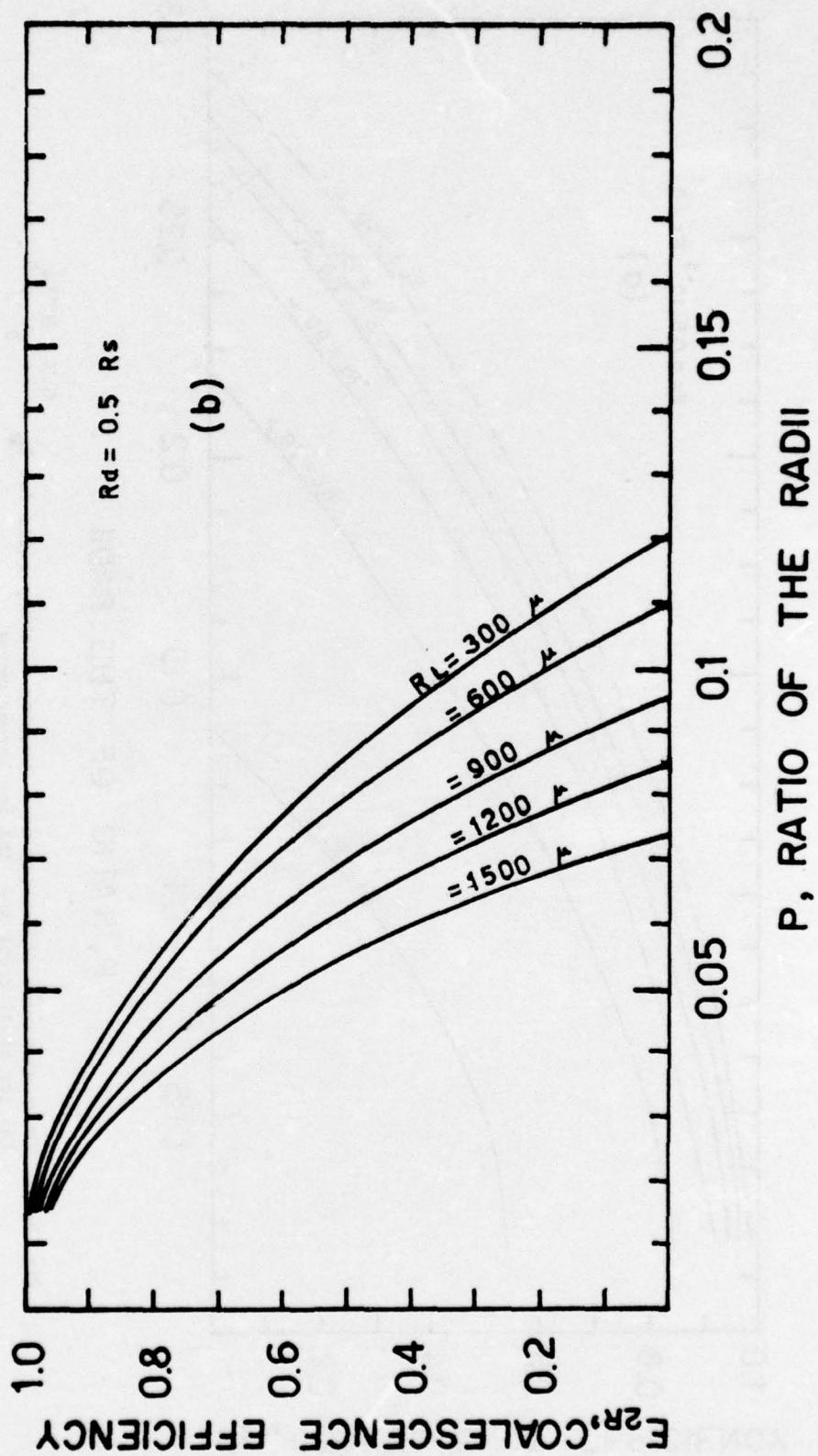


Fig. 5-10. The coalescence efficiency as a function of the ratio of the radii,  $p$ , for  $R_D = 0.5R_S$ . (a) for small drops and (b) for larger drops.



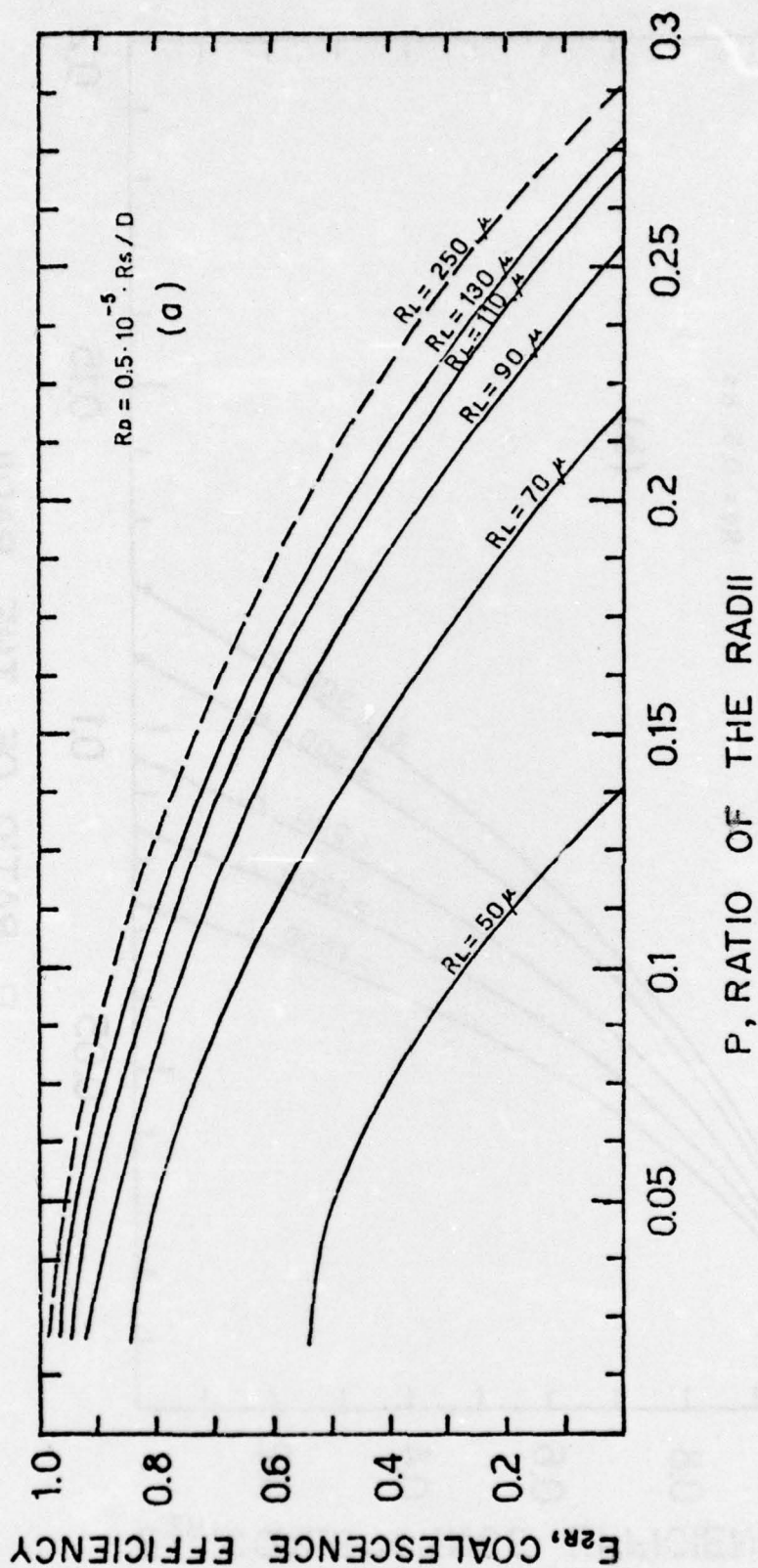
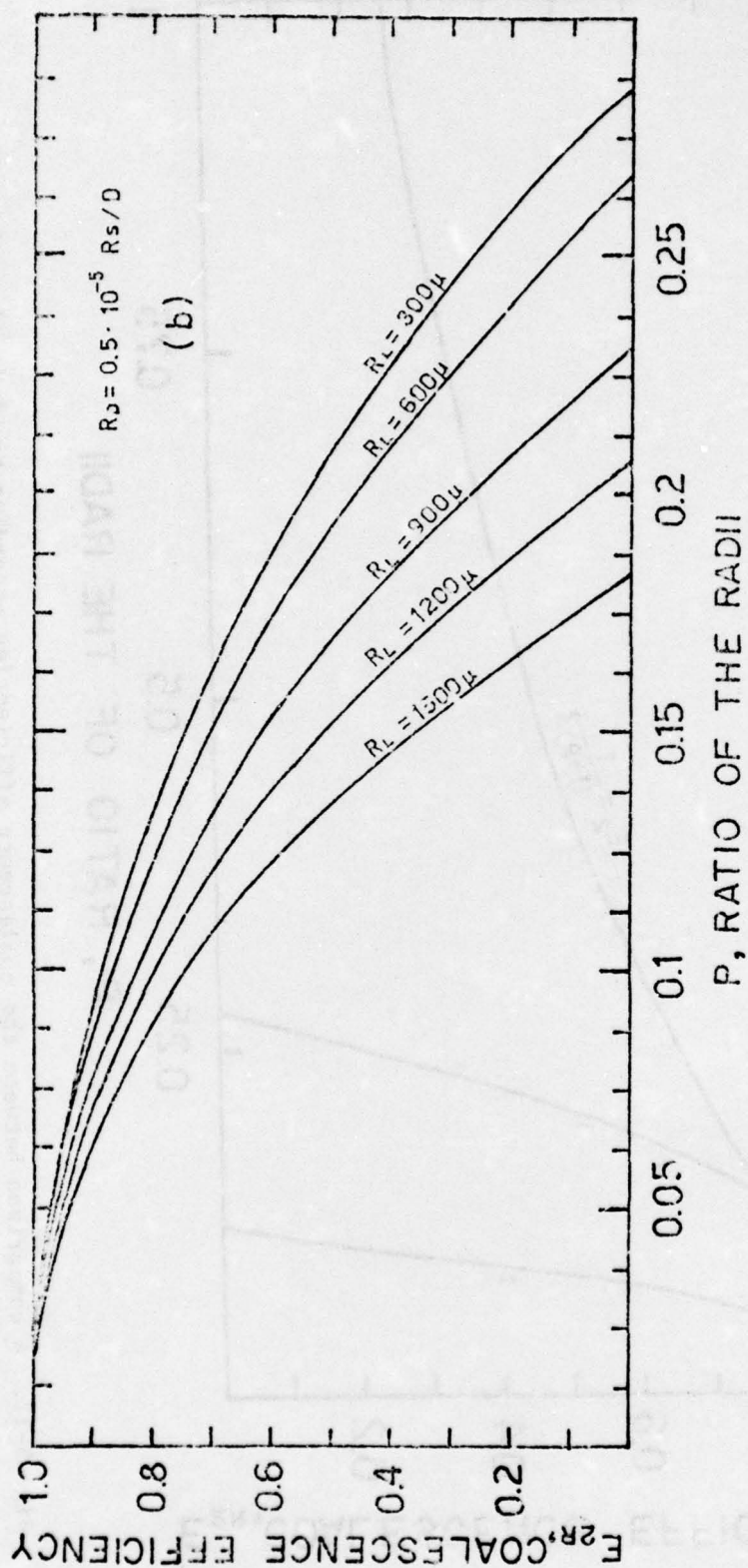


Fig. 5-11. The coalescence efficiency as a function of the p ratio for  $R_D = \frac{0.5 \times 10^{-5} R_s}{D}$ .  
 (a) for small drops and (b) for larger drops.



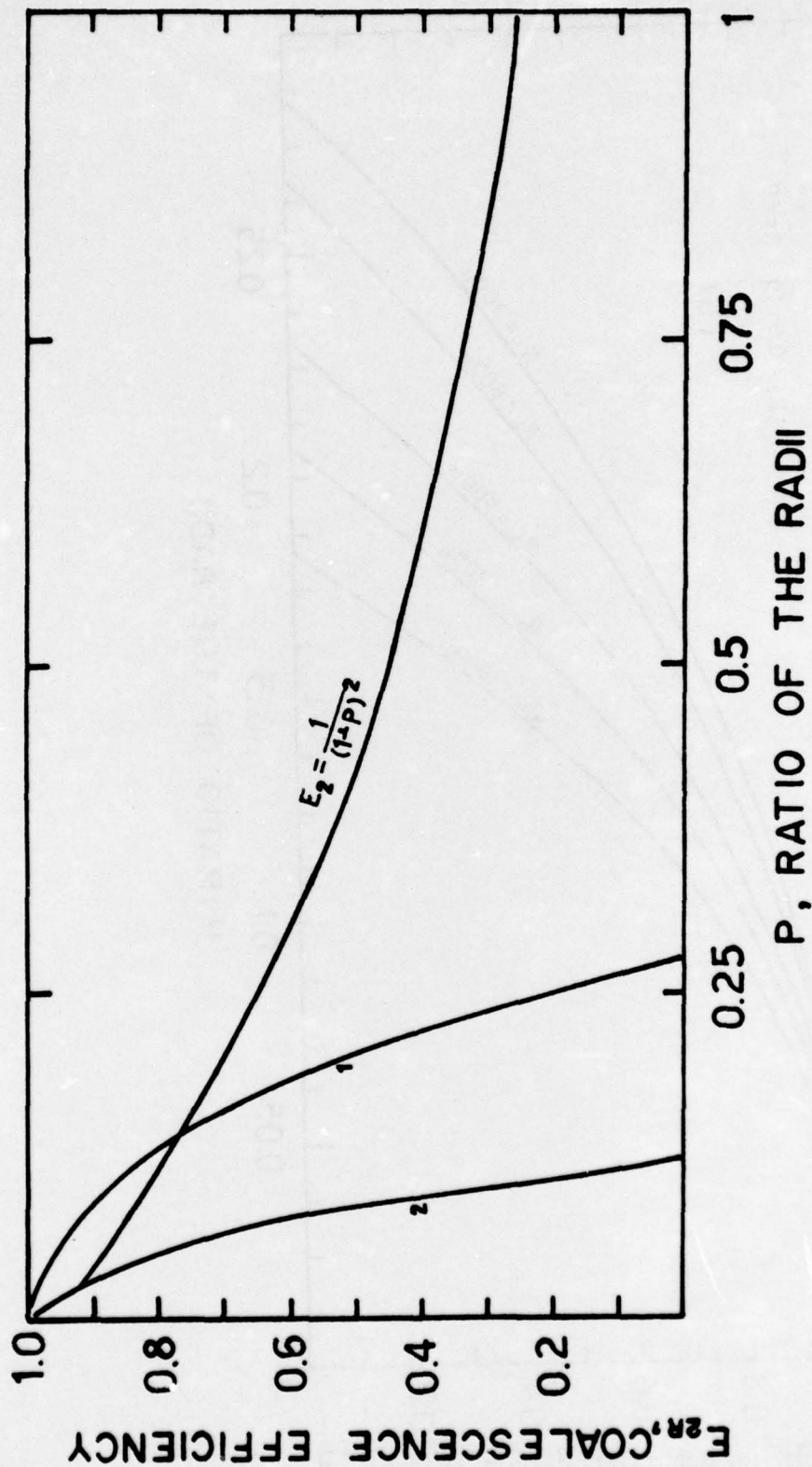
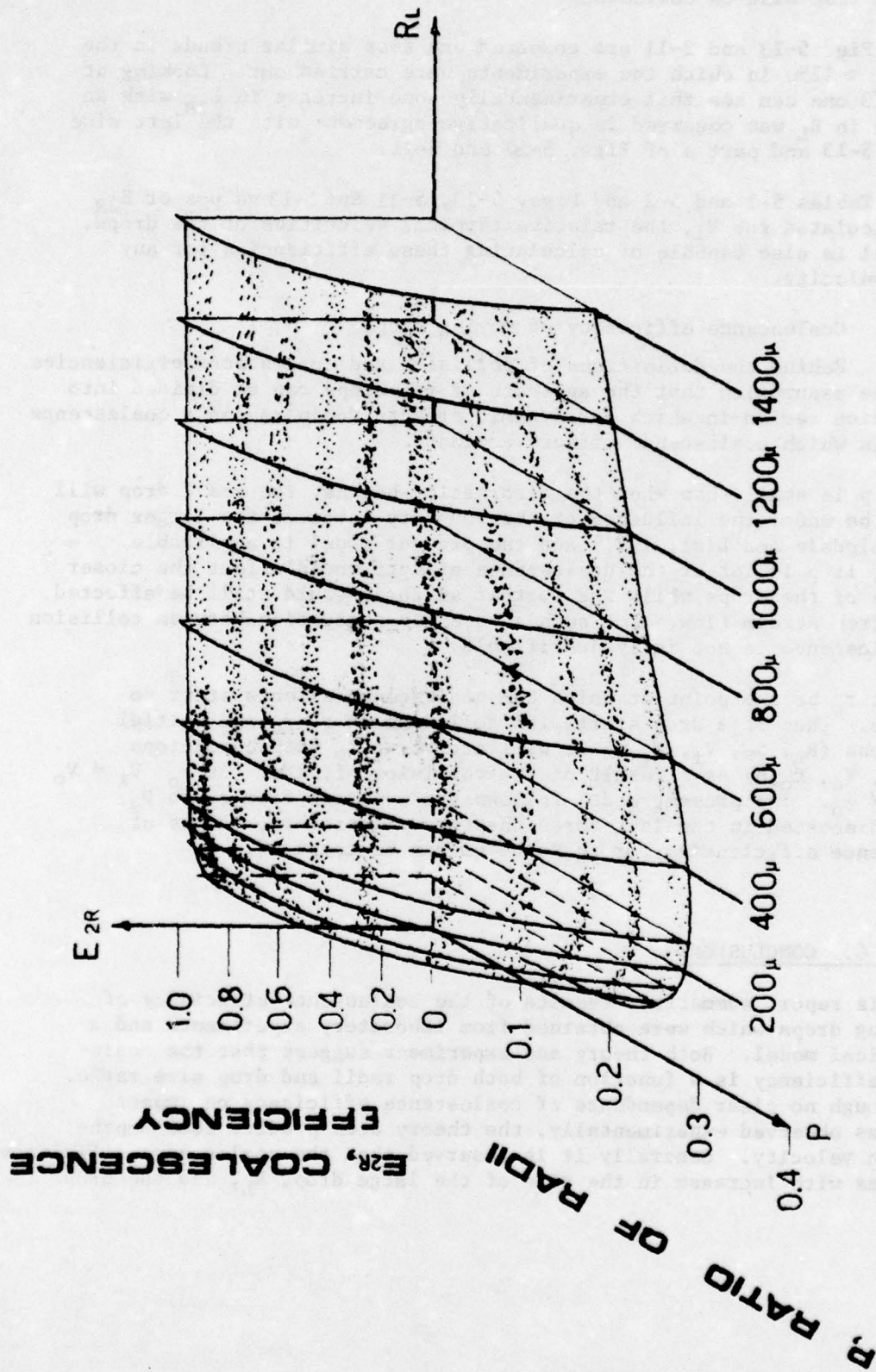


Fig. 5-12. A comparison between the coalescence efficiencies according to Whelpdale and List (1971) and the present results. Curve 1 is for  $R_D = 0.5 R_s$  and curve 2 for  $R_D = \frac{0.5 \times 1.0^{-5} R_s}{D}$ .



### $R_L$ , RADIUS OF THE LARGER DROP

Fig. 5-13. A three dimensional representation of the coalescence efficiency as a function of the radius of the large drop,  $R_L$ , and the p ratio. Here  $R_D = \frac{0.5 \times 1.0^{-5} R_s}{D}$ .

obtained from head-on collisions.

If Fig. 5-13 and 2-11 are compared one sees similar trends in the range  $R_L > 125\mu$  in which the experiments were carried out. Looking at Fig. 2-10 one can see that experimentally some increase in  $E_{2R}$  with an increase in  $R_L$  was observed in qualitative agreement with the left side of Fig. 5-13 and part a of Figs. 5-10 and 5-11.

In Tables 5-1 and 5-2 and Figs. 5-10, 5-11 and 5-13, values of  $E_{2R}$  were calculated for  $V_i$ , the relative terminal velocities of the drops. The model is also capable of calculating these efficiencies for any impact velocity.

#### iv. Coalescence efficiency of moving drops

Behind the definitions of collision and coalescence efficiencies rests the assumption that the approach of two drops can be divided into a collision region in which aerodynamic effects dominate and a coalescence region in which coalescence effects dominate.

If  $p$  is small than when the deformation begins, the small drop will already be under the influence of the boundary layer of the larger drop (see Whelpdale and List, 1971) and the present model is applicable. However, if  $p$  is larger the coalescence effects would affect the closer surfaces of the drops while the further surfaces would still be affected by the free stream flow. For such a case the separation between collision and coalescence is not fully justifiable.

Let  $r_0$  be the point at which the coalescence effects start to dominate. Then if a drop starts its collision at  $r > r_0$  and initial conditions  $(R_L, R_s, V_i, x_i, \eta)$  it will arrive at  $r_0$  with conditions  $(R_L, R_s, V_0, x_0, \eta)$  as a result of the collision effects. At  $r_0$   $V_i \neq V_0$  and  $x_i \neq x_0$ . The present model follows the approach from  $r_0$  to  $D_s$ , as was discussed in the last three chapters. Therefore, values of coalescence efficiencies for these cases can be computed.

## CHAPTER 6. CONCLUSIONS

This report summarises results of the coalescence efficiency of colliding drops which were obtained from laboratory experiments and a theoretical model. Both theory and experiment suggest that the coalescence efficiency is a function of both drop radii and drop size ratio. Even though no clear dependence of coalescence efficiency on impact speed was observed experimentally, the theory does predict some dependence on velocity. Generally it is observed that the coalescence efficiency decreases with increase in the size of the large drop,  $R_L$ , and the drop

ratio,  $p$ . However, for small  $R_L$  a decrease in the efficiency was also shown.

Both theory and experiment demonstrate the strong dependence of coalescence on impact angle. The theory is able to predict the efficiency of coalescence for different impact speeds and not only the relative terminal velocities of the drops. It is also capable of calculating the coalescence efficiency of all impacts on stationary targets and the coalescence efficiencies for moving drops when the  $p$  ratio is small. From the experiments two empirical equations were obtained which relate the coalescence efficiencies and partial coalescence efficiencies with  $p$  and  $R_L$ . These could easily be used in numerical models of cloud and rain development. Even though the present results provide physical understanding and numerical values of the coalescence efficiency, the problem is far from being fully understood. It is hoped that this investigation will continue in order to find values of coalescence efficiency for much smaller drops and for all  $p$  ratios.

It should be pointed out that the theoretical derived values of the coalescence efficiency were generally lower than our experimental results.

We feel that the inclusion of surface waves on the deformed surfaces in the theory would increase the theoretical values and bring them closer to those of the experiment. We plan to continue our theoretical investigation in this direction.

## References

- Abbott, C.E. and T.W. Cannon, 1972: A droplet generator with electronic control of production rate and charge. *Rev. Sci. Inst.*, 43, 1313-1317.
- Adamson, A.W., 1967: "Physical Chemistry of Surfaces". Second ed. John Wiley & Sons, New York.
- Allan, R.S., G.E. Charles and S.G. Mason, 1961: The approach of gas bubbles to a gas/liquid interface. *J. Coll. Sci.*, 16, 150-165.
- Bartlett, J.T., 1971: The effect of revised collision efficiencies on the growth of cloud droplets by coalescence. *Quart. J. Roy. Met. Soc.*, 96, 730-738.
- Beard, K.V. and H.R. Pruppacher, 1968: An experimental test of theoretically calculated collision efficiencies of cloud drops. *J. Geophy. Res.*, 73, 6407, 6414.
- Brazier-Smith, P.R., S.G. Jennings and J. Latham, 1972: The interaction of falling water drops: Coalescence. *Proc. Roy. Soc.*, A326, 393-408.
- Browne, I.C., H.P. Palmer and T.W. Wormell, 1954: Physics of rain clouds. *Quart. J. Roy. Met. Soc.*, 80, 291-327.
- Burrill, K.A. and D.R. Woods, 1969: Change in interface and film shapes for a deformable drop at a deformable liquid-liquid interface: Part I film hydrodynamic pressure distribution and interface shapes. *J. Coll. and Inter. Sci.*, 30, 511-524.
- Canlas, D.C., 1960: An experimental investigation on the effects of ambient pressure, temperature and relative humidity on the coalescence of water drops. Ph.D. thesis, New York University.
- Charles, G.E. and S.G. Mason, 1960: The coalescence of liquid drops with flat liquid/liquid interfaces. *J. Collo. Sci.*, 15, 236-277.
- Cotton, W.R. and N.R. Gokhale, 1967: Collision coalescence and break-up of large water drops in a vertical wind tunnel. *J. Geophy. Res.*, 72, 4041-4049.
- Deryagin, B.V. and M. Kussakov, 1939: Anomalous properties of thin poly-molecular solvate (adsorbed) films as applied to the development of a mathematical theory of the stability of colloids. *Acta Physicochim URSS*, 10, 25-44.

- Foote, G.B., 1971: A theoretical investigation of the dynamics of liquid drops. Ph.D. thesis, University of Arizona.
- Foote, G.B., 1975: The water drop rebound problem: Dynamics of collision. J. Atmos. Sci., 32, 390-402.
- Frankel, S.P. and K.J. Mysels, 1962: On the dimpling during the approach of two interfaces. J. Phys. Chem., 66, 190-191.
- Hocking, L.M., 1959: The collision efficiency of water drops. Quart. J. Roy. Met. Soc., 85, 44-50.
- Hocking, L.M. and P.R. Jonas, 1970: Theoretical collision efficiencies of small drops. Quart. J. Roy. Met. Soc., 96, 722-729.
- Jayarathne, O.W. and B.J. Mason, 1964: The coalescence and bouncing of water drops at an air/water interface. Proc. Roy. Soc., 280, 545-548.
- Landau, L.D. and E.M. Lifshitz, 1959: "Fluid Mechanics", Addison-Wesley, Reading Mass.
- Levin, Z., M. Neiburger and L. Rodriguez, 1973: Experimental evaluation of collection and coalescence effects in cloud drops. J. Atmos. Sci., 30, 944-946.
- Levin, Z. and B. Machnes, 1976: Experimental study of the coalescence of rain drops. Inter. Cloud Phys. Conf. Boulder, Color. In Press.
- Lindblad, N.R., 1964: Effects of relative humidity and electric charge on the coalescence of curved water surfaces. J. Coll. Sci., 19, 729-743.
- Mackay, G.D.N. and S.C. Mason, 1963: Some effects of interface diffusion on the gravity coalescence of liquid drops. J. Coll. Sci., 18, 674-683.
- Neiburger, M., Z. Levin and L. Rodriguez, 1972: Experimental determination of the collection efficiency of cloud drops. J. Rech. Atmos., 6, 393-397.
- Neiburger, M., I.Y. Lee, E. Lobl and L. Rodriguez, 1974: Computed collision efficiencies and experimental collection efficiencies of cloud drops. Conf. on Cloud Physics. Tucson, Ariz. Amer. Met. Soc., 73-78.
- Nelson, A.R. and N.R. Gokhale, 1973: Delay time as a function of velocity for the collision of freely suspended waterdrops. J. Geophys. Res., 78, 1472-1474.

- Park, R.H., 1970: Behavior of drops colliding in humid nitrogen. Ph.D. thesis, Univer. of Wisconsin.
- Picknett, E.T., 1960: "Collection Efficiency for Water Drops in Air: Aerodynamic Capture of Particles". Pergamon Press, London.
- Plumlee, H.R., 1964: Effect of electrostatic forces on drop collision and coalescence in air. Ph.D. thesis, Univer. of Illinois and Ill. State Water Survey.
- Prokhorov, P.S., 1949: Explanation of the new mechanism of non-coalescence of water drops during collision. Lawrence Rad. Lab. UCRL Translation 601, Berkeley, Calif., 1960 (unpublished).
- Prokhorov, P.S., 1954: The effects of humidity deficit on coagulation processes and the coalescence of liquid drops. Disc. Faraday Soc., 18, 41-51.
- Rayleigh, Lord, 1882: Further observation upon liquid jets in continuation of those recorded in the society's "Proceedings" for March and May 1879. Proc. Roy. Soc., 34, 130-145.
- Ryley, D.J. and M.R. Wood, 1965-1966: The collision, in free flight, of water droplets in atmospheres of air and steam. Proc. Inst. Mech. Engr., 180, Part 30, 73-87.
- Sartor, J.D. and C.E. Abbott, 1972: Some details of coalescence and charge transfer between freely falling drops in different electrical environments. J. De. Rech. Atmos., 6, 479-493.
- Schotland, R.M., 1960: Experimental results relating to the coalescence of water drops with water surfaces. Disc. Faraday Soc., 30, 72-77.
- Scott, W.D. and Z. Levin, 1975: A stochastic electrical model of an infinite cloud: charge generation and precipitation development. J. Atmos. Sci., 52, 1814-1828.
- Selman, J.R., 1961: An investigation on the effect of ambient pressure and vapor pressure on the coalescence of drops. M.Sc. thesis, Univer. of Wisconsin.
- Shafrir, U. and M. Neiburger, 1963: Collision efficiencies of two spheres falling in a viscous medium. J. Geophy. Res., 68, 4141-4147.

- Swinbank, W.C., 1947: Collisions of cloud droplets. *Nature*, 159, 849-850.
- Telford, J. and N.S. Thorndike, 1961: Observation of small drops collisions. *J. Met.*, 18, 382-389.
- Tubman, K.A., 1968: The collisional behaviour of water drops in free flight within an atmosphere of low pressure steam. M. Eng. thesis, Univer. of Liverpool.
- Tverskaya, N.P., 1954: Trudy Glavnoi Geofiz. Obs. No. 47, 112.
- Whelpdale, D.M. and R. List, 1971: The coalescence process in rain drop growth. *J. Geophy. Res.*, 76, 2836-2856.
- Woods, J.D. and B.J. Mason, 1964: Experimental determination of collection efficiencies for small water droplets in air. *Quart. J. Roy. Met. Soc.*, 90, 373-381.